

Supporting Information

Solvatomorphism of a 2,6-pyridyl- dicarboxamide-based Foldamer

Sena Ozturk,^[a] Alexander R. Davis,^[a] Colin C. Seaton,^[b] Louise
Male,^[a] and Sarah J. Pike*^[a]

^[a]School of Chemistry, University of Birmingham, Edgbaston, Birmingham, B15 2TT, UK.

^[b]School of Chemistry and Biosciences, Faculty of Life Sciences, University of Bradford,
Bradford, West Yorkshire, BD7 1DP, UK

Email: s.j.pike@bham.ac.uk

Contents

Crystallographic Details	4
Crystal Data and Structural Refinement	8
a) 1A	8
b) 1A'	9
c) 1B	10
d) 1·THF	11
e) 1·butanone	12
f) 1·DCM	13
g) 1·MeOH	14
h) 1·DMSO	15
Crystallisation Solvents and Conditions for 1 Screened in This Study	16
Helical Pitch Values of Studied Structures	17
Cavity Values of Studied Structures	18
Synthetic Scheme to Access Foldamer 1	19
Solid-State Analysis	20
a) Solid State Analysis of 1A	20
b) Solid State Analysis of 1A'	28
c) Solid State Analysis of 1B	35
d) Solid State Analysis of 1·THF	44
e) Solid State Analysis of 1·butanone	51
f) Solid state analysis of 1·DCM	60
g) Solid state analysis of 1·MeOH	66
h) Solid state analysis of 1·DMSO	74
Cavity space and channel calculation	83
a) Void Analysis of 1A and 1A'	84
b) Void Analysis of 1B	85
c) Void Analysis of 1·THF	86
d) Void Analysis of 1·butanone	87
e) Void Analysis of 1·DCM	89
f) Void Analysis of 1·MeOH	90
g) Void Analysis of 1·DMSO	91
References	93

General Experimental Details

The diamine terminated foldamer **1** was synthesised in accordance with known literature procedures using a multi-step synthetic route as outlined in Scheme 1.^{1,2} The following solvents were either used to grow (or attempt to grow) crystals that were suitable for single crystal X-ray diffraction analysis for this study.

Chloroform, dichloromethane, pyridine, toluene, acetone, anisole, methanol, ethanol and *N,N*-dimethylformamide were purchased from Thermofisher scientific chemicals. Dimethyl sulfoxide, α,α,α -trifluorotoluene, acetonitrile, 2-hexanone, diethyl ether and diisopropyl ether were purchased from Sigma-Aldrich. Tetrahydrofuran and ethyl acetate were purchased from VWR. 1,4-dioxane and 2-decanone were purchased from Thermo Scientific. Xylene was purchased from Honeywell. Butanone was purchased from Scientific Lab Supplies. 2-ethoxyethanol was purchased from Merck. All chemicals were used as received.

The following abbreviations are employed: DMSO = dimethylsulfoxide, Et = ethyl, ^{*i*}Pr = isopropyl, Me = methyl, DCM = dichloromethane, THF = tetrahydrofuran, (Boc)₂O = Di-*tert*-butyl decarbonate, MS = molecular sieves.

Crystallographic Details

The dataset for **1·DCM** was measured on a Bruker APEX-II CCD diffractometer. The datasets for **1A**, **1A'** and **1·Butanone** were measured on a Rigaku XtaLAB Synergy diffractometer using a HyPix detector. The datasets for **1·THF** and **1·DMSO** were measured on an Agilent SuperNova diffractometer using an Atlas detector. These latter five data collections were driven and processed and absorption corrections were applied using CrysAlisPro.³ The datasets for **1B** and **1·MeOH** were measured at the Diamond Light Source, Beamline I19-1, using a Dectris PILATUS 2M detector.⁴ These datasets were processed and absorption corrections were applied using DIALS 3, XIA2 and AIMLESS.⁵⁻⁹

Using OLEX2,¹⁰ all eight structures were solved using ShelXT,¹¹ and were refined by a full-matrix least-squares procedure on F^2 in ShelXL.¹² All non-hydrogen atoms were refined with anisotropic displacement parameters. Hydrogen atom treatment is discussed for each structure individually. Crystal structures were visualised using Mercury.¹³

1A: $C_{31}H_{25}N_9O_2$ ($M = 555.60$ g/mol): monoclinic, space group $P2_1/c$ (no. 14), $a = 11.56410(10)$ Å, $b = 38.6957(4)$ Å, $c = 12.34340(10)$ Å, $\beta = 104.4570(10)^\circ$, $V = 5348.54(9)$ Å³, $Z = 8$, $T = 103(6)$ K, $\mu(\text{Cu K}\alpha) = 0.743$ mm⁻¹, $D_{\text{calc}} = 1.380$ g/cm³, 39445 reflections measured ($7.742^\circ \leq 2\Theta \leq 149.002^\circ$), 10243 unique ($R_{\text{int}} = 0.0287$, $R_{\text{sigma}} = 0.0246$) which were used in all calculations. The final R_1 was 0.0465 ($I > 2\sigma(I)$) and wR_2 was 0.1357 (all data).

The structure contains two crystallographically-independent molecules. The hydrogen atoms bonded to N(2), N(5), N(6), N(9), N(102), N(105), N(106), N(109) were located in the electron density and the positions and isotropic thermal parameters were refined, subject to N-H distance restraints where necessary. The remaining hydrogen atoms were fixed as riding models with the isotropic thermal parameters (U_{iso}) being based on the U_{eq} of the parent atom.

1A': $C_{31}H_{25}N_9O_2$ ($M = 555.60$ g/mol): monoclinic, space group $P2_1/c$ (no. 14), $a = 11.57690(10)$ Å, $b = 38.7107(2)$ Å, $c = 12.34610(10)$ Å, $\beta = 104.7550(10)^\circ$, $V = 5350.45(7)$ Å³, $Z = 8$, $T = 99.99(10)$ K, $\mu(\text{Cu K}\alpha) = 0.743$ mm⁻¹, $D_{\text{calc}} = 1.379$ g/cm³, 71800 reflections measured ($7.75^\circ \leq 2\Theta \leq 157.238^\circ$), 10856 unique ($R_{\text{int}} = 0.0295$, $R_{\text{sigma}} = 0.0161$) which were used in all calculations. The final R_1 was 0.0376 ($I > 2\sigma(I)$) and wR_2 was 0.1024

(all data).

The structure contains two crystallographically-independent molecules. The hydrogen atoms bonded to N(2), N(5), N(6), N(9), N(102), N(105), N(106), N(109) were located in the electron density and the positions and isotropic thermal parameters were refined, subject to N-H distance restraints where necessary. The remaining hydrogen atoms were fixed as riding models with the isotropic thermal parameters (U_{iso}) being based on the U_{eq} of the parent atom.

1B: $C_{31}H_{25}N_9O_2$ ($M=555.60$ g/mol): monoclinic, space group $P2_1/c$ (no. 14), $a = 17.58120(10)$ Å, $b = 42.4637(2)$ Å, $c = 7.06860(5)$ Å, $\beta = 95.5710(10)^\circ$, $V = 5252.23(5)$ Å³, $Z = 8$, $T = 100.15$ K, $\mu(\text{Synchrotron}) = 0.088$ mm⁻¹, $D_{calc} = 1.405$ g/cm³, 115588 reflections measured ($2.256^\circ \leq 2\theta \leq 72.228^\circ$), 25728 unique ($R_{int} = 0.0610$, $R_{sigma} = 0.0791$) which were used in all calculations. The final R_1 was 0.0580 ($I > 2\sigma(I)$) and wR_2 was 0.1615 (all data).

The structure contains two crystallographically-independent molecules. The aminophenyl groups C(13)-C(18), N(5) / C(13A)-C(18A), N(5A), C(26)-C(31), N(9) / C(26A)-C(31A), N(9A) and C(126)-C(131), N(109) / C(26B)-C(31B), N(9B) are disordered over two positions at refined percentage occupancy ratios of 91.0 (2) : 9.0 (2), 87.9 (2) : 12.1 (2) and 93.4 (2) : 6.6 (2) respectively. The hydrogen atoms bonded to N(2), N(5), N(6), N(9), N(102), N(105), N(106), N(109) were located in the electron density and the positions and isotropic thermal parameters were refined, subject to N-H distance restraints where necessary. The remaining hydrogen atoms were fixed as riding models with the isotropic thermal parameters (U_{iso}) being based on the U_{eq} of the parent atom.

1·THF: $C_{35}H_{33}N_9O_3$ ($M=627.70$ g/mol): monoclinic, space group $P2_1$ (no. 4), $a = 11.5123(5)$ Å, $b = 10.4201(5)$ Å, $c = 12.7453(5)$ Å, $\beta = 92.318(4)^\circ$, $V = 1527.67(12)$ Å³, $Z = 2$, $T = 100.00(10)$ K, $\mu(\text{Cu } K\alpha) = 0.738$ mm⁻¹, $D_{calc} = 1.365$ g/cm³, 24759 reflections measured ($7.686^\circ \leq 2\theta \leq 136.456^\circ$), 4334 unique ($R_{int} = 0.0283$, $R_{sigma} = 0.0263$) which were used in all calculations. The final R_1 was 0.0445 ($I > 2\sigma(I)$) and wR_2 was 0.1152 (all data).

The structure contains a molecule of tetrahydrofuran, disordered over two positions at a refined percentage occupancy ratio of 74.4 (6) : 25.6 (6). The hydrogen atoms bonded to N(4) and N(6) were located in the electron density and the positions refined. The remaining hydrogen

atoms were fixed as riding models and the isotropic thermal parameters (U_{iso}) of all hydrogen atoms were based on the U_{eq} of the parent atom.

1•Butanone: $\text{C}_{35}\text{H}_{33}\text{N}_9\text{O}_3$ ($M=627.70$ g/mol): monoclinic, space group $\text{P}2_1$ (no. 4), $a = 11.7137(2)$ Å, $b = 10.3944(2)$ Å, $c = 12.6481(2)$ Å, $\beta = 93.4610(10)^\circ$, $V = 1537.18(5)$ Å³, $Z = 2$, $T = 99.99(16)$ K, $\mu(\text{Cu K}\alpha) = 0.733$ mm⁻¹, $D_{\text{calc}} = 1.356$ g/cm³, 28058 reflections measured ($7.002^\circ \leq 2\Theta \leq 140.142^\circ$), 5534 unique ($R_{\text{int}} = 0.0390$, $R_{\text{sigma}} = 0.0288$) which were used in all calculations. The final R_1 was 0.0440 ($I > 2\sigma(I)$) and wR_2 was 0.1215 (all data).

The aminophenyl group C(26)-C(31), N(9) / C(26A)-C(31A), N(9A) is disordered over two positions at refined percentage occupancy ratio of 69.5 (7) : 30.5 (7). The phenyl ring C(26A)-C(31A) is subject to a rigid body restraint.

The structure contains a molecule of butanone, disordered over two positions at a refined percentage occupancy ratio of 70.2 (7) : 29.8 (7). The hydrogen atoms bonded to N(2), N(5), N(6) and N(9) were located in the electron density and the positions were refined. The remaining hydrogen atoms were fixed as riding models and the isotropic thermal parameters (U_{iso}) of all hydrogen atoms were based on the U_{eq} of the parent atom.

1•DCM: $\text{C}_{32}\text{H}_{27}\text{Cl}_2\text{N}_9\text{O}_2$ ($M=640.52$ g/mol): orthorhombic, space group $\text{Pna}2_1$ (no. 33), $a = 22.019(10)$ Å, $b = 12.786(6)$ Å, $c = 10.554(4)$ Å, $V = 2971(2)$ Å³, $Z = 4$, $T = 99.94$ K, $\mu(\text{MoK}\alpha) = 0.267$ mm⁻¹, $D_{\text{calc}} = 1.432$ g/cm³, 21038 reflections measured ($5.004^\circ \leq 2\Theta \leq 56.582^\circ$), 6993 unique ($R_{\text{int}} = 0.1788$, $R_{\text{sigma}} = 0.2249$) which were used in all calculations. The final R_1 was 0.0788 ($I > 2\sigma(I)$) and wR_2 was 0.2322 (all data).

The structure contains a molecule of dichloromethane. The hydrogen atoms were fixed as riding models with the isotropic thermal parameters (U_{iso}) being based on the U_{eq} of the parent atom.

1•MeOH: $\text{C}_{32}\text{H}_{29}\text{N}_9\text{O}_3$ ($M=587.64$ g/mol): monoclinic, space group $\text{P}2_1/c$ (no. 14), $a = 20.5174(2)$ Å, $b = 10.26200(10)$ Å, $c = 26.9629(2)$ Å, $\beta = 91.1290(10)^\circ$, $V = 5675.92(9)$ Å³, $Z = 8$, $T = 100.15$ K, $\mu(?) = 0.088$ mm⁻¹, $D_{\text{calc}} = 1.375$ g/cm³, 67755 reflections measured ($2.928^\circ \leq 2\Theta \leq 49.676^\circ$), 10749 unique ($R_{\text{int}} = 0.0469$, $R_{\text{sigma}} = 0.0393$) which were used in all calculations. The final R_1 was 0.0495 ($I > 2\sigma(I)$) and wR_2 was 0.1468 (all data).

The structure contains two crystallographically-independent foldamers and one molecule of methanol per foldamer. The hydrogen atoms bonded to N(2), N(5), N(6), N(9), O(201) and O(301) were located in the electron density and the positions and isotropic thermal parameters were refined, subject to N-H and O-H distance restraints where necessary. The remaining hydrogen atoms were fixed as riding models with the isotropic thermal parameters (U_{iso}) being based on the U_{eq} of the parent atom.

1•DMSO: $\text{C}_{33}\text{H}_{31}\text{N}_9\text{O}_3\text{S}$ ($M = 633.73$ g/mol): monoclinic, space group $\text{P}2_1$ (no. 4), $a = 11.5089(5)$ Å, $b = 10.4369(4)$ Å, $c = 12.6459(5)$ Å, $\beta = 90.842(4)^\circ$, $V = 1518.83(11)$ Å³, $Z = 2$, $T = 100.00(10)$ K, $\mu(\text{Cu K}\alpha) = 1.373$ mm⁻¹, $D_{\text{calc}} = 1.386$ g/cm³, 23584 reflections measured ($6.99^\circ \leq 2\theta \leq 155.288^\circ$), 6284 unique ($R_{\text{int}} = 0.0442$, $R_{\text{sigma}} = 0.0350$) which were used in all calculations. The final R_1 was 0.0788 ($I > 2\sigma(I)$) and wR_2 was 0.2337 (all data).

The aminophenyl group C(26)-C(31), N(9) / C(26A)-C(31A), N(9A) is disordered over two positions at refined percentage occupancy ratio of 64.6 (10) : 35.4 (10).

The structure contains a molecule of DMSO, disordered over two positions at a refined percentage occupancy ratio of 63.0 (6) : 37.0 (6). The hydrogen atoms bonded to N(2), N(5) and N(6) were located in the electron density and the positions and isotropic thermal parameters were refined, subject to N-H distance restraints where necessary. The remaining hydrogen atoms were fixed as riding models with the isotropic thermal parameters (U_{iso}) being based on the U_{eq} of the parent atom.

CCDC 2426430 (**1A**), 2426870 (**1A'**), 2426871 (**1B**), 2426432 (**1•THF**), 2426872 (**1•Butanone**), 2426431 (**1•DCM**), 2426873 (**1•MeOH**) and 2426874 (**1•DMSO**) contain the supplementary crystallographic data for this paper. These data can be obtained free of charge from The Cambridge Crystallographic Data Centre via www.ccdc.cam.ac.uk/data_request/cif.

Crystal Data and Structural Refinement

a) 1A

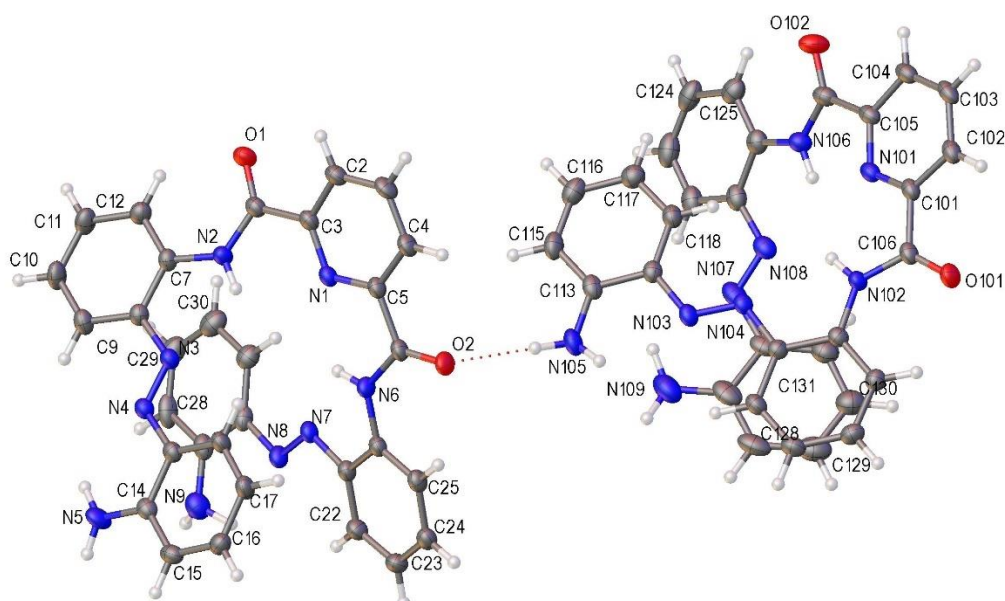


Table S1 Crystal data and structure refinement for **1A**

Identification code	1A
Empirical formula	$C_{31}H_{25}N_9O_2$
Formula weight	555.60
Temperature/K	103(6)
Crystal system	monoclinic
Space group	$P2_1/c$
$a/\text{\AA}$	11.56410(10)
$b/\text{\AA}$	38.6957(4)
$c/\text{\AA}$	12.34340(10)
$\alpha/^\circ$	90
$\beta/^\circ$	104.4570(10)
$\gamma/^\circ$	90
Volume/ \AA^3	5348.54(9)
Z	8
$\rho_{\text{calc}}/\text{g/cm}^3$	1.380
μ/mm^{-1}	0.743
F(000)	2320.0
Crystal size/ mm^3	0.313 × 0.217 × 0.168
Radiation	Cu $K\alpha$ ($\lambda = 1.54184$)
2 θ range for data collection/ $^\circ$	7.742 to 149.002
Index ranges	-14 ≤ h ≤ 11, -46 ≤ k ≤ 48, -15 ≤ l ≤ 15
Reflections collected	39445
Independent reflections	10243 [$R_{\text{int}} = 0.0287$, $R_{\text{sigma}} = 0.0246$]
Data/restraints/parameters	10243/2/805
Goodness-of-fit on F^2	1.108
Final R indexes [$I \geq 2\sigma(I)$]	$R_1 = 0.0469$, $wR_2 = 0.1200$
Final R indexes [all data]	$R_1 = 0.0555$, $wR_2 = 0.1369$
Largest diff. peak/hole / $e \text{\AA}^{-3}$	1.34/-0.45

b) 1A`

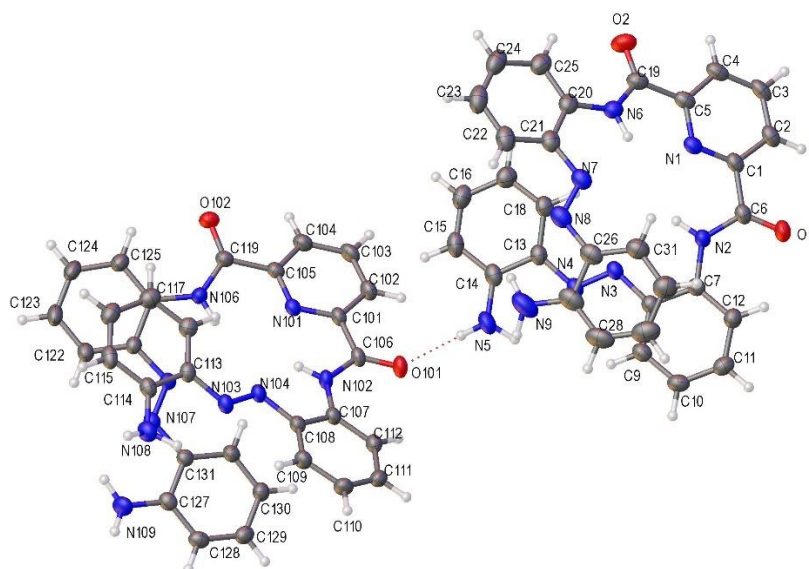


Table S2 Crystal data and structure refinement for 1A`

Identification code	1A`
Empirical formula	C₃₁H₂₅N₉O₂
Formula weight	555.60
Temperature/K	99.99(10)
Crystal system	monoclinic
Space group	P2₁/c
a/Å	11.57690(10)
b/Å	38.7107(2)
c/Å	12.34610(10)
α/°	90
β/°	104.7550(10)
γ/°	90
Volume/Å ³	5350.45(7)
Z	8
ρ _{calc} /cm ³	1.379
μ/mm ⁻¹	0.743
F(000)	2320.0
Crystal size/mm ³	0.148 × 0.078 × 0.074
Radiation	Cu Kα (λ = 1.54184)
2θ range for data collection/°	7.75 to 157.238
Index ranges	-14 ≤ h ≤ 14, -46 ≤ k ≤ 47, -14 ≤ l ≤ 15
Reflections collected	71800
Independent reflections	10856 [R_{int} = 0.0295, R_{sigma} = 0.0161]
Data/restraints/parameters	10856/4/805
Goodness-of-fit on F ²	1.037
Final R indexes [I ≥ 2σ (I)]	R₁ = 0.0376, wR₂ = 0.1001
Final R indexes [all data]	R₁ = 0.0415, wR₂ = 0.1024
Largest diff. peak/hole / e Å ⁻³	0.46/-0.19

c) 1B

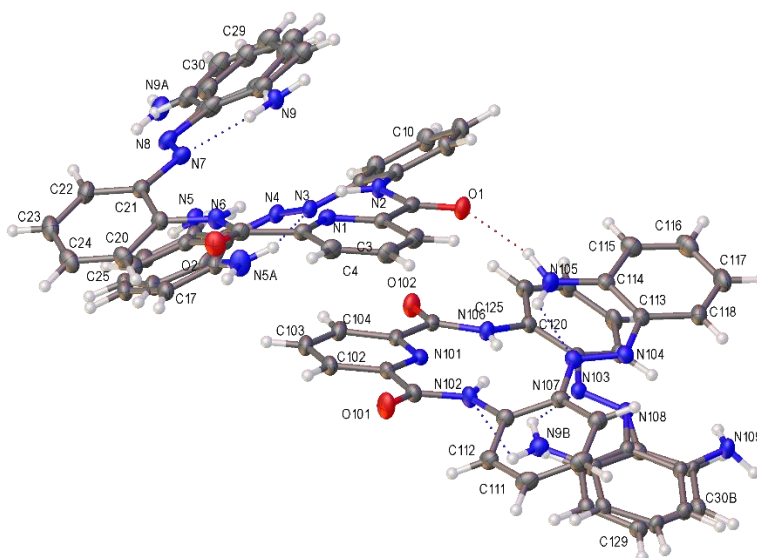


Table S3 Crystal data and structure refinement for **1B**

Identification code	1B
Empirical formula	C ₃₁ H ₂₅ N ₉ O ₂
Formula weight	555.60
Temperature/K	100.15
Crystal system	monoclinic
Space group	P2 ₁ /c
a/Å	17.58120(10)
b/Å	42.4637(2)
c/Å	7.06860(5)
α/°	90
β/°	95.5710(10)
γ/°	90
Volume/Å ³	5252.23(5)
Z	8
ρ _{calc} /cm ³	1.405
μ/mm ⁻¹	0.088
F(000)	2320.0
Crystal size/mm ³	0.15 × 0.012 × 0.0097
Radiation	Synchrotron (λ = 0.6889)
2θ range for data collection/°	2.256 to 72.228
Index ranges	-30 ≤ h ≤ 29, -71 ≤ k ≤ 69, -11 ≤ l ≤ 11
Reflections collected	115588
Independent reflections	25728 [R _{int} = 0.0610, R _{sigma} = 0.0791]
Data/restraints/parameters	25728/1687/997
Goodness-of-fit on F ²	1.029
Final R indexes [I ≥ 2σ (I)]	R ₁ = 0.0580, wR ₂ = 0.1483
Final R indexes [all data]	R ₁ = 0.1041, wR ₂ = 0.1615
Largest diff. peak/hole / e Å ⁻³	0.53/-0.44

d) 1·THF

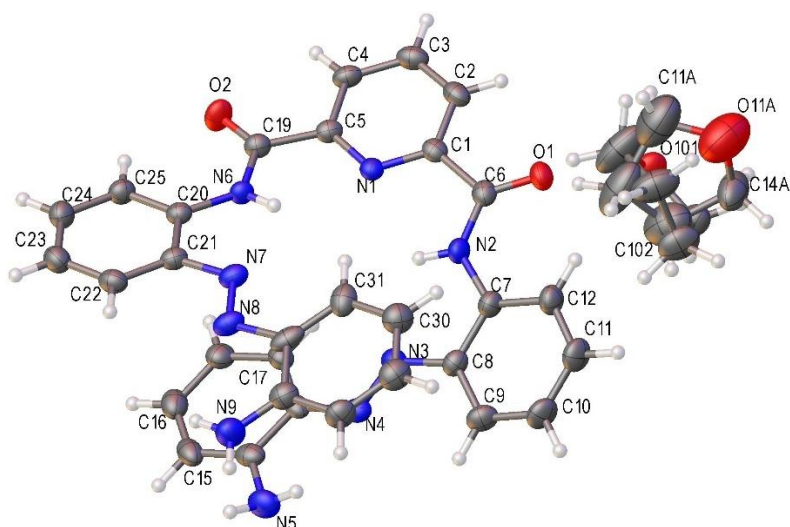


Table S4 Crystal data and structure refinement for 1·THF

Identification code	1·THF
Empirical formula	C ₃₅ H ₃₃ N ₉ O ₃
Formula weight	627.70
Temperature/K	100.00(10)
Crystal system	monoclinic
Space group	P2 ₁
a/Å	11.5123(5)
b/Å	10.4201(5)
c/Å	12.7453(5)
α/°	90
β/°	92.318(4)
γ/°	90
Volume/Å ³	1527.67(12)
Z	2
ρ _{calc} /cm ³	1.365
μ/mm ⁻¹	0.738
F(000)	660.0
Crystal size/mm ³	0.305 × 0.101 × 0.083
Radiation	CuKα (λ = 1.54184)
2θ range for data collection/°	7.686 to 136.456
Index ranges	-12 ≤ h ≤ 13, -12 ≤ k ≤ 9, -15 ≤ l ≤ 13
Reflections collected	24759
Independent reflections	4334 [R _{int} = 0.0283, R _{sigma} = 0.0263]
Data/restraints/parameters	4334/137/477
Goodness-of-fit on F ²	1.055
Final R indexes [I ≥ 2σ (I)]	R ₁ = 0.0448, wR ₂ = 0.1112
Final R indexes [all data]	R ₁ = 0.0505, wR ₂ = 0.1161
Largest diff. peak/hole / e Å ⁻³	0.46/-0.24
Flack parameter	0.12(7)

e) **1•butanone**

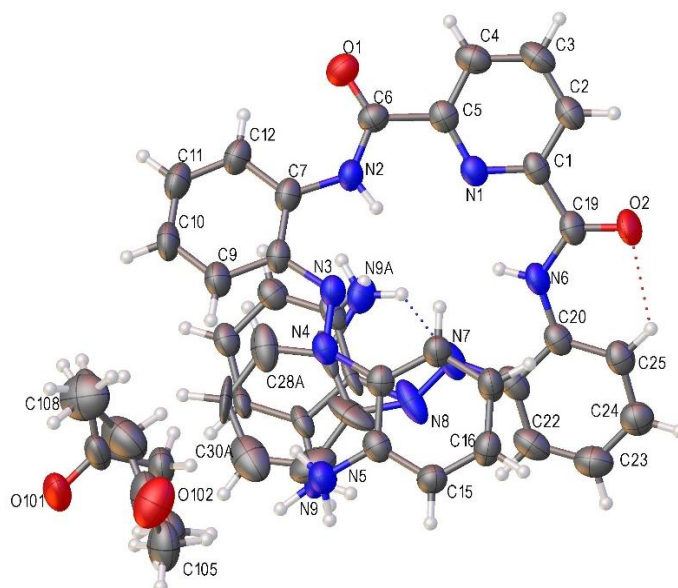


Table S5 Crystal data and structure refinement for 1•butanone

Identification code	1•butanone
Empirical formula	C ₃₅ H ₃₃ N ₉ O ₃
Formula weight	627.70
Temperature/K	99.99(16)
Crystal system	monoclinic
Space group	P2 ₁
a/Å	11.7137(2)
b/Å	10.3944(2)
c/Å	12.6481(2)
α/°	90
β/°	93.4610(10)
γ/°	90
Volume/Å ³	1537.18(5)
Z	2
ρ _{calc} /cm ³	1.356
μ/mm ⁻¹	0.733
F(000)	660.0
Crystal size/mm ³	0.43 × 0.12 × 0.03
Radiation	Cu Kα (λ = 1.54184)
2θ range for data collection/°	7.002 to 140.142
Index ranges	-14 ≤ h ≤ 14, -10 ≤ k ≤ 12, -15 ≤ l ≤ 14
Reflections collected	28058
Independent reflections	5534 [R _{int} = 0.0390, R _{sigma} = 0.0288]
Data/restraints/parameters	5534/127/544
Goodness-of-fit on F ²	1.054
Final R indexes [I ≥ 2σ(I)]	R ₁ = 0.0440, wR ₂ = 0.1189
Final R indexes [all data]	R ₁ = 0.0475, wR ₂ = 0.1217
Largest diff. peak/hole / e Å ⁻³	0.31/-0.29
Flack parameter	-0.03(11)

f) **1·DCM**

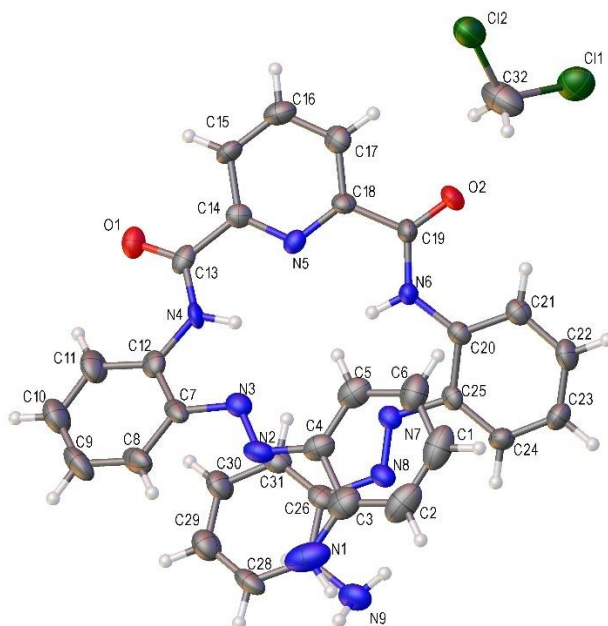


Table S6 Crystal data and structure refinement for **1·DCM**

Identification code	1·DCM
Empirical formula	$C_{32}H_{27}Cl_2N_9O_2$
Formula weight	640.52
Temperature/K	99.94
Crystal system	orthorhombic
Space group	$Pna2_1$
$a/\text{\AA}$	22.019(10)
$b/\text{\AA}$	12.786(6)
$c/\text{\AA}$	10.554(4)
$\alpha/^\circ$	90
$\beta/^\circ$	90
$\gamma/^\circ$	90
Volume/ \AA^3	2971(2)
Z	4
$\rho_{\text{calc}}/\text{cm}^3$	1.432
μ/mm^{-1}	0.267
F(000)	1328.0
Crystal size/ mm^3	$0.53 \times 0.097 \times 0.04$
Radiation	$\text{MoK}\alpha$ ($\lambda = 0.71073$)
2θ range for data collection/ $^\circ$	5.004 to 56.582
Index ranges	$-28 \leq h \leq 29, -13 \leq k \leq 16, -13 \leq l \leq 13$
Reflections collected	21038
Independent reflections	6993 [$R_{\text{int}} = 0.1788, R_{\text{sigma}} = 0.2249$]
Data/restraints/parameters	6993/1/408
Goodness-of-fit on F^2	0.931
Final R indexes [$I \geq 2\sigma(I)$]	$R_1 = 0.0788, wR_2 = 0.1666$
Final R indexes [all data]	$R_1 = 0.2424, wR_2 = 0.2322$
Largest diff. peak/hole / $e \text{\AA}^{-3}$	0.35/-0.47
Flack parameter	0.09(9)

g) 1·MeOH

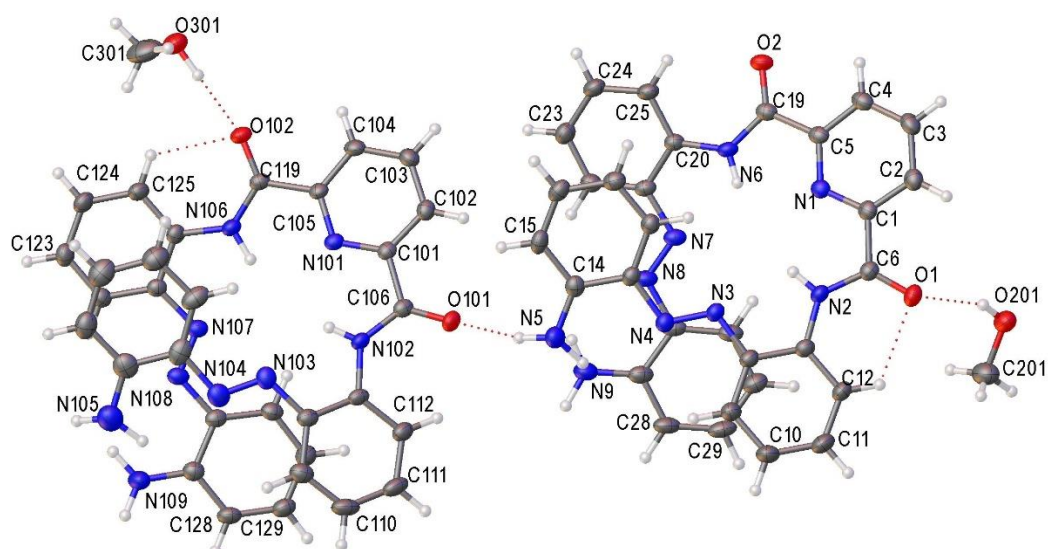


Table S7 Crystal data and structure refinement for 1·MeOH

Identification code	1·MeOH
Empirical formula	C ₃₂ H ₂₉ N ₉ O ₃
Formula weight	587.64
Temperature/K	100.15
Crystal system	monoclinic
Space group	P2 ₁ /c
a/Å	20.5174(2)
b/Å	10.26200(10)
c/Å	26.9629(2)
α/°	90
β/°	91.1290(10)
γ/°	90
Volume/Å ³	5675.92(9)
Z	8
ρ _{calc} /cm ³	1.375
μ/mm ⁻¹	0.088
F(000)	2464.0
Crystal size/mm ³	0.078 × 0.022 × 0.01
Radiation	? (λ = 0.6889)
2θ range for data collection/°	2.928 to 49.676
Index ranges	-25 ≤ h ≤ 25, -12 ≤ k ≤ 12, -32 ≤ l ≤ 32
Reflections collected	67755
Independent reflections	10749 [R _{int} = 0.0469, R _{sigma} = 0.0393]
Data/restraints/parameters	10749/3/849
Goodness-of-fit on F ²	1.051
Final R indexes [I ≥ 2σ (I)]	R ₁ = 0.0495, wR ₂ = 0.1391
Final R indexes [all data]	R ₁ = 0.0659, wR ₂ = 0.1468
Largest diff. peak/hole / e Å ⁻³	0.54/-0.39

h) 1·DMSO

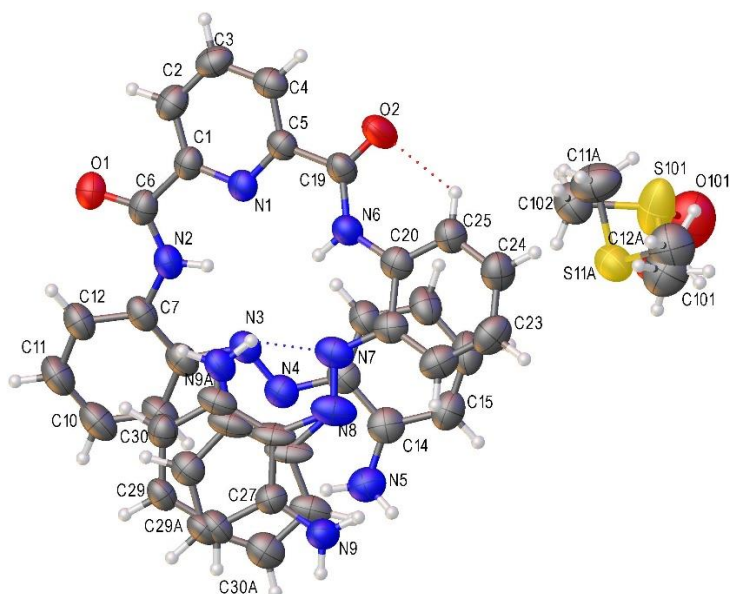


Table S8 Crystal data and structure refinement for 1·DMSO

Identification code	1·DMSO
Empirical formula	C₃₃H₃₁N₉O₃S
Formula weight	633.73
Temperature/K	100.00(10)
Crystal system	monoclinic
Space group	P2 ₁
a/Å	11.5089(5)
b/Å	10.4369(4)
c/Å	12.6459(5)
α/°	90
β/°	90.842(4)
γ/°	90
Volume/Å ³	1518.83(11)
Z	2
ρ _{calc} /cm ³	1.386
μ/mm ⁻¹	1.373
F(000)	664.0
Crystal size/mm ³	0.24 × 0.104 × 0.058
Radiation	Cu Kα (λ = 1.54184)
2θ range for data collection/°	6.99 to 155.288
Index ranges	-14 ≤ h ≤ 14, -13 ≤ k ≤ 13, -15 ≤ l ≤ 12
Reflections collected	23584
Independent reflections	6284 [R _{int} = 0.0442, R _{sigma} = 0.0350]
Data/restraints/parameters	6284/363/532
Goodness-of-fit on F ²	1.040
Final R indexes [I ≥ 2σ (I)]	R ₁ = 0.0788, wR ₂ = 0.2116
Final R indexes [all data]	R ₁ = 0.0938, wR ₂ = 0.2337
Largest diff. peak/hole / e Å ⁻³	0.60/-0.67
Flack parameter	0.00(2)

Crystallisation Solvents and Conditions for 1 Screened in This Study

Crystallisation Solvent(s)	Crystallisation Technique	Single Crystals Suitable for X-ray Diffraction Analysis Obtained
Chloroform	Slow evaporation	Yes
Anisole	Slow evaporation	No
Trifluorotoluene/dichloromethane	Slow evaporation	Yes
Tetrahydrofuran	Vapour diffusion with Et ₂ O	Yes
Butanone	Slow evaporation	Yes
Dichloromethane	Vapour diffusion with Et ₂ O	Yes
Methanol	Slow evaporation	Yes
Dimethylsulfoxide	Saturated solution ^a	Yes
Acetone	Vapour diffusion with Et ₂ O	No
Ethanol	Slow evaporation	No
Ethanol	Vapour diffusion with Et ₂ O	No
1,4-dioxane	Vapour diffusion with Et ₂ O	No
Pyridine	Slow evaporation	No
Pyridine	Vapour diffusion with Et ₂ O	No
Dimethylformamide	Vapour diffusion with Et ₂ O	No
Ethyl Acetate	Slow evaporation	No
Ethyl Acetate	Vapour diffusion with Et ₂ O	No
Toluene	Slow evaporation	No
Toluene	Vapour diffusion with Et ₂ O	No
Acetonitrile	Slow evaporation	No
Acetonitrile	Vapour diffusion with Et ₂ O	No
Xylene	Slow evaporation	No
Xylene	Vapour diffusion with Et ₂ O	No
Xylene	Vapour diffusion with ⁱ Pr ₂ O	No
2-Decanone	Slow evaporation	No
2-Decanone	Vapour diffusion with Et ₂ O	No
2-Decanone	Vapour diffusion with ⁱ Pr ₂ O	No
2-Hexanone	Slow evaporation	No
2-Hexanone	Vapour diffusion with Et ₂ O	No
2-Hexanone	Vapour diffusion with ⁱ Pr ₂ O	No
3-Hexanone	Slow evaporation	No
3-Hexanone	Vapour diffusion with Et ₂ O	No
3-Hexanone	Vapour diffusion with ⁱ Pr ₂ O	No
2-ethoxyethanol	Slow evaporation	No
2-ethoxyethanol	Vapour diffusion with Et ₂ O	No
2-ethoxyethanol	Vapour diffusion with ⁱ Pr ₂ O	No

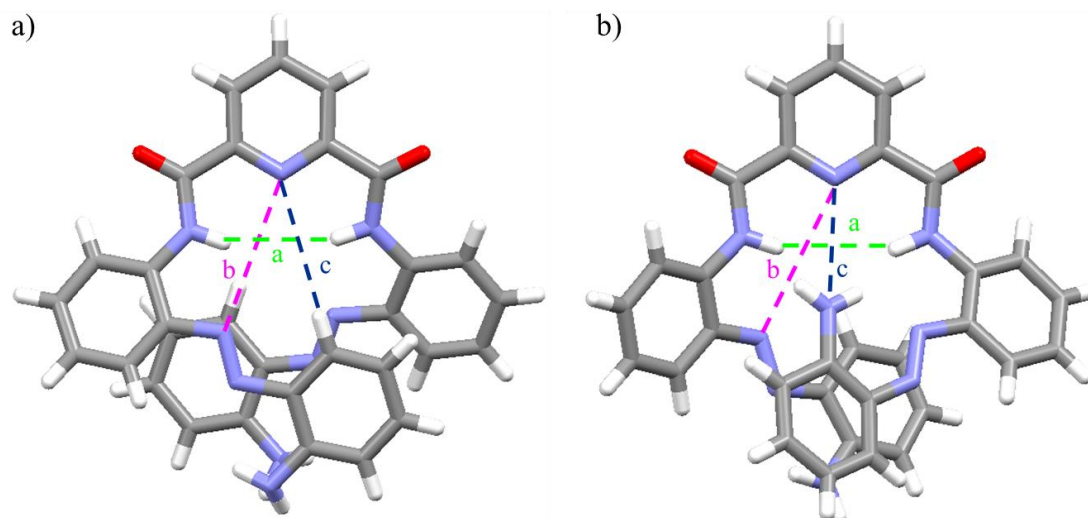
Table S9. Summary of the crystallisation solvents and conditions for **1** screened in this study. ^aSingle crystals suitable for X-ray crystallographic analysis were grown at ambient temperature in a saturated solution of **1** in DMSO over 12 weeks.

Helical Pitch Values of Studied Structures

<i>Compound</i>	<i>Crystallisation Solvent</i>	<i>Helical Pitch (Å)</i>
1A	Chloroform	3.5 and 4.3
1A'	Trifluorotoluene/dichloromethane	3.5 and 4.3
1B	Dimethylformamide	3.6 and 3.6 / 3.3 and 3.9*
1·THF	Tetrahydrofuran	3.4
1·butanone	Butanone	3.4
1·DCM	Dichloromethane	3.3
1·MeOH	Methanol	3.3
1·DMSO	Dimethylsulfoxide	3.3

Table S10. Summary of solid state analysis showing the helical pitch of the foldamers in the solid state structures of **1** and its five solvatomorphs. *Helical pitch measurement of minor disorder component.

Cavity Values of Studied Structures

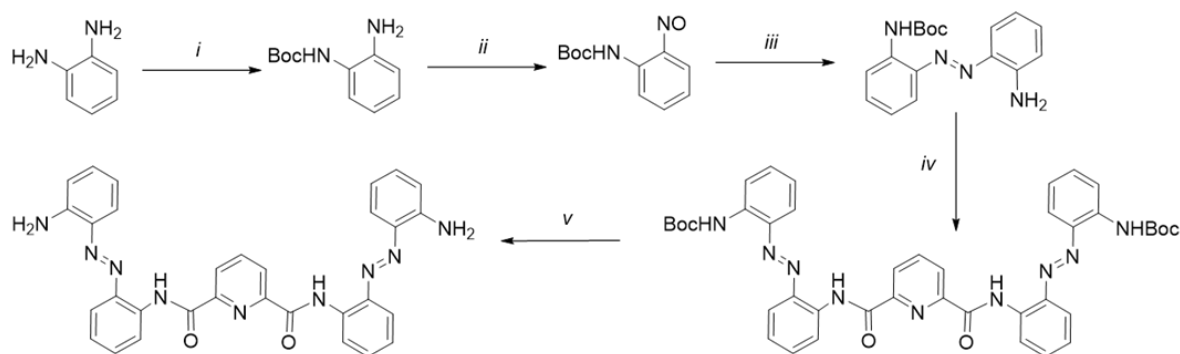


Scheme 1. Distances measured in table below, where represents a) molecules which possess aniline moieties facing out of the helix and b) molecules which possess positional disorder in the aniline moiety where the amine faces into the helix.

Structure	<i>a</i> (Å)	<i>b</i> (Å)	<i>c</i> (Å)
1A (I)	3.00(3)	4.161(2) / 4.173(2)	3.7592(16) / 3.6582(16)
1A (II)	3.04(4)	4.133(2) / 4.212(2)	4.2979(15) / 3.7028(15)
1A` (I)	2.98(3)	4.2129(16) / 4.1290(17)	3.6742(11) / 4.2820(11)
1`A (II)	3.02(2)	4.1542(15) / 4.1729(16)	3.7211(11) / 3.6381(12)
1B-a (I)	2.94(2)	4.3833(12) / 4.3483(13)	3.8550(9) / 3.8268(15) ^a
1B-b (I)	3.01(2)	4.3323(12) / 4.2829(13)	3.6731(12) ^a / 3.8290(9)
1B-a (II)	2.94(2)	4.3833(12) / 4.3483(13)	3.790(11) ^a / 3.9088(9)
1B-b (II)	3.01(2)	4.3323(12) / 4.2829(13)	3.6731(12) ^a / 3.621(15) ^a
1•THF	3.16(6)	4.091(4) / 4.311(4)	3.467(3) / 3.941(3)
1•Butanone-a	3.12(6)	4.163(3) / 4.313(4)	3.573(3) / 3.826(3)
1•Butanone-b	3.12(6)	4.163(3) / 4.313(4)	3.573(3) / 4.115(12) ^a
1•DCM	2.9800(11)	4.190(11) / 4.308(11)	3.802(7) / 4.030(7)
1•MeOH (I)	3.10(4)	4.133(2) A / 4.223(2)	3.6851(16) / 3.9241(16)
1•MeOH (II)	3.06(4)	4.225(2) / 4.040(3)	3.9691(16) / 3.5271(16)
1•DMSO-a	3.14(9)	4.109(7) / 4.381(7)	3.475(5) / 3.940(5)
1•DMSO-b	3.14(9)	4.109(7) / 4.381(7)	3.475(5) / 4.096(15) ^a

Table S11. Solid state analysis of contact distances a, b, and c (as seen above in graphic) for each of the studied foldamers. ^aDistance measured using the nitrogen of the flipped NH₂.

Synthetic Scheme to Access Foldamer 1



Scheme 2. i) (Boc)₂O, THF, rt, 16 h, 48%, ii) oxone, CH₂Cl₂/H₂O, rt, 1 h, 46%; iii) *o*-phenylenediamine, toluene, acetic acid, 60 °C, 18 h, 78%; iv) 2,6-pyridinedicarbonyl dichloride, pyridine, CH₂Cl₂, 4 Å MS, 48 h, 65%; v) trifluoroacetic acid, CH₂Cl₂, 0 °C → rt, 16 h, 98%.

Solid-State Analysis

a) Solid State Analysis of 1A

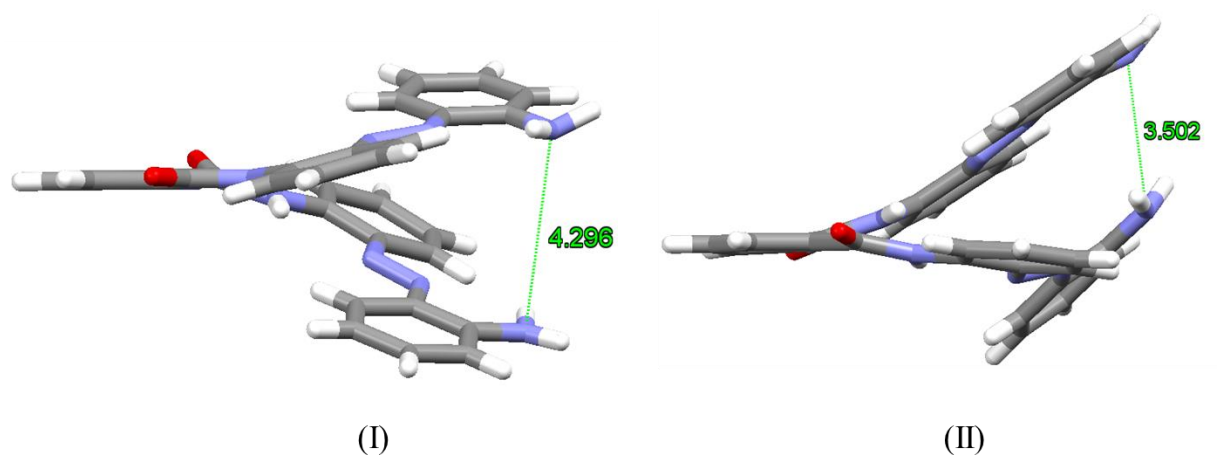


Figure S1. Solid state analysis of the two crystallographically unique molecules the unit cell of **1A**, showing helical pitch (distance between N atoms at each terminus).

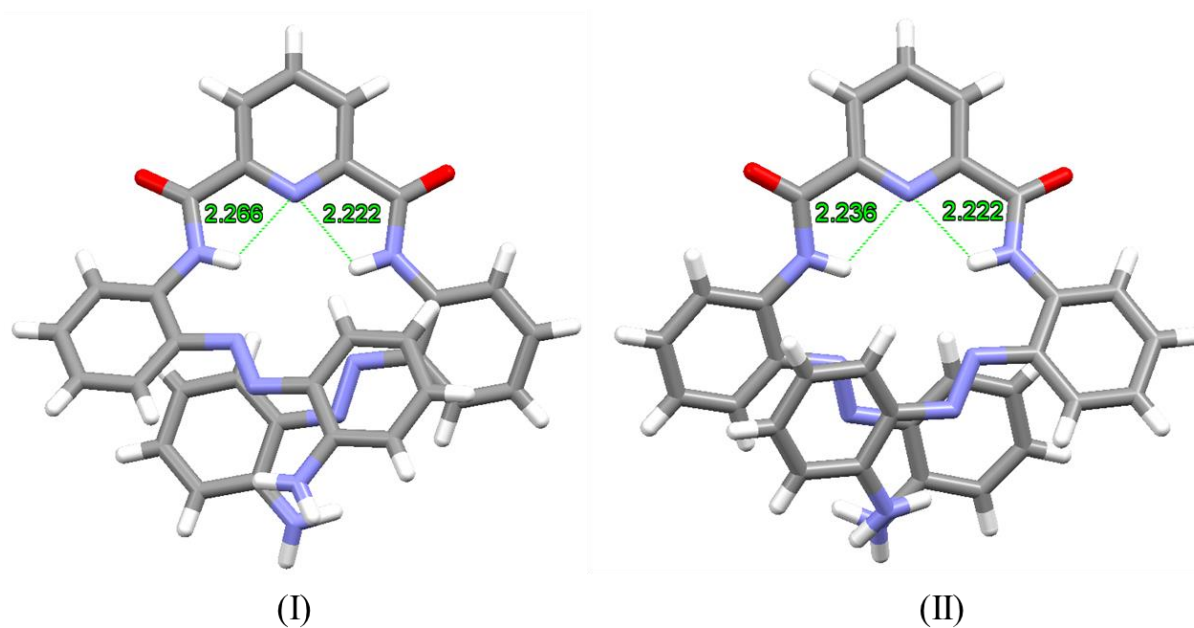


Figure S2. Solid state analysis of the two crystallographically unique molecules of **1A** in the unit cell, highlighting the presence of bifurcated¹⁴ intramolecular N-H...N hydrogen bonding interactions¹⁴ involving the N atom of the pyridine and the two NH's of the adjacent amide bonds leading to the *syn-syn* conformation about the central pyridinecarboxamide unit.¹⁵

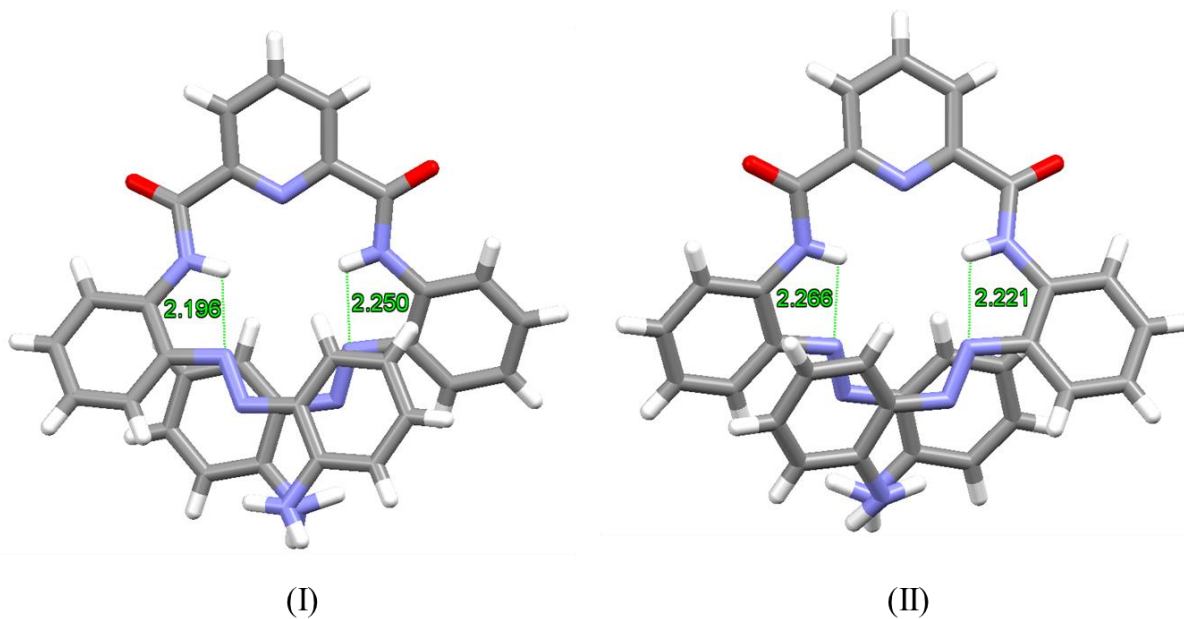


Figure S3. Solid state analysis of the two crystallographically unique molecules (**I** on left and **II** on the right) in the unit cell of **1A**, highlighting the close contacts between the pyridyl amide NHs and the adjacent azo N atoms.¹⁶

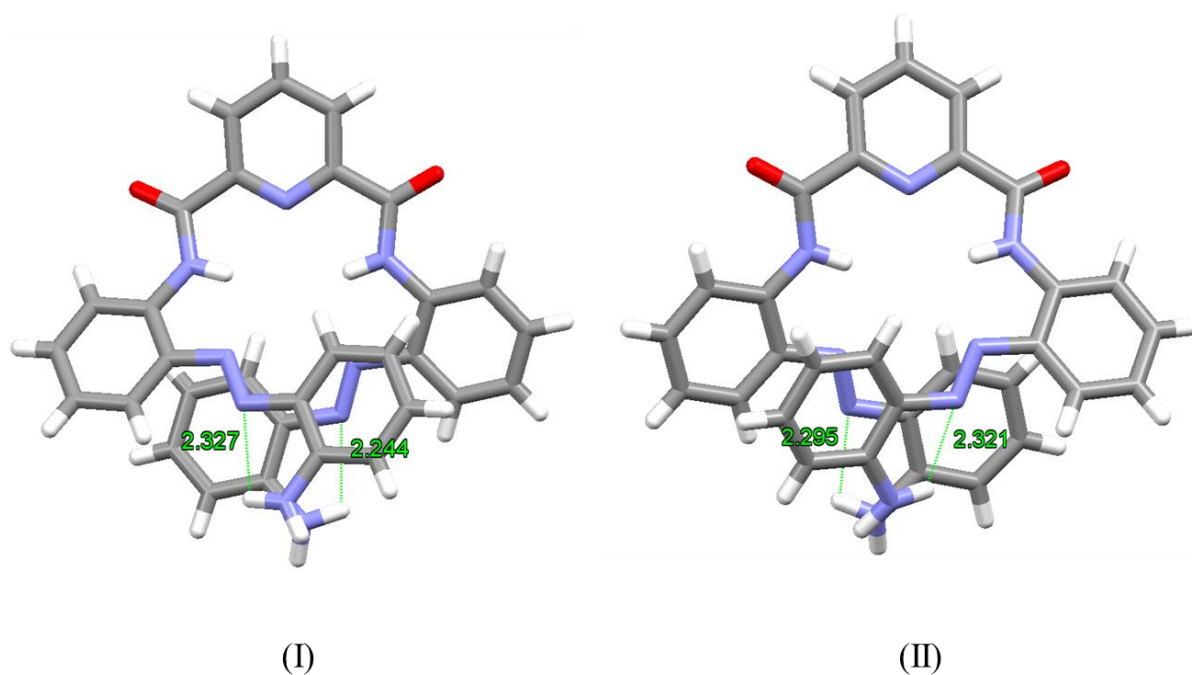


Figure S4. Solid state analysis of the two crystallographically unique molecules in the unit cell of **1A**, highlighting the close contacts between the terminal acetyl amide and the adjacent azo N atoms.¹⁶

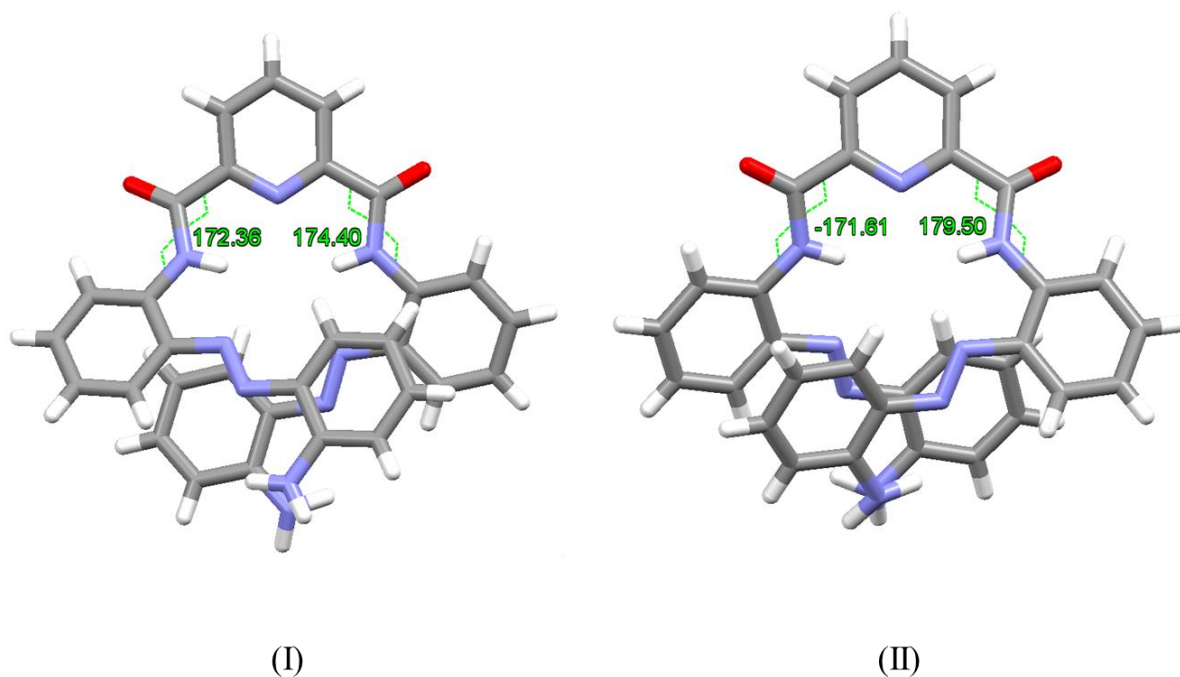


Figure S5. Solid state analysis of the two crystallographically unique molecules one molecule in the unit cell of **1A**, highlighting the torsion angles of the internal peptide bonds.

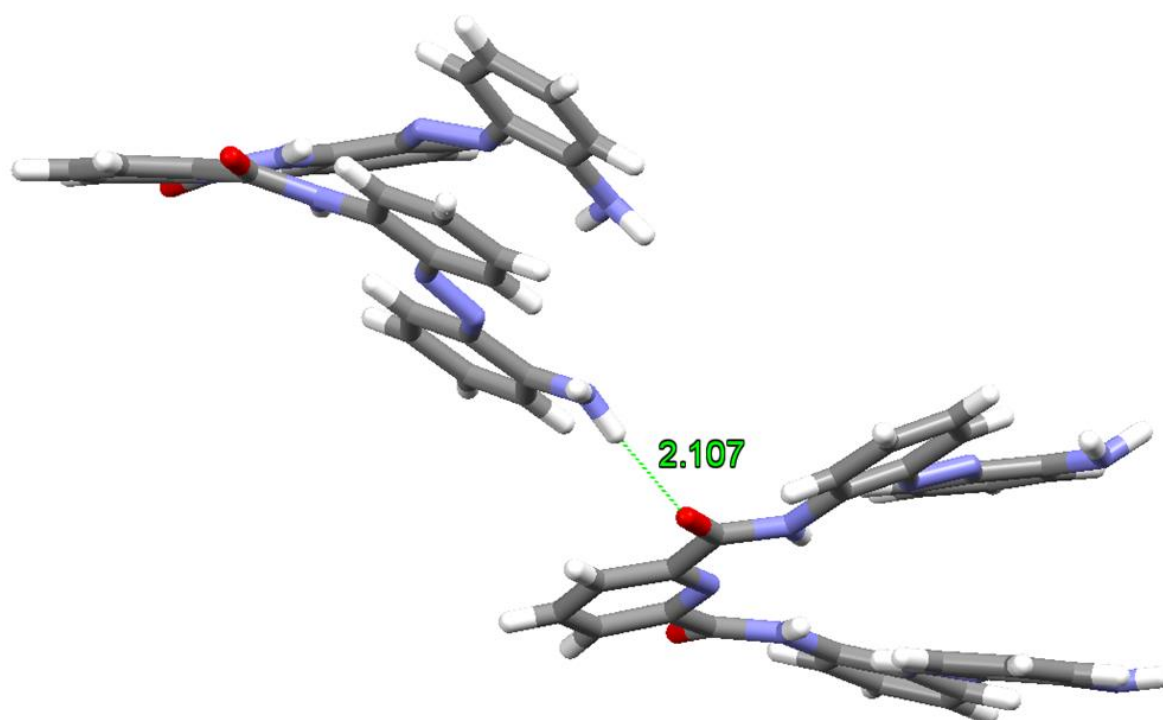


Figure S6. Solid state analysis of **1A** highlighting the presence of intermolecular N-H...O hydrogen-bonding interactions¹⁷ between an NH of a terminal amine functionality on the foldamer molecule **1A(II)** and the O atom of a carbonyl group in the carboxamide unit of an adjacent foldamer molecule **1A(I)**.

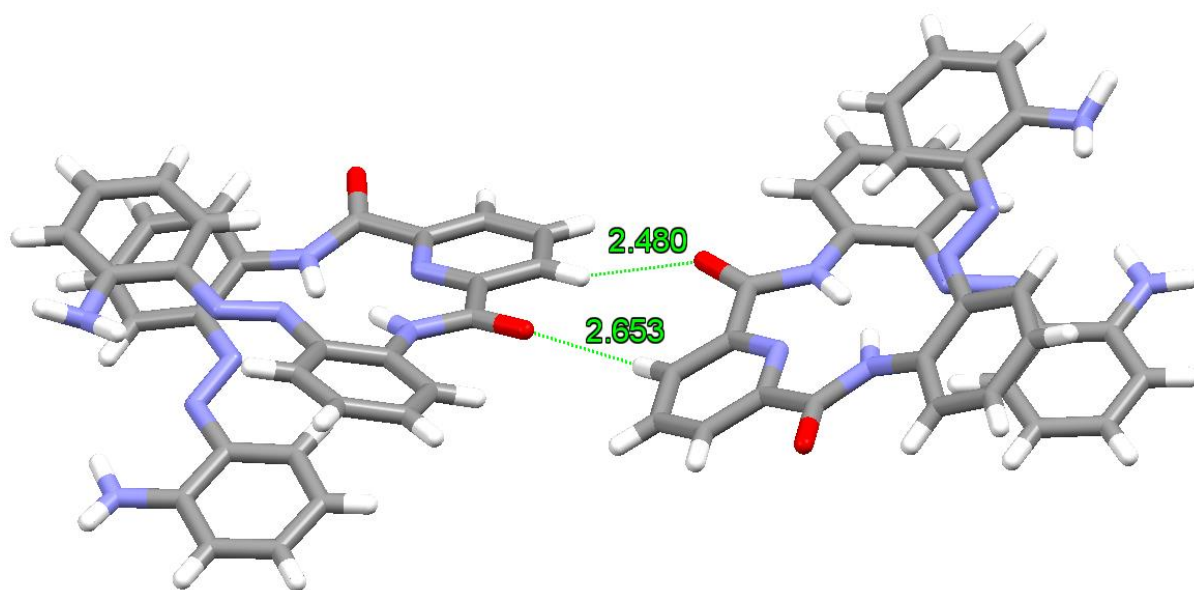


Figure S7. Solid state analysis of **1A** highlighting the presence of intermolecular reciprocal C-H...O hydrogen-bonding interactions¹⁷ between aromatic protons on the pyridine ring of one foldamer molecule **I** and the O atoms of a carbonyl group in the carboxamide unit of an adjacent foldamer molecule **I**.

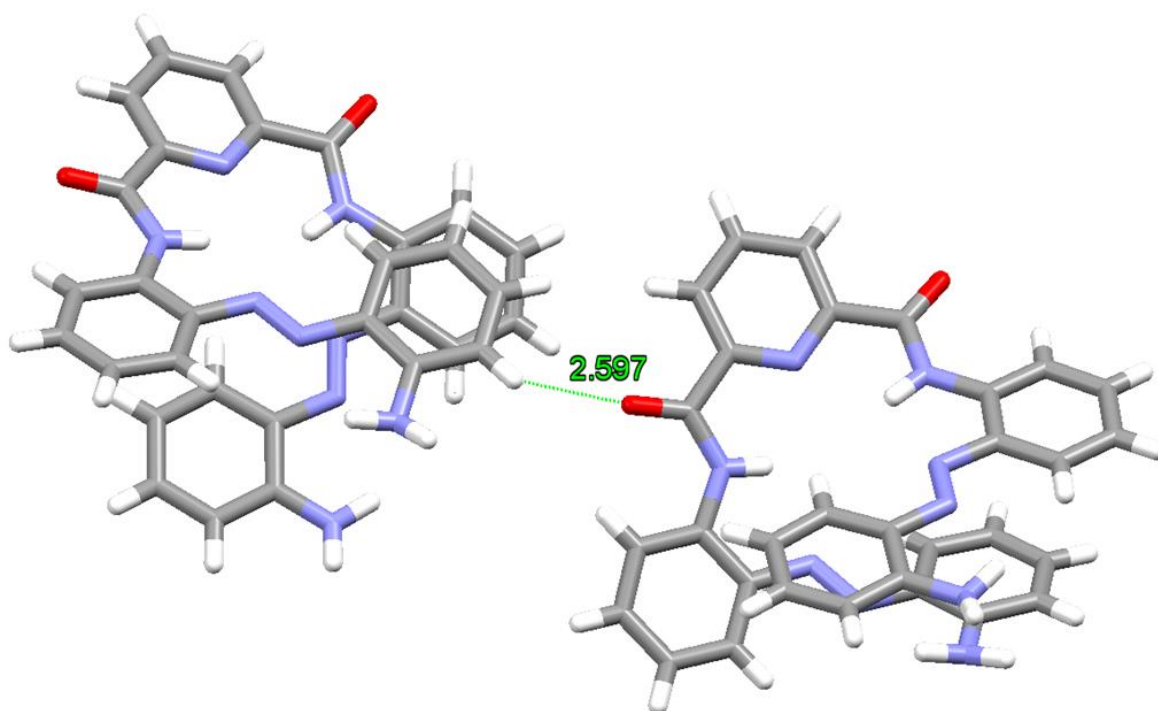


Figure S8. Solid state analysis of **1A** highlighting the presence of intermolecular C-H...O hydrogen-bonding interactions¹⁷ between aromatic proton on the aniline ring of one foldamer molecule **1A(I)** and the O atom of a carbonyl group in the carboxamide unit of an adjacent foldamer molecule **1A(I)**.

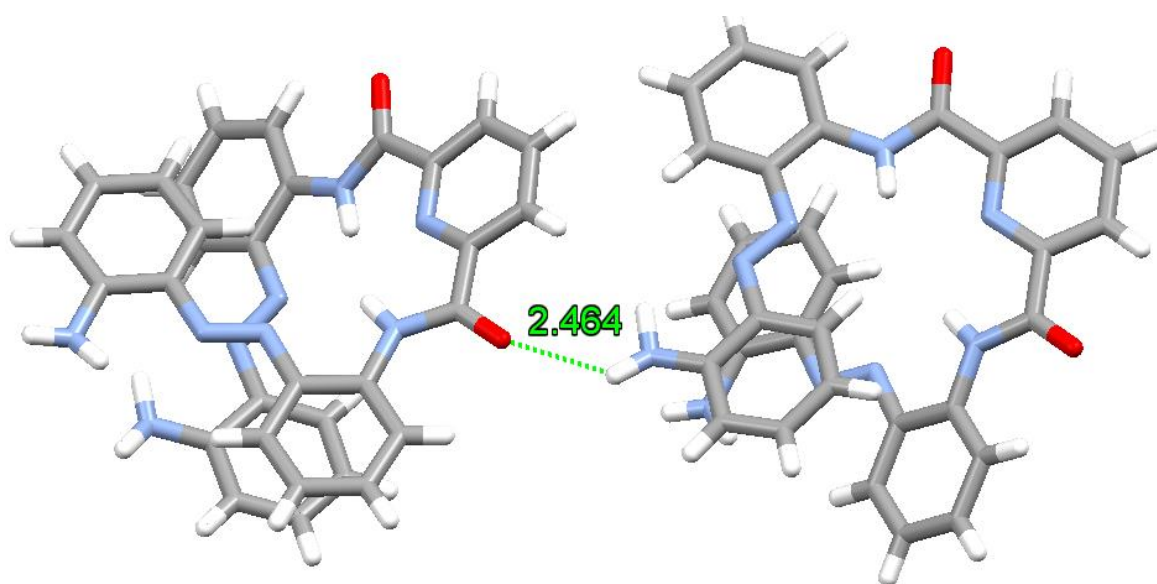


Figure S9. Solid state analysis of **1A** highlighting the presence of intermolecular N-H...O hydrogen-bonding interactions¹⁷ between an NH atom of a terminal amine functionality on one foldamer molecule of **1A(I)** and the O atom of a carbonyl group in the carboxamide unit of an adjacent foldamer molecule of **1A(II)**.

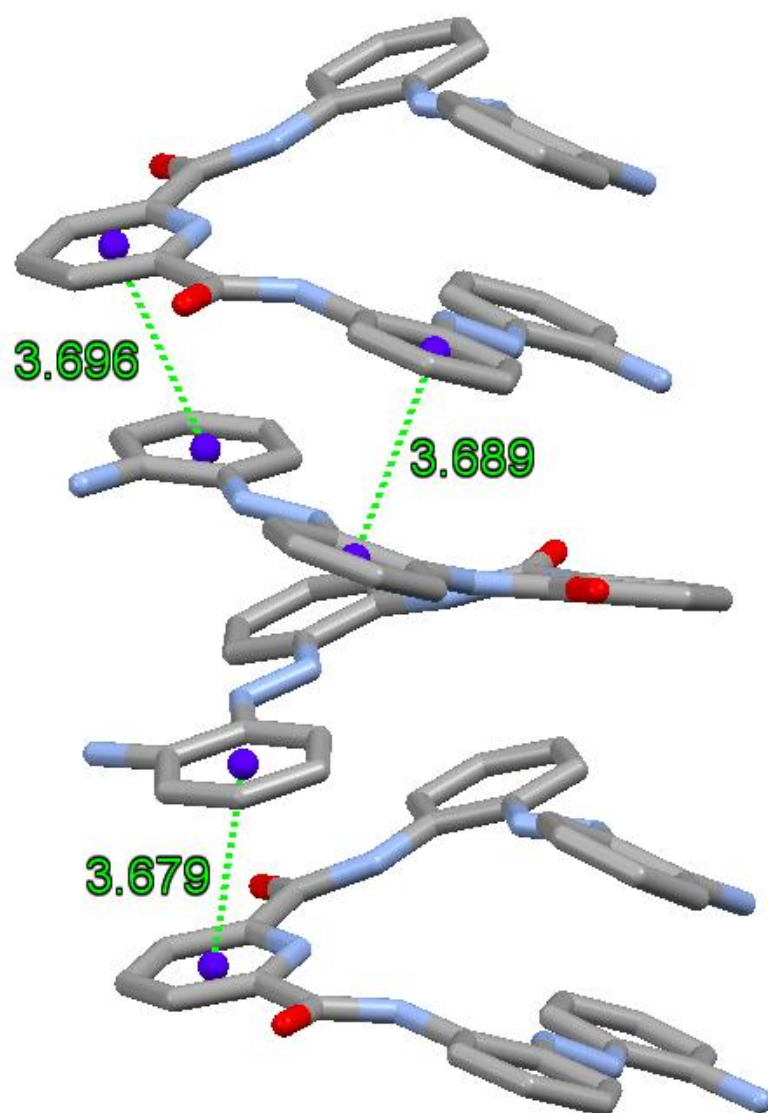


Figure S10. Solid state analysis of the offset face-to-face π - π stacking interactions¹⁸ observed between molecules of **1A**, stacking in a II-I-II manner. Hydrogen atoms have been removed for clarity.

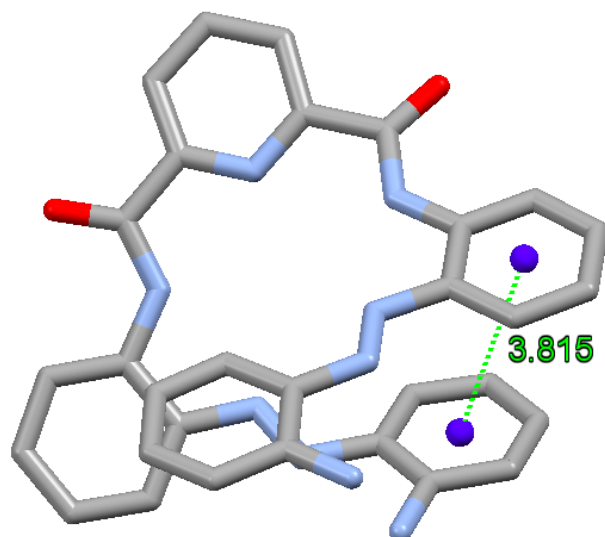


Figure S11. Solid state analysis of the intramolecular offset face-to-face π - π stacking interaction¹⁸ within crystallographically unique foldamer II in the unit cell of **1A**.

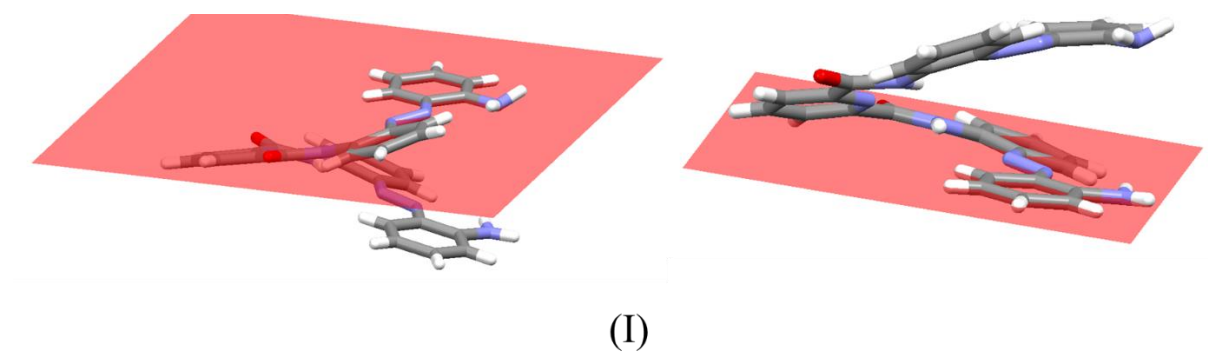


Figure S12. Solid state analysis of crystallographically unique molecule I in the unit cell of **1A**, highlighting the plane of one of the terminal aniline groups.

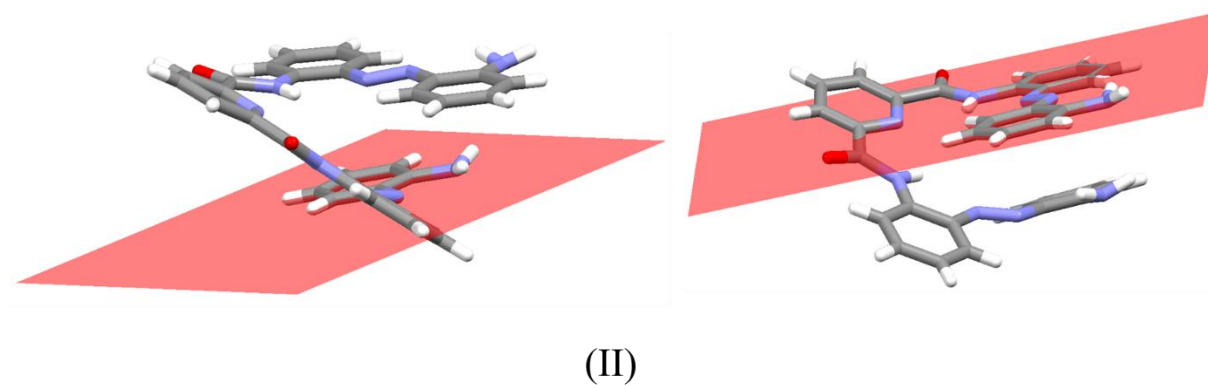


Figure S13. Solid state analysis of crystallographically unique molecule I in the unit cell of **1A**, highlighting the plane of one of the terminal aniline groups.

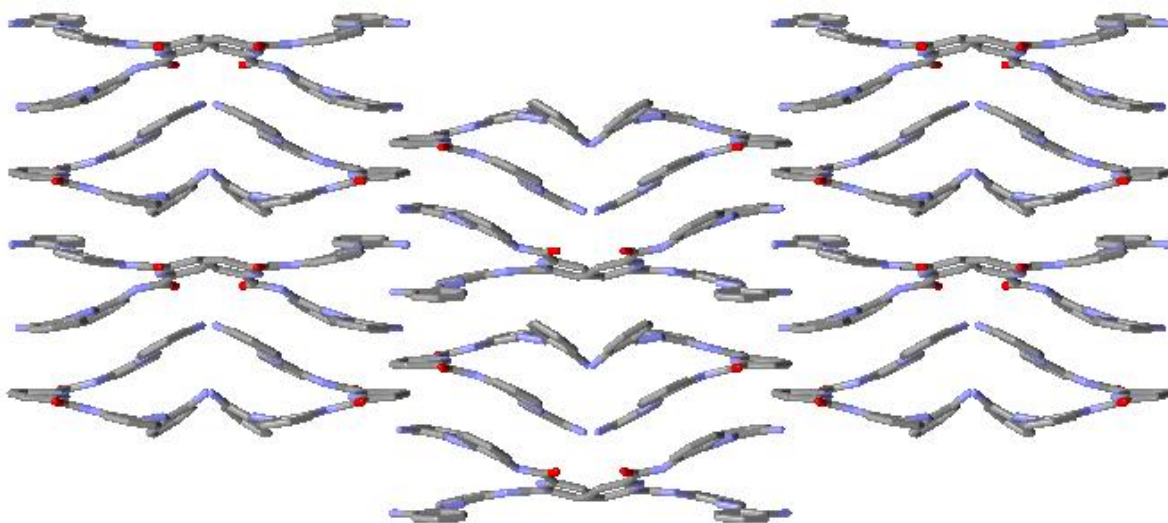


Figure S14. Solid state analysis showing the crystal packing of **1A** as viewed along the *c* axis. H atoms have been removed for clarity.

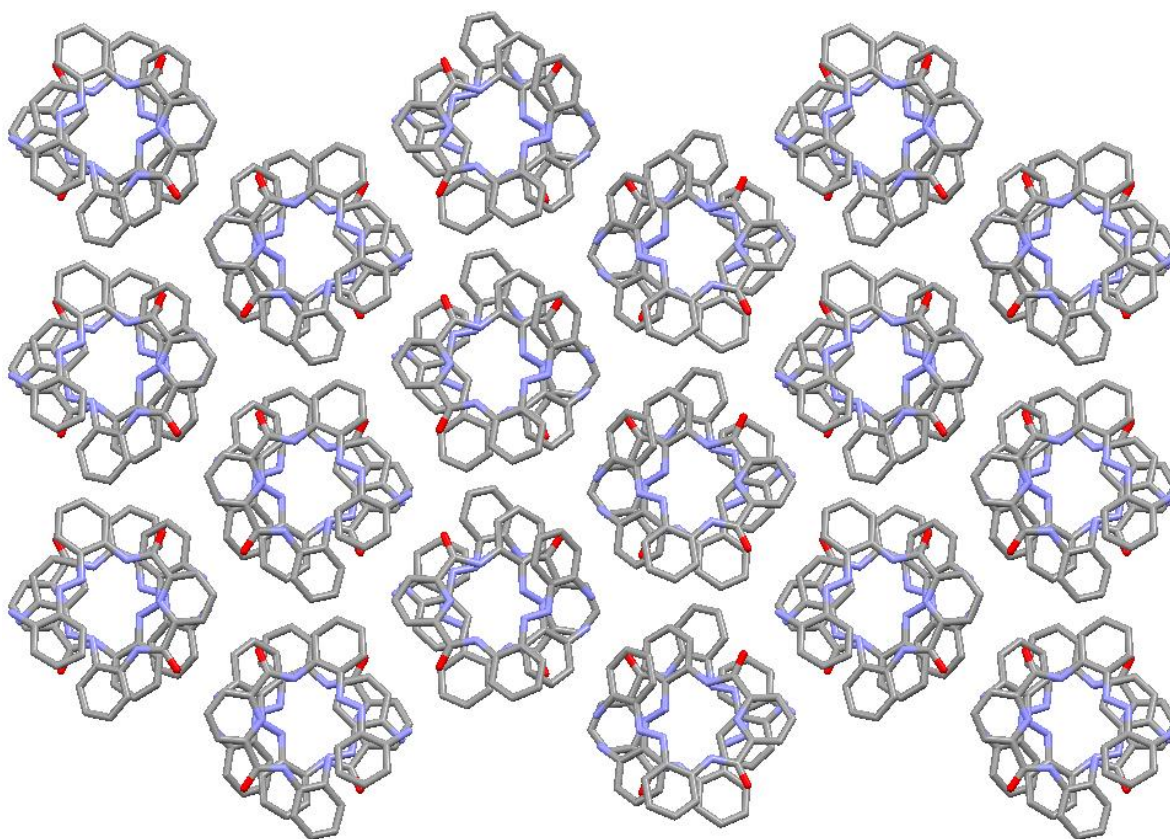


Figure S15. Solid state analysis showing the crystal packing of **1A** as viewed along the *a* axis. H atoms have been removed for clarity.

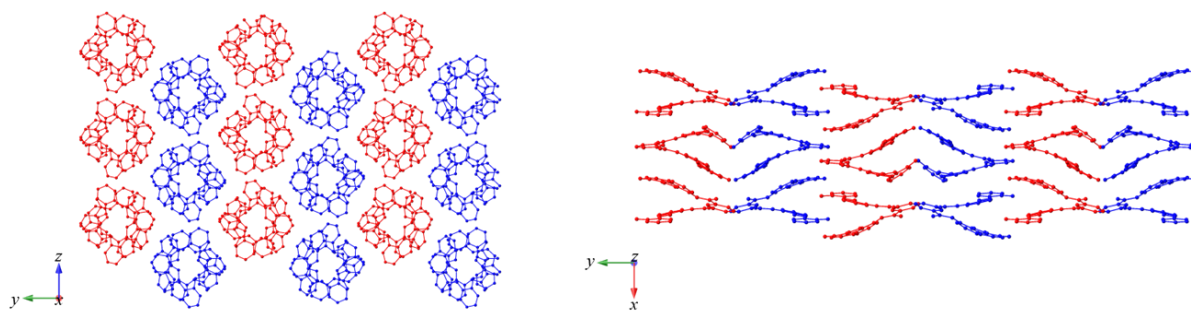


Figure S16. Solid state analysis showing the crystal packing of **1A** showing columns of like-handed stacks, which alternate handedness between columns. Hydrogen atoms have been removed for clarity, molecules have been coloured in accordance with handedness, where red represents left (M), and blue represents right (P).

b) Solid State Analysis of **1A**

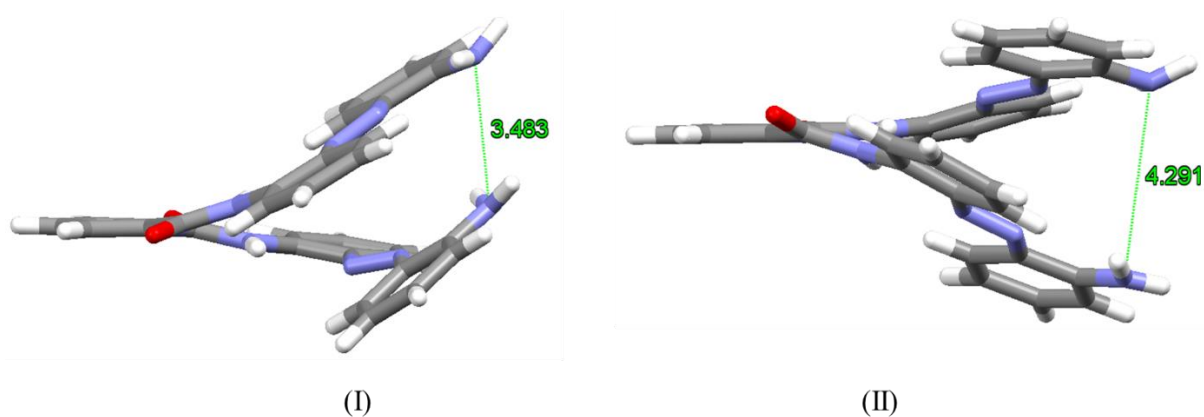


Figure S17. Solid state analysis of the two crystallographically unique in the unit cell of **1A**, showing helical pitch (distance between N atoms at each terminus).

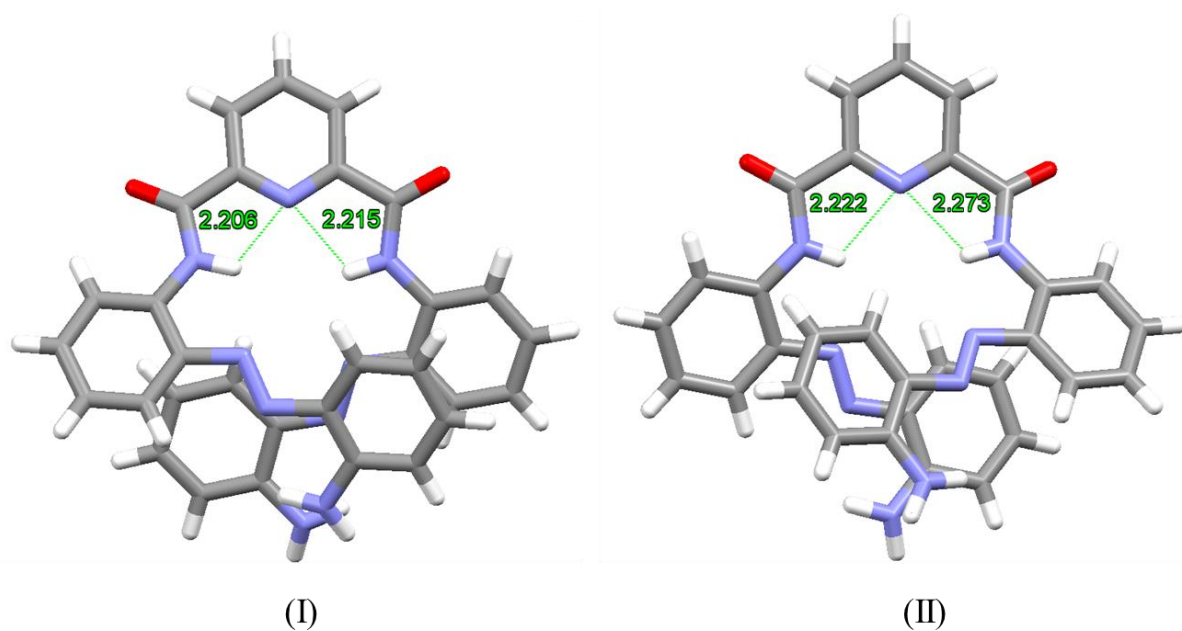


Figure S18. Solid state analysis of the two crystallographically unique molecules of **1A'** in the unit cell, highlighting the presence of bifurcated¹⁴ intramolecular N-H...N hydrogen bonding interactions¹⁴ involving the N atom of the pyridine and the two NH's of the adjacent amide bonds leading to the *syn-syn* conformation about the central pyridinecarboxamide unit.¹⁵

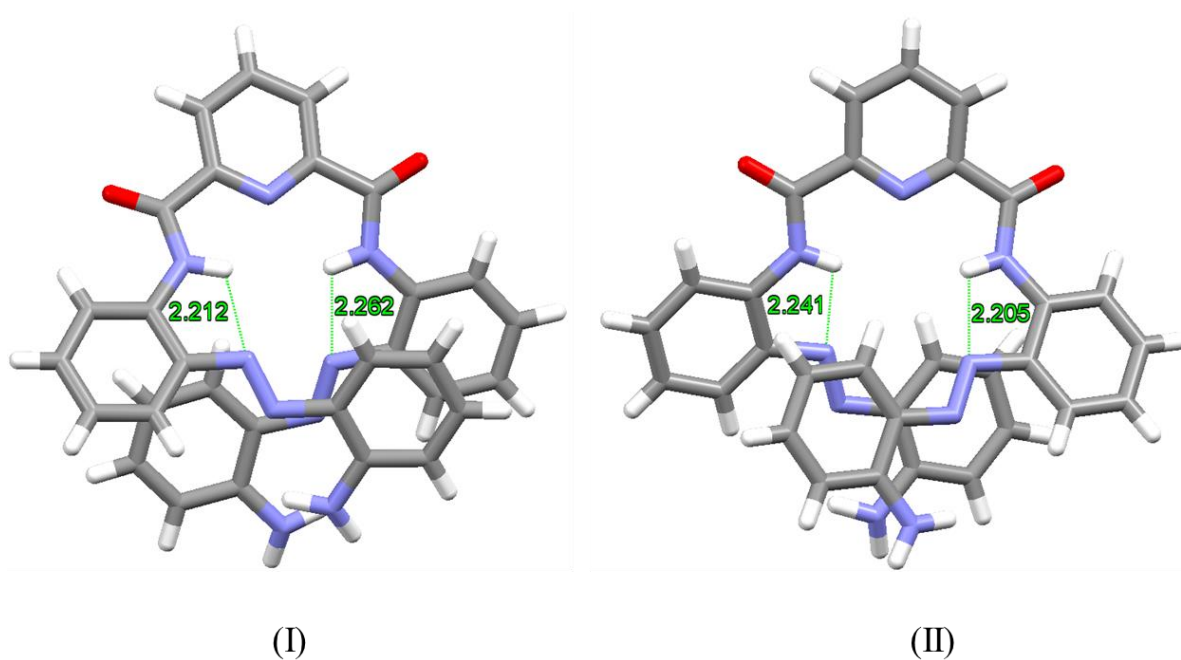


Figure S19. Solid state analysis of the two crystallographically unique molecules in the unit cell of **1A'**, highlighting the close contacts between the pyridyl amide NHs and the adjacent azo N atoms.¹⁶

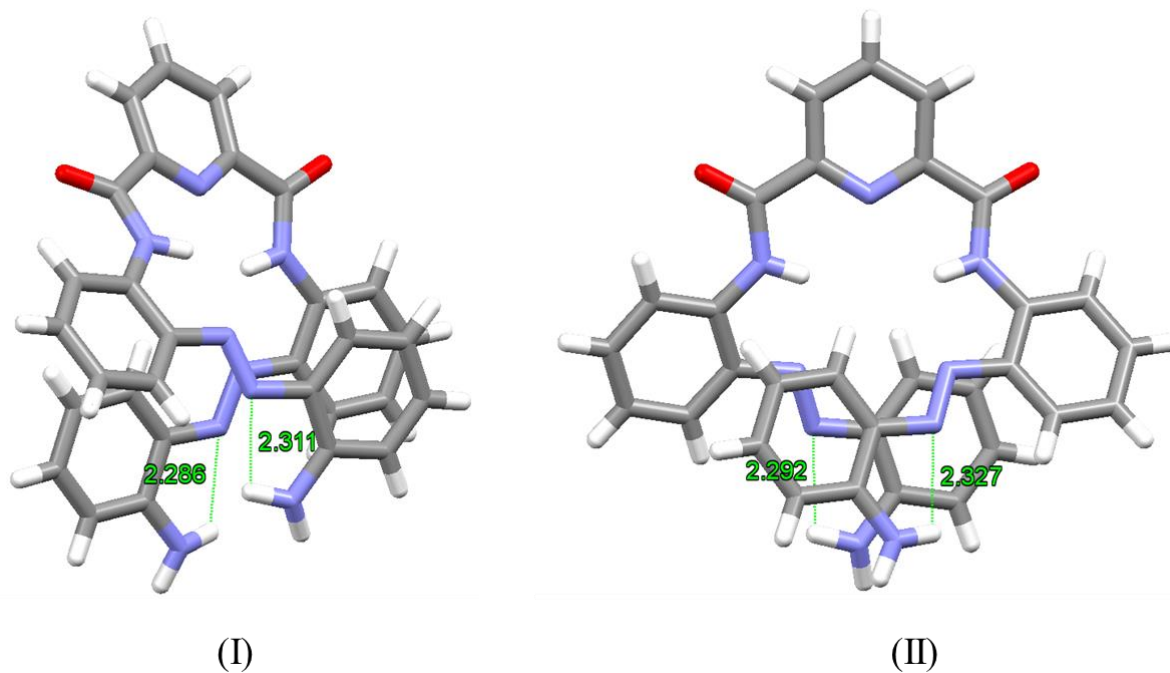


Figure S20. Solid state analysis of the two crystallographically unique molecules in the unit cell of **1A'**, highlighting the close contacts between the terminal acetyl amide and the adjacent azo N atoms.¹⁶

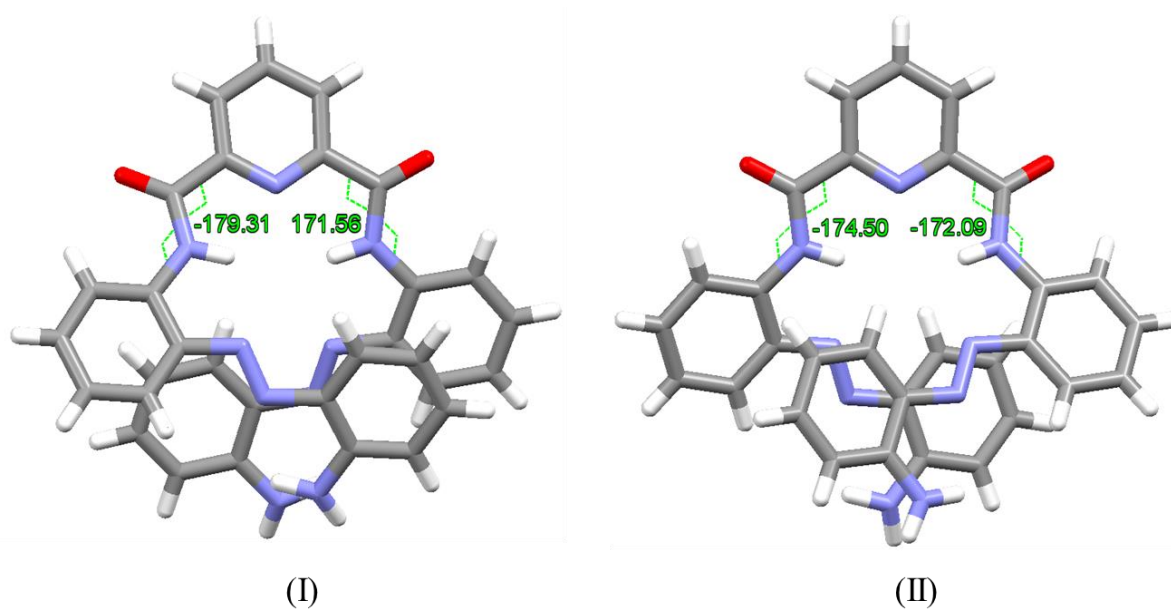


Figure S21. Solid state analysis of the two crystallographically unique molecules in the unit cell of **1A'**, highlighting the torsion angles of the internal peptide bonds.

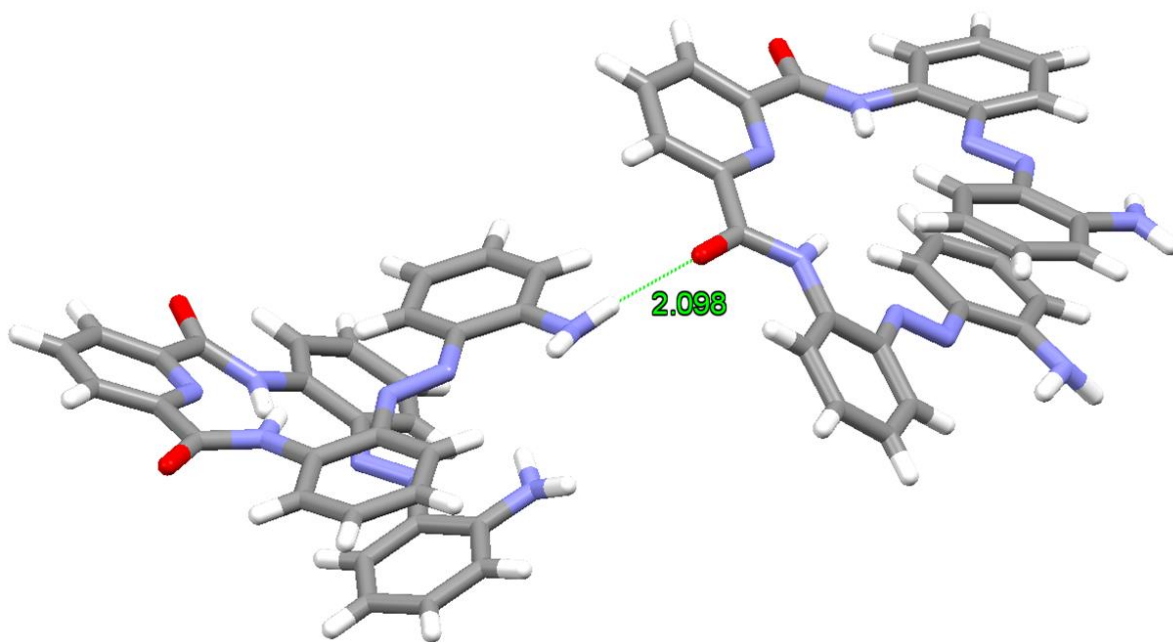


Figure S22. Solid state analysis of **1A'** highlighting the presence of intermolecular N-H...O hydrogen-bonding interactions¹⁷ between an NH of a terminal amine functionality on the foldamer molecule **1A'**(I) and the O atom of a carbonyl group in the carboxamide unit of an adjacent foldamer molecule **1A'**(II).

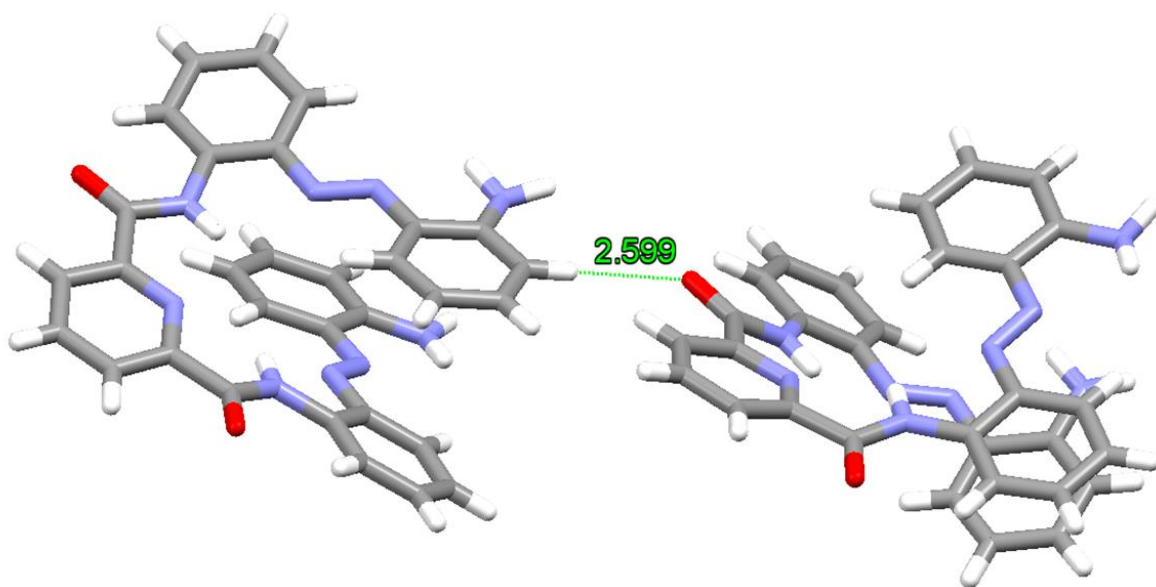


Figure S23. Solid state analysis of **1A'** highlighting the presence of intermolecular reciprocal C-H...O hydrogen-bonding interactions¹⁷ between aromatic protons on the phenyl of one molecule of II and the O atoms of a carbonyl group in the carboxamide unit of an adjacent foldamer molecule of I.

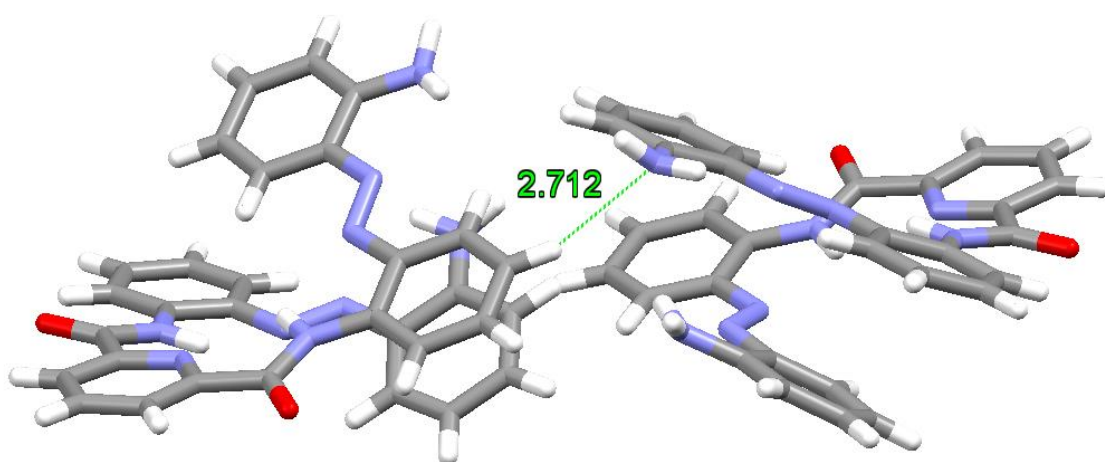


Figure S24. Solid state analysis of **1A'** highlighting the presence of intermolecular C-H...N hydrogen-bonding interactions¹⁷ between an aromatic proton on the phenyl ring of one molecule of foldamer **1A'**(I) and the N atom of an aniline unit of an adjacent foldamer **1A'**(I) molecule.

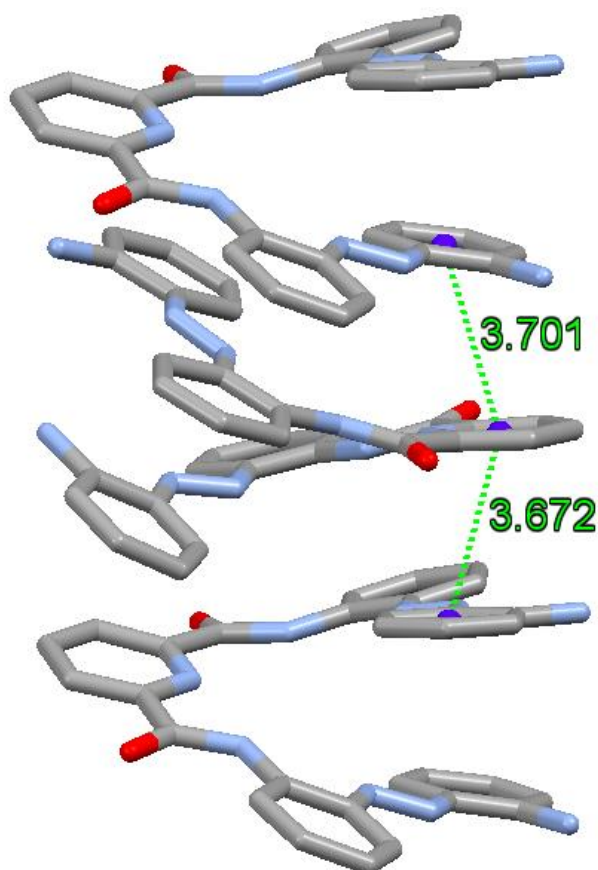


Figure S25. Solid state analysis of the offset face-to-face π - π stacking interactions¹⁸ observed between molecules of **1A'**. Hydrogen atoms have been removed for clarity. Between the aniline phenyl rings of molecule II and the pyridyl ring of a molecule of I.

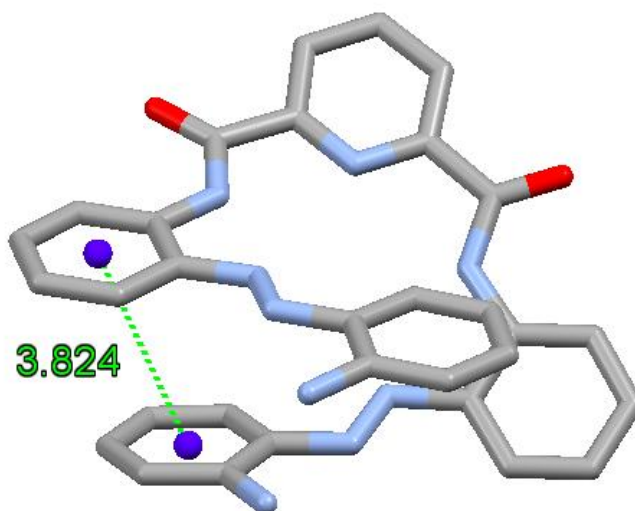
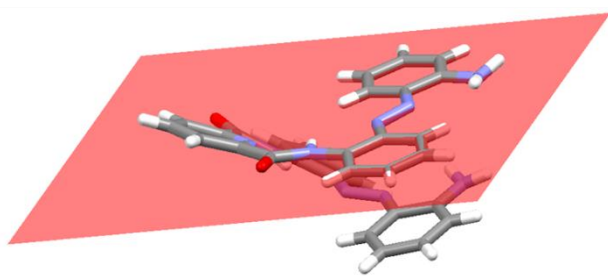


Figure S26. Solid state analysis of the offset face-to-face π - π stacking interactions¹⁸ observed within molecule **1A'**(I). Hydrogen atoms have been removed for clarity.



(I)

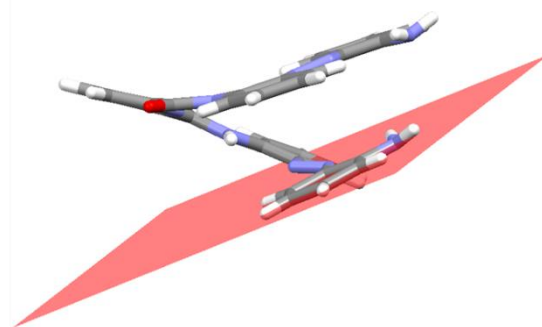
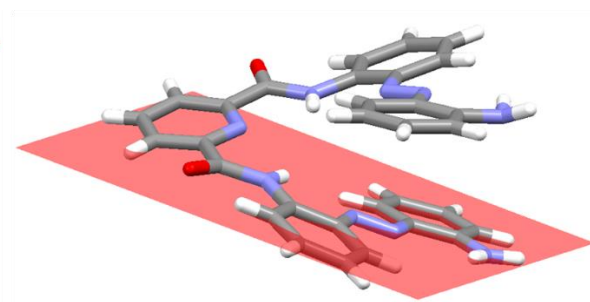
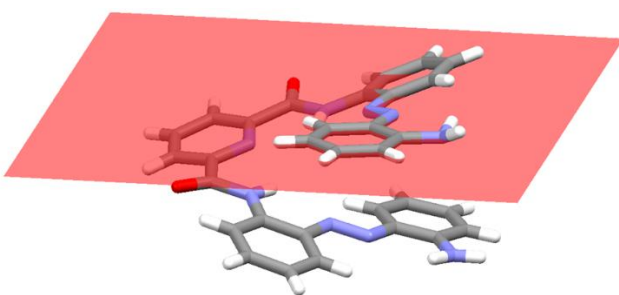


Figure S27. Solid state analysis of molecule I in the unit cell of **1A'**, highlighting the plane of one of the terminal aniline groups.



(II)

Figure S28. Solid state analysis of molecule II in the unit cell of **1A'**, highlighting the plane of one of the terminal aniline groups.

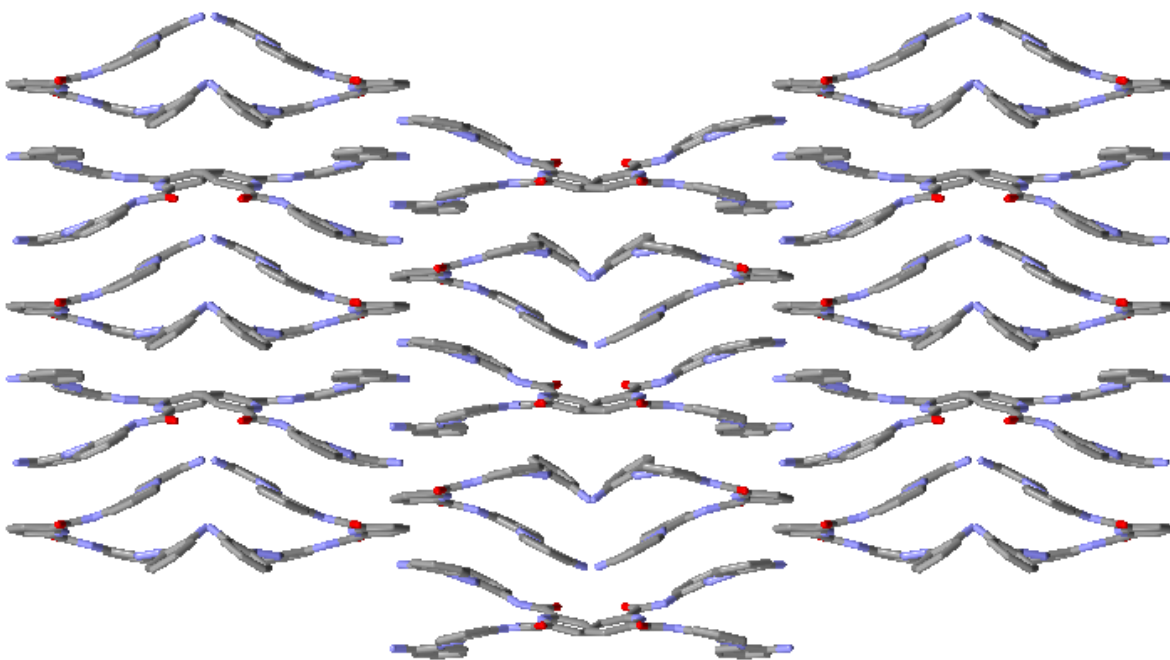


Figure S29. Solid state analysis showing the crystal packing of **1A'** as viewed along the *c* axis. H atoms have been removed for clarity.

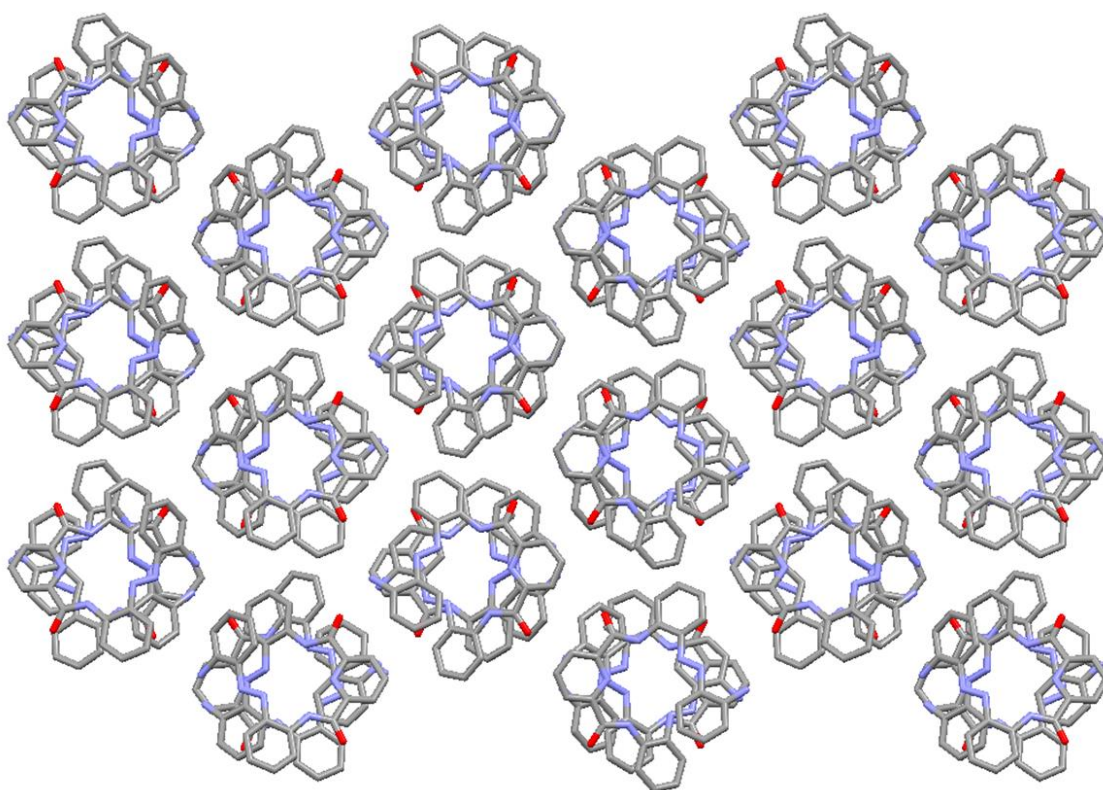


Figure S30. Solid state analysis showing the crystal packing of **1A'** as viewed along the *a* axis. H atoms have been removed for clarity.

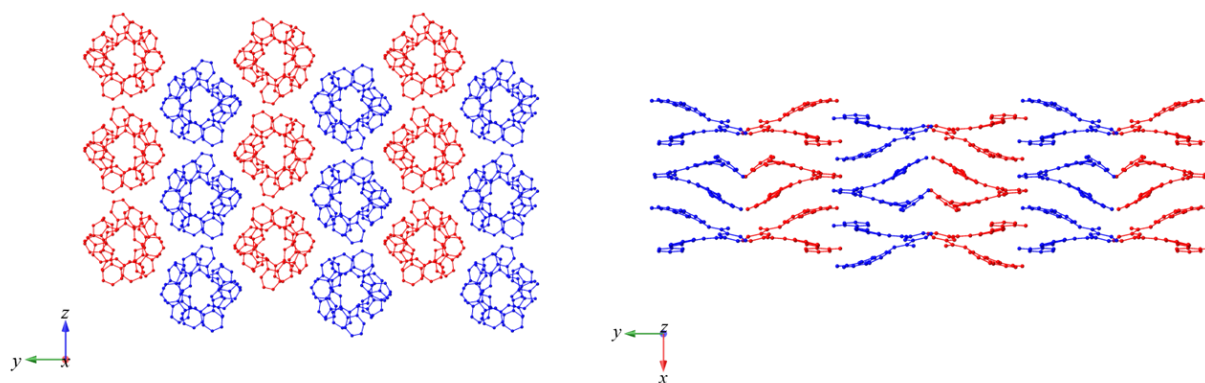


Figure S31. Solid state analysis showing the crystal packing of **1A** showing columns of like-handed stacks, which alternate handedness between columns. Hydrogen atoms have been removed for clarity, molecules have been coloured in accordance with handedness, where red represents left (M), and blue represents right (P).

c) Solid State Analysis of **1B**

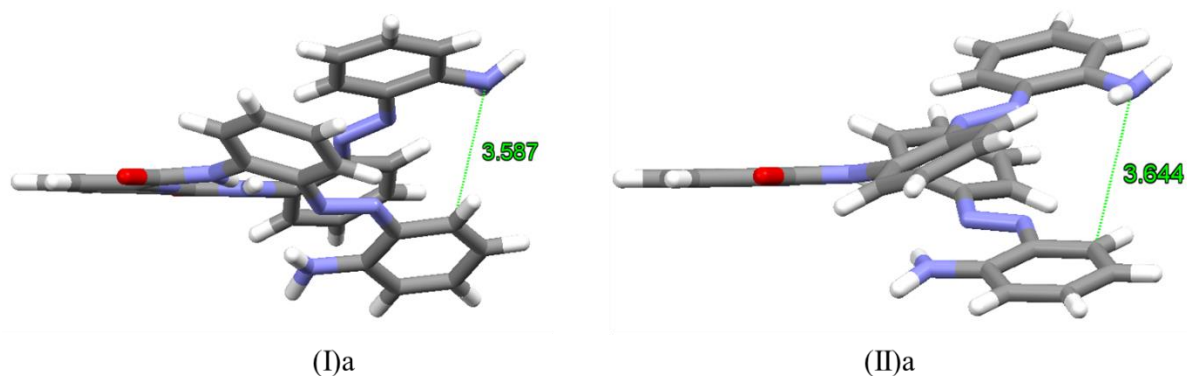
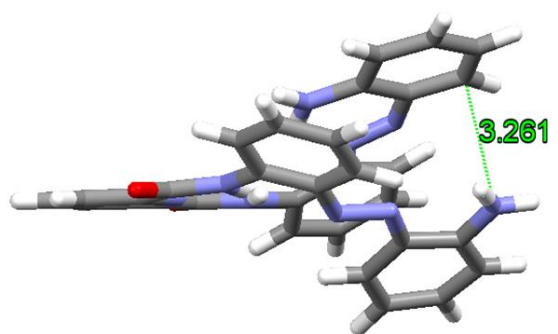
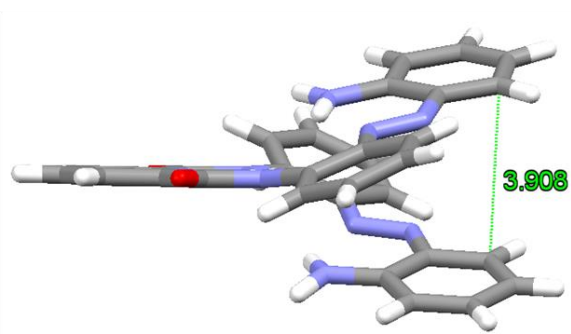


Figure S32. Solid state analysis of the majority components at 93.4(2)% occupancy of the two crystallographically unique molecules in the unit cell of **1B**, showing helical pitch. The structure shows positional disorder of the aniline moieties on one end of each molecule.

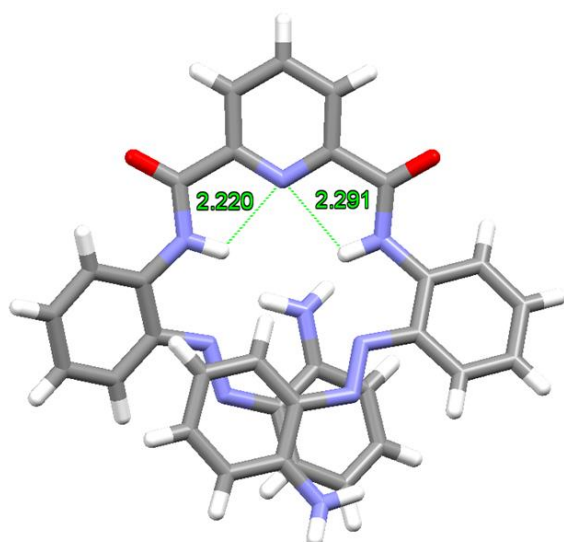


(I)b

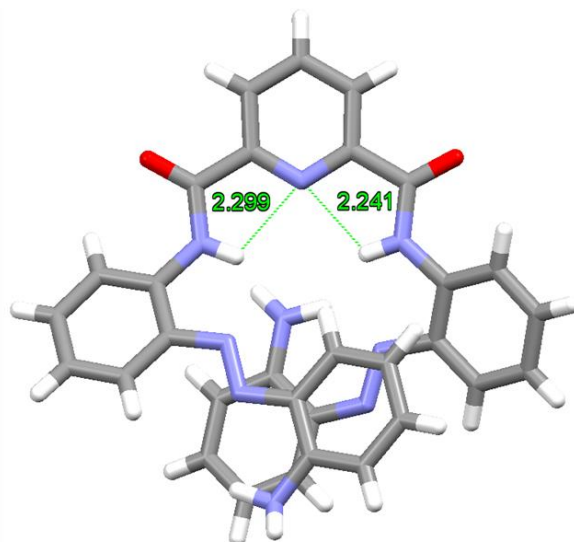


(II)b

Figure S33. Solid state analysis of the minority components at 6.6(2)% occupancy of the two crystallographically unique molecules in the unit cell of **1B**, showing helical pitch. The structure shows positional disorder of the aniline moieties on one end of each molecule.



(I)



(II)

Figure S34. Solid state analysis of the two crystallographically unique molecules (**I** on left and **II** on the right) of **1B** in the unit cell, highlighting the presence of bifurcated¹⁴ intramolecular N-H...N hydrogen bonding interactions¹⁴ involving the N atom of the pyridine and the two NH's of the adjacent amide bonds leading to the *syn-syn* conformation about the central pyridinecarboxamide unit.¹⁵

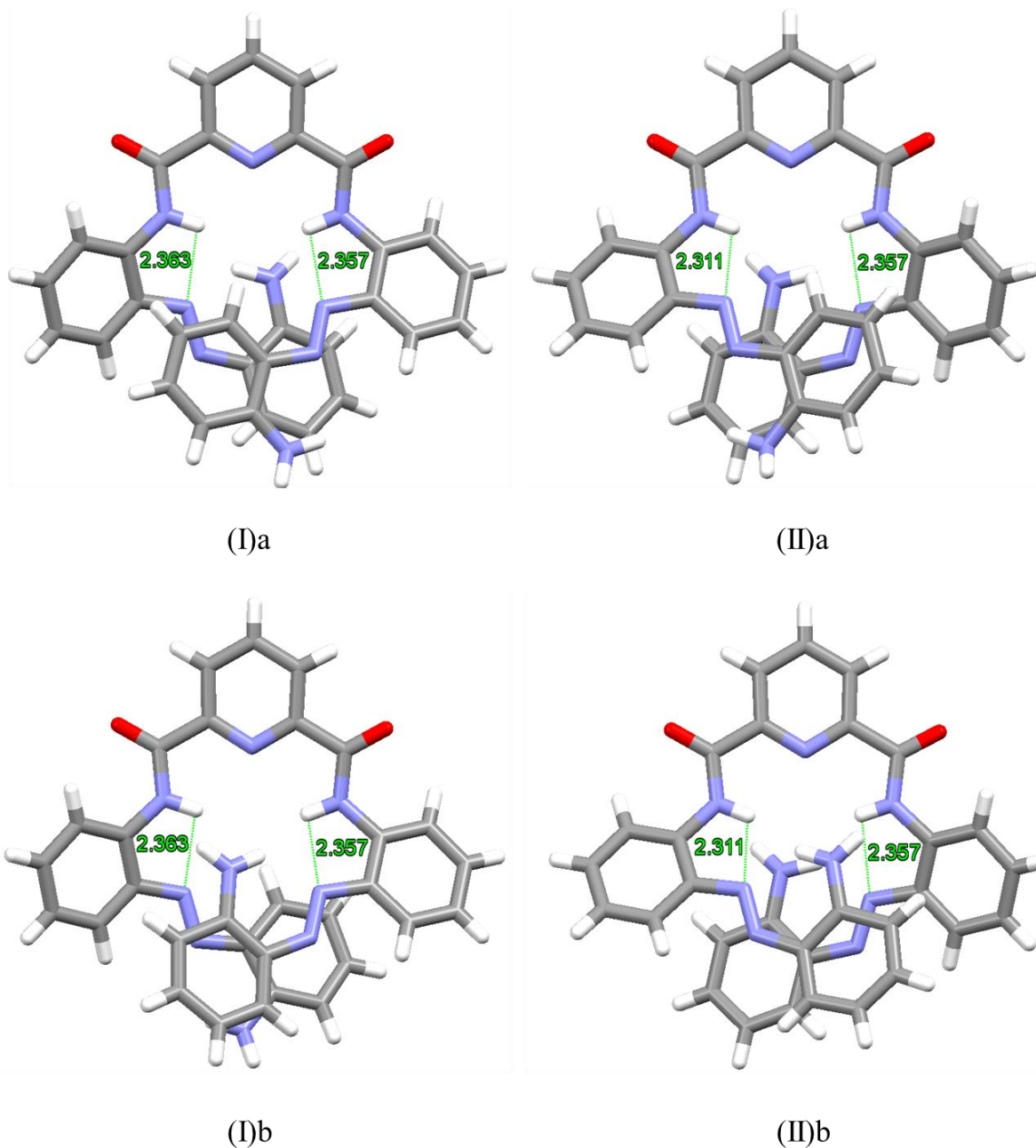
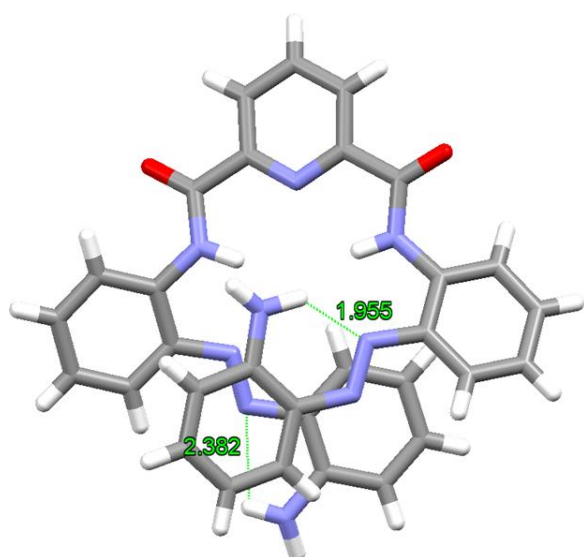
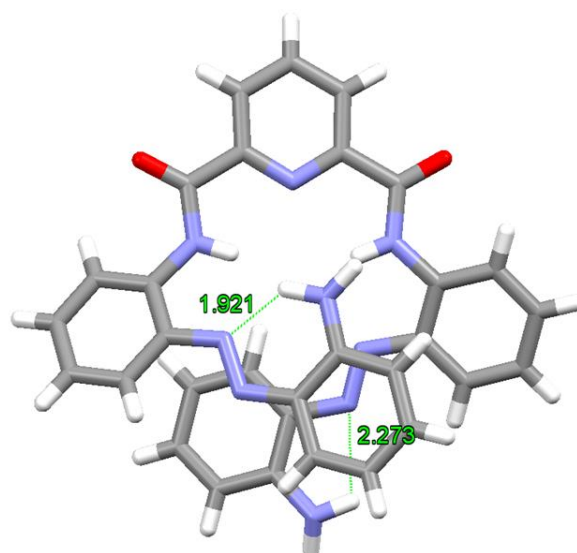


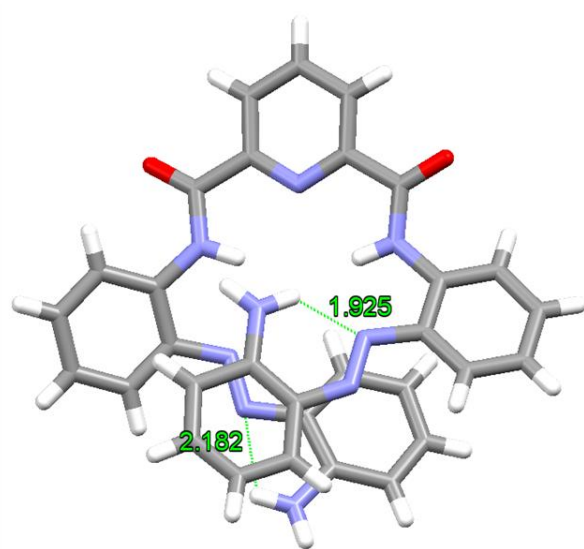
Figure S35. Solid state analysis of the two crystallographically unique molecules in the unit cell of **1B**, where the disordered occupancy is denoted using ‘a’ for the majority component and ‘b’ for the minority component, highlighting the close contacts between the pyridyl amide NHs and the adjacent azo N atoms.¹⁶



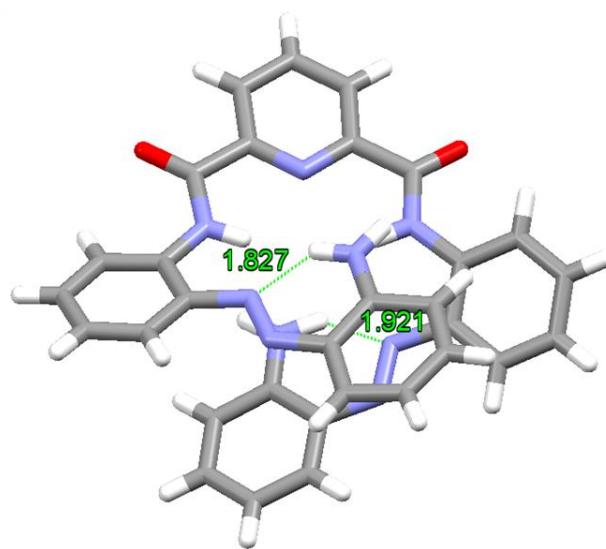
(I)a



(II)a



(I)b



(II)b

Figure S36. Solid state analysis of the two crystallographically unique molecules in the unit cell of **1B**, where the disordered occupancy is denoted using ‘a’ for the majority component and ‘b’ for the minority component, highlighting the close contacts between the terminal acetyl amide and the adjacent azo N atoms.¹⁶

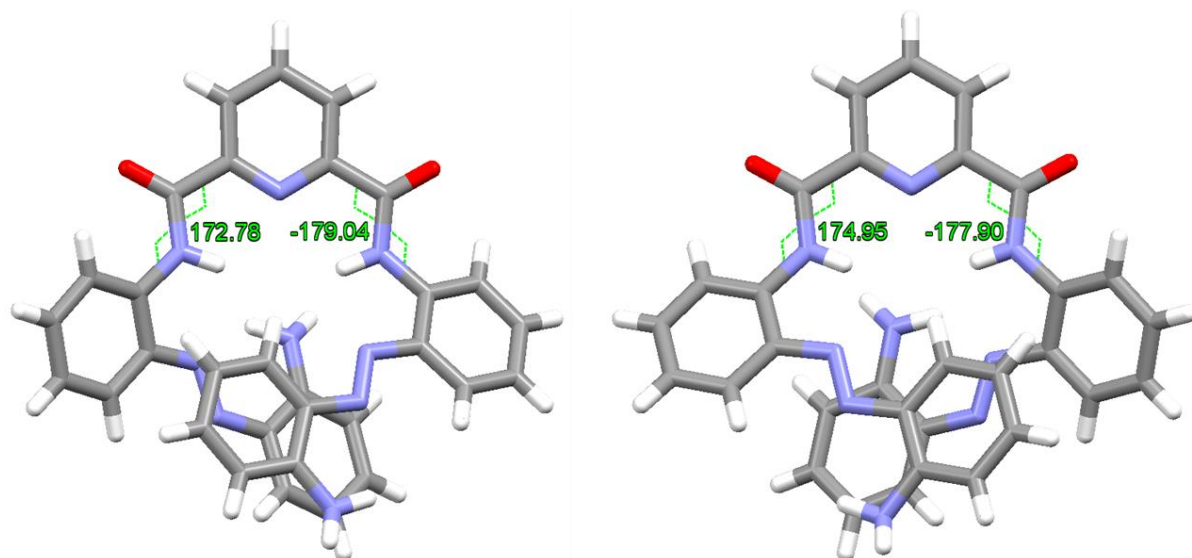


Figure S37. Solid state analysis of the two crystallographically unique molecules in the unit cell of **1B**, highlighting the torsion angles of the internal peptide bonds.

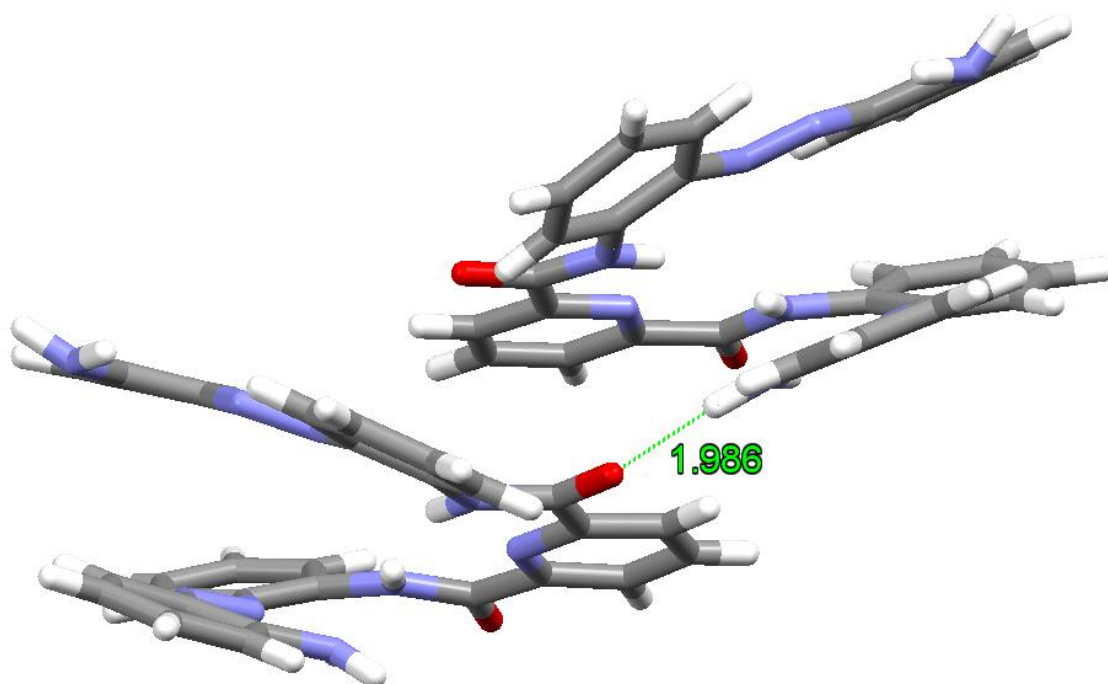


Figure S38. Solid state analysis of **1B** highlighting the presence of intermolecular C-H...O hydrogen-bonding interactions¹⁷ between an aromatic hydrogen of a foldamer molecule of **1B(I)** and the oxygen of an internal amide functionality of foldamer molecule **1B(II)**.

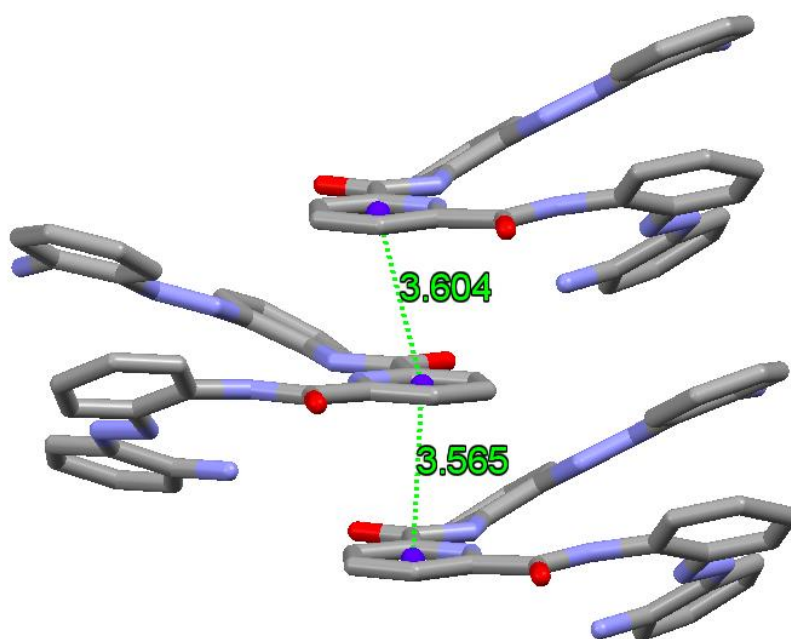


Figure S39. Solid state analysis of the offset face-to-face π - π stacking interactions¹⁸ observed between molecules of **1B**.

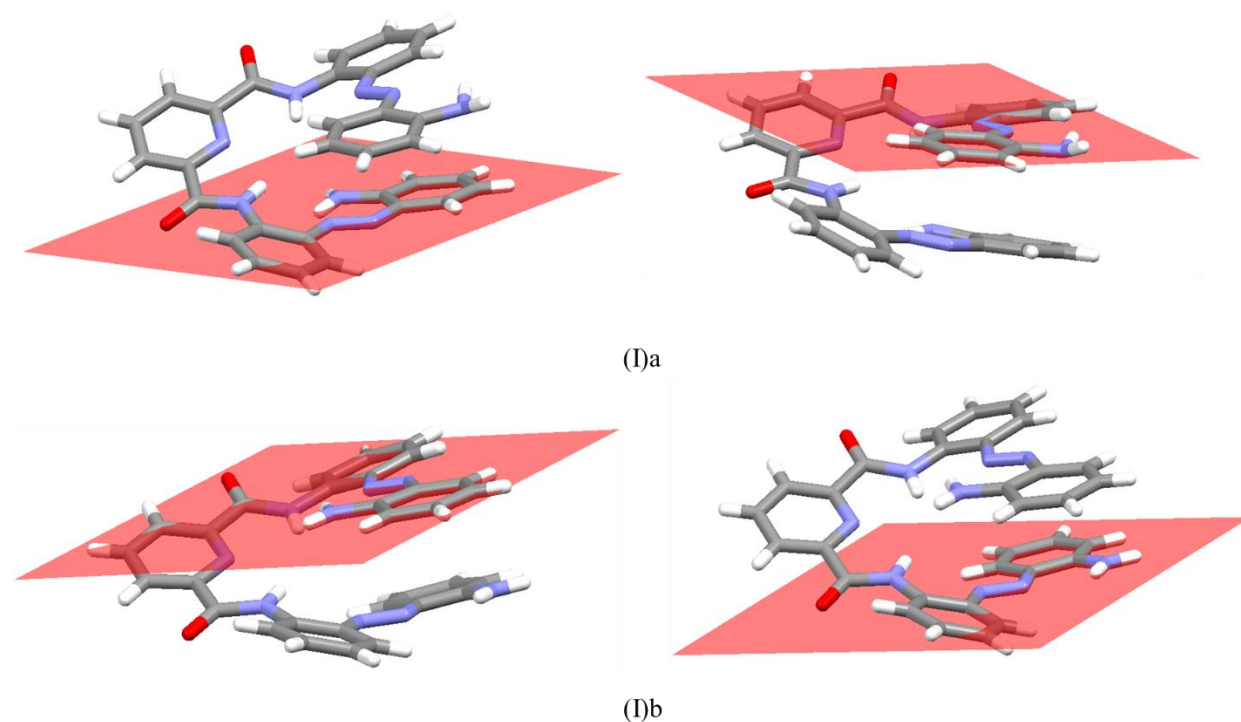


Figure S40. Solid state analysis of crystallographically unique molecule I in the unit cell of **1B**, where the disordered occupancy is denoted using ‘a’ for the majority component and ‘b’ for the minority component, highlighting the plane of the terminal aniline groups.

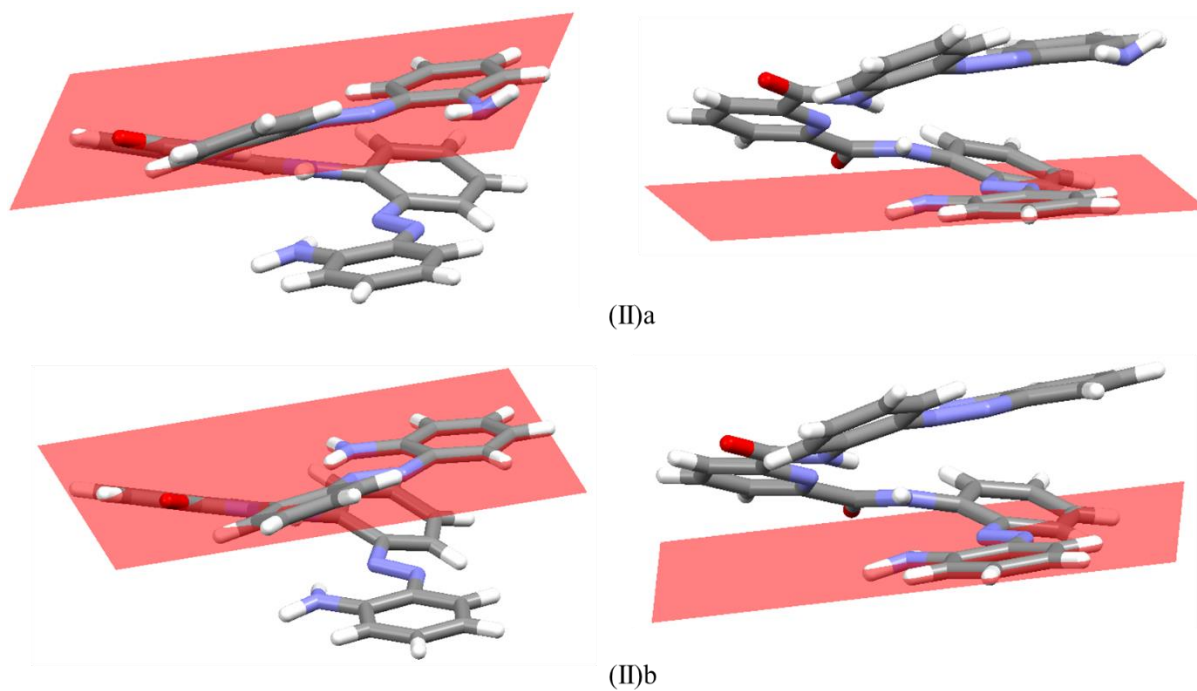


Figure S41. Solid state analysis of crystallographically unique molecule **II** in the unit cell of **1B**, where the disordered occupancy is denoted using ‘a’ for the majority component and ‘b’ for the minority component, highlighting the plane of one of the terminal aniline groups.

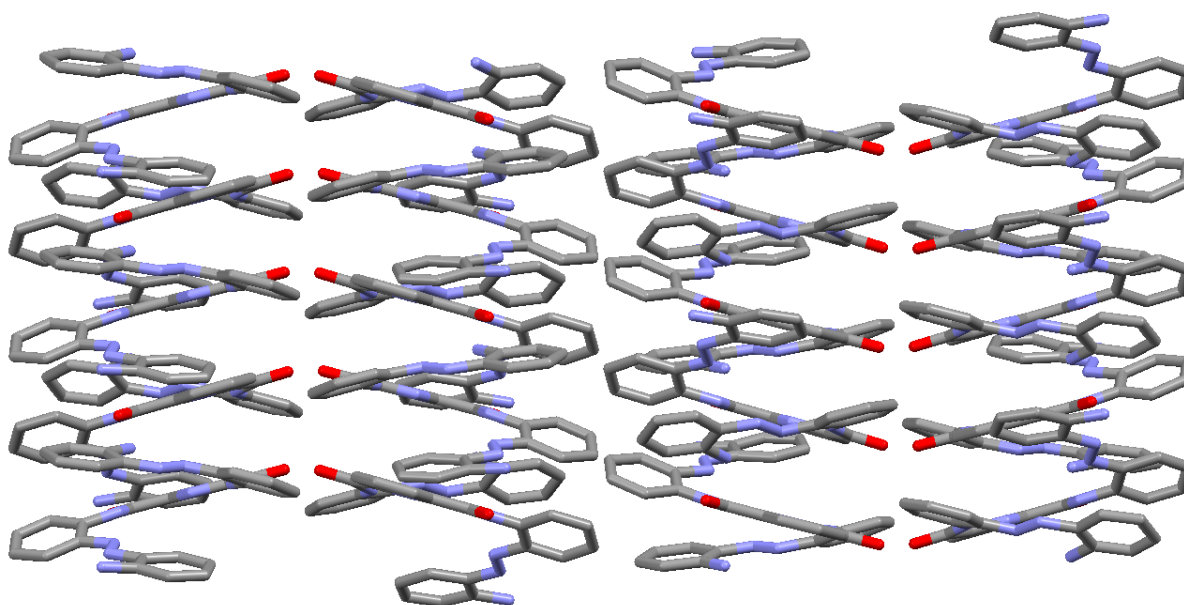


Figure S42. Solid state analysis showing the crystal packing of the majority components of **1B** as viewed along the *a* axis. H atoms have been removed for clarity.

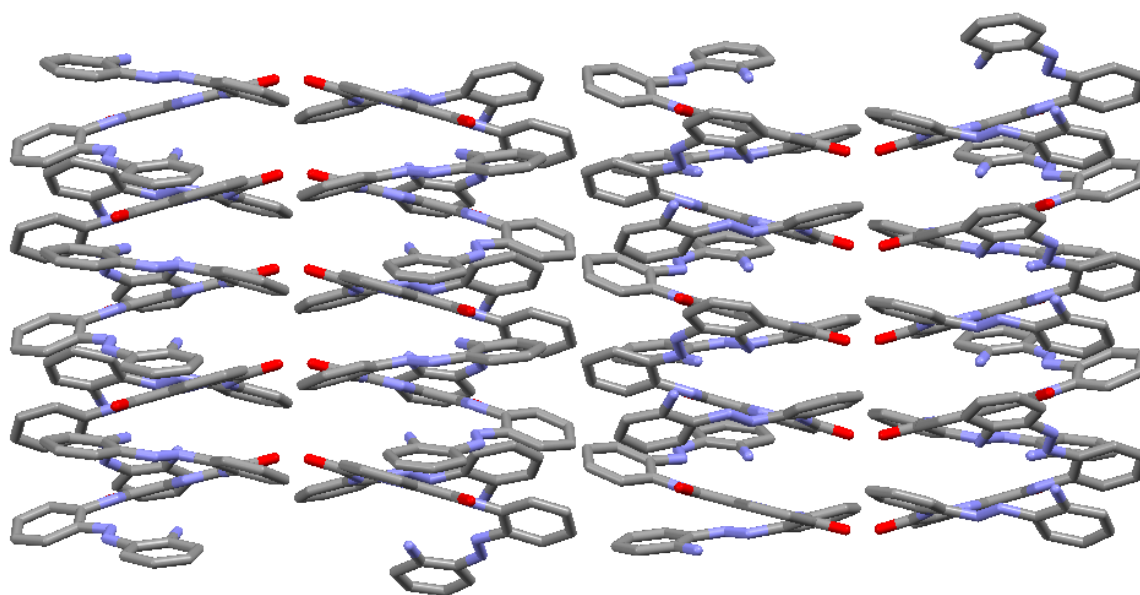


Figure S43. Solid state analysis showing the crystal packing of the minority components of **1B** as viewed along the *a* axis. H atoms have been removed for clarity.

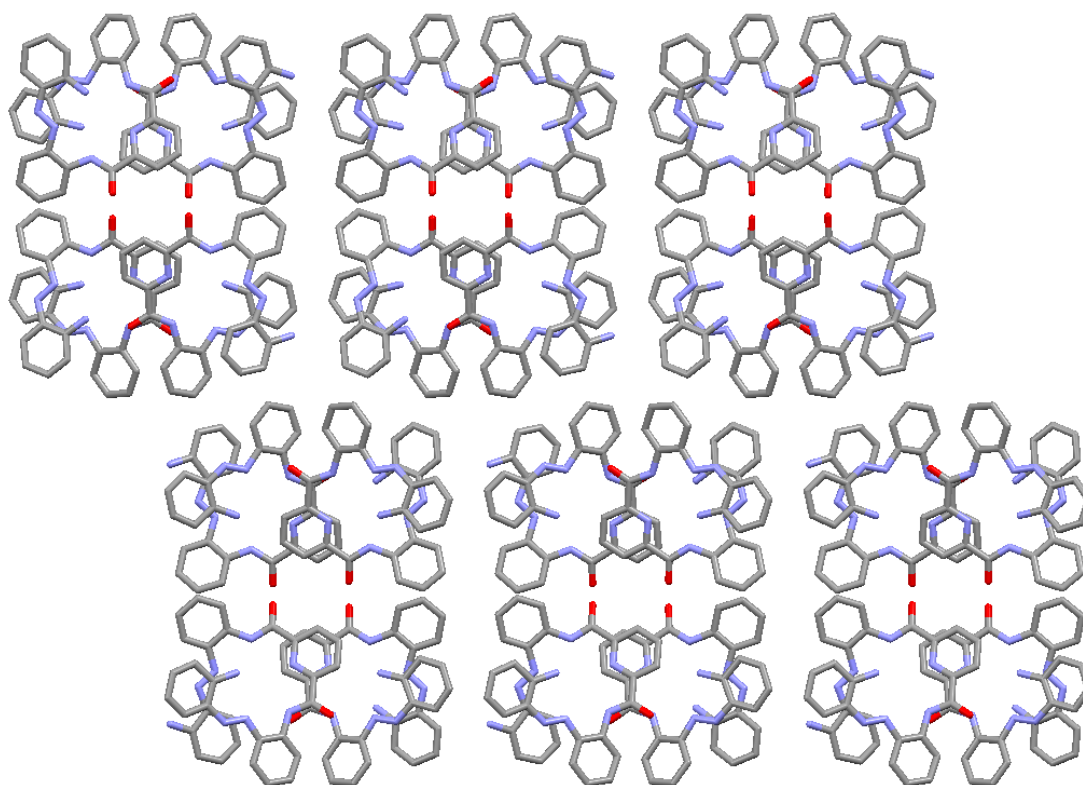


Figure S44. Solid state analysis showing the crystal packing of the majority components of **1B** as viewed along the *c* axis. H atoms have been removed for clarity.

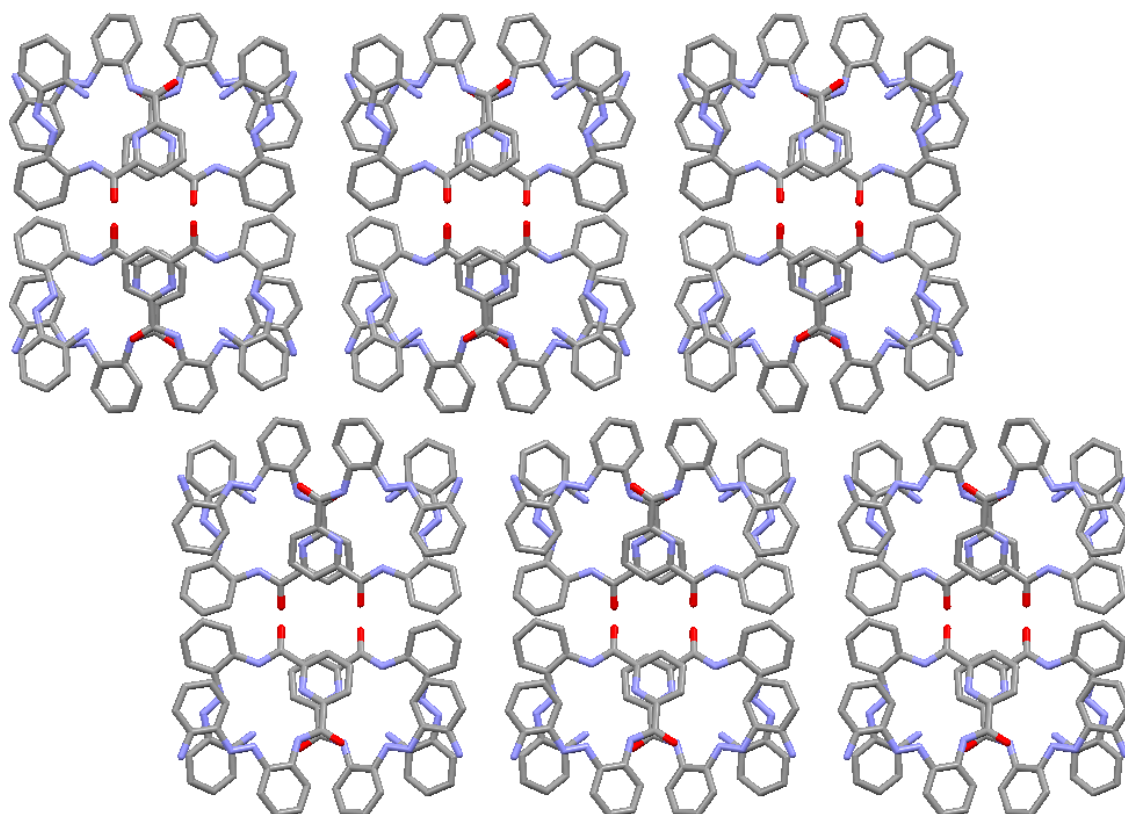


Figure S45. Solid state analysis showing the crystal packing of the minority components of **1B** as viewed along the *c* axis. H atoms have been removed for clarity.

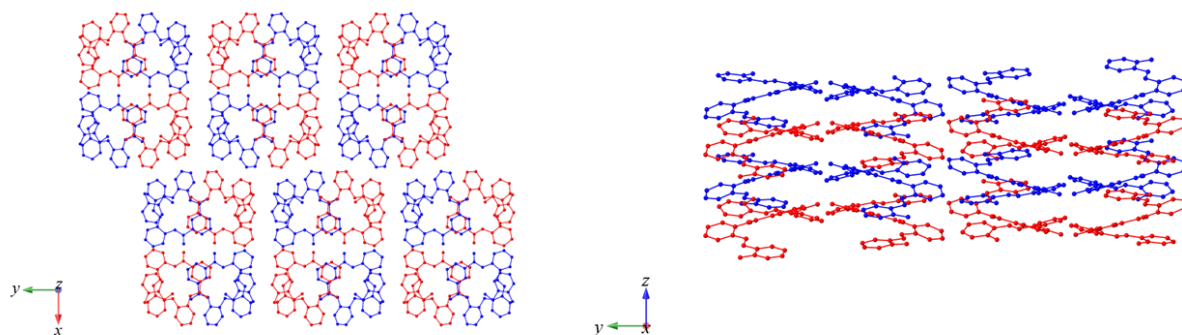


Figure S46. Solid state analysis showing the crystal packing of the majority component of **1B** showing units made up of four columns of alternating handedness. Hydrogen atoms have been removed for clarity, molecules have been coloured in accordance with handedness, where red represents left (M), and blue represents right (P).

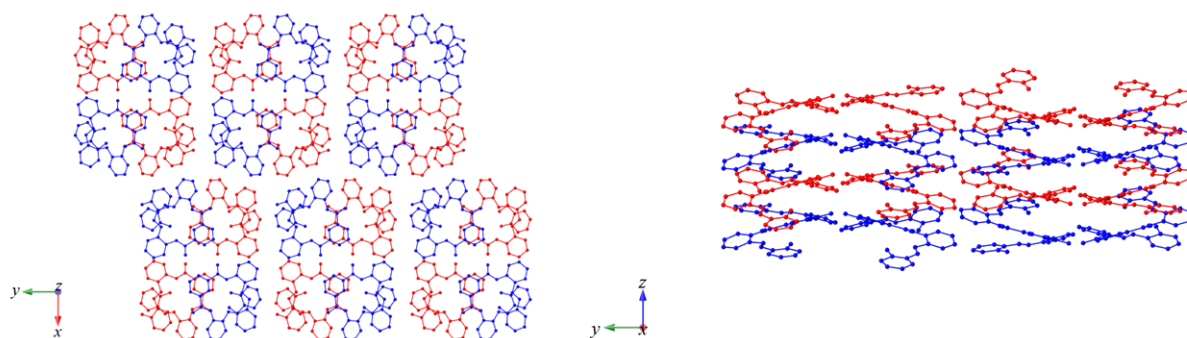


Figure S47. Solid state analysis showing the crystal packing of the minority component of **1B** showing units made up of four columns of alternating handedness. Hydrogen atoms have been removed for clarity, molecules have been coloured in accordance with handedness, where red represents left (M), and blue represents right (P).

d) Solid State Analysis of **1**·THF

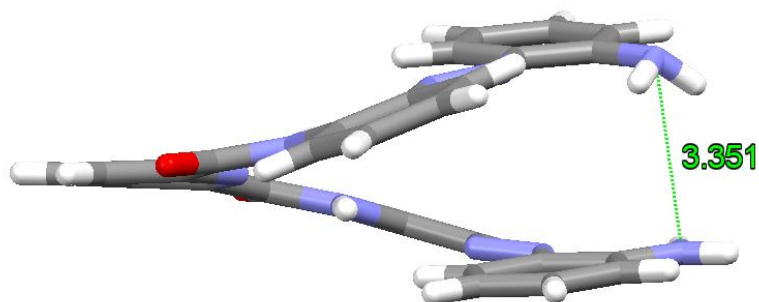


Figure S48. Solid state analysis of **1**·THF, showing helical pitch (distance between N atoms at each terminus).

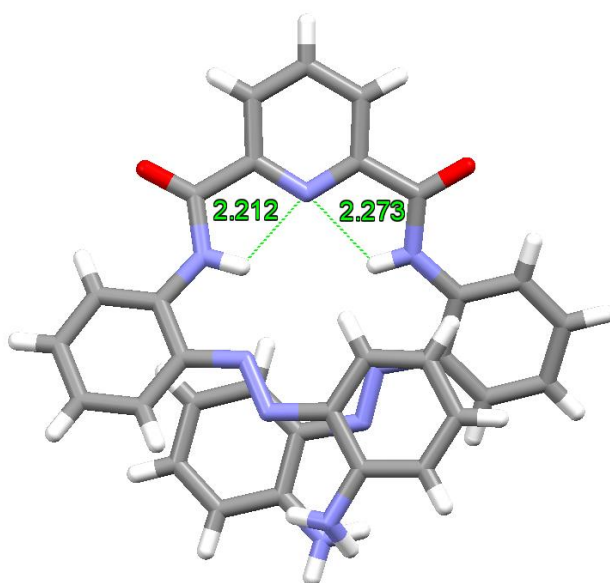


Figure S49. Solid state analysis of **1**·THF in the unit cell highlighting the presence of bifurcated¹⁴ intramolecular N-H···N hydrogen bonding interactions¹⁴ involving the N atom of the pyridine and the two NH's of the adjacent amide bonds leading to the *syn-syn* conformation about the central pyridinecarboxamide unit.¹⁵

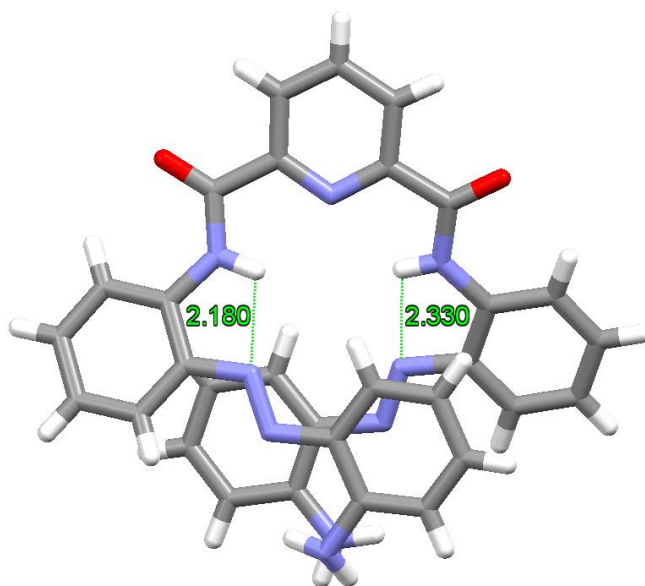


Figure S50. Solid state analysis of **1**·THF in the unit cell highlighting the close contacts between the pyridyl amide NHs and the adjacent azo N atoms.¹⁶

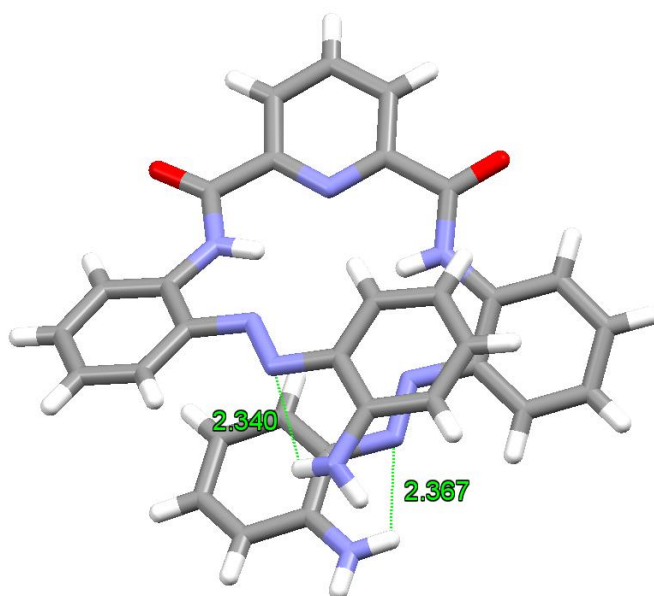


Figure S51. Solid state analysis of **1**·THF in the unit cell highlighting the close contacts between the terminal acetyl amide and the adjacent azo N atoms.¹⁶

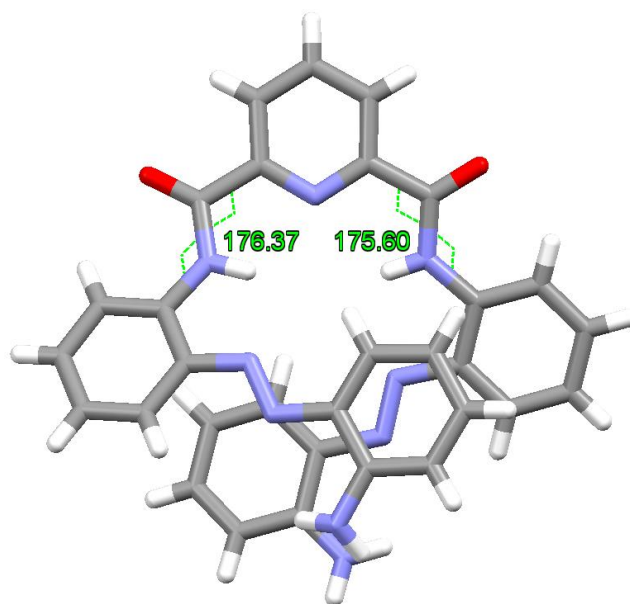


Figure S52. Solid state analysis of **1·THF** in the unit cell highlighting the torsion angles of the internal peptide bonds.

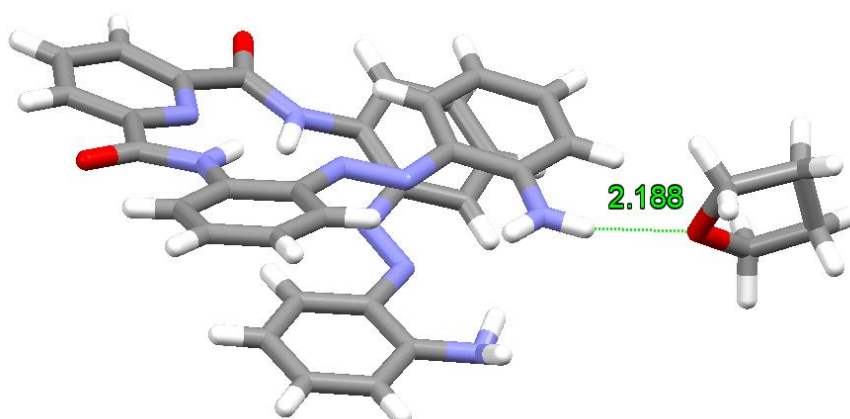


Figure S53. Solid state analysis of **1·THF** highlighting the presence of intermolecular N-H...O hydrogen-bonding interactions¹⁷ between an NH of a terminal amine functionality on the foldamer molecule and the O atom of the majority tetrahydrofuran solvent molecule at 74.3(6)% occupancy.

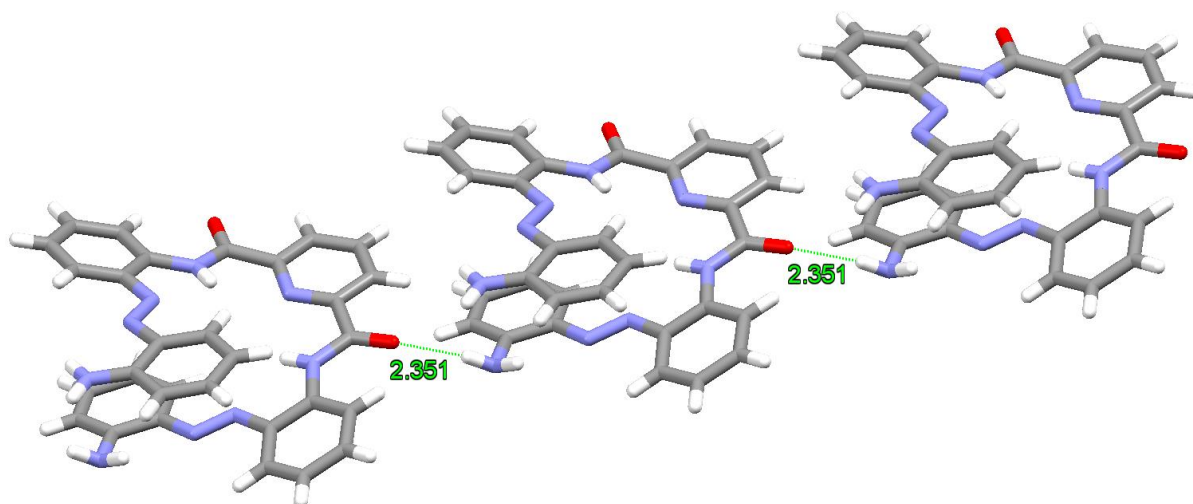


Figure S54. Solid state analysis of **1·THF** highlighting the presence of an intermolecular N-H \cdots O hydrogen-bonding interaction¹⁷ between the NH atoms of the terminal amine functionalities on one molecule and O atom of a carbonyl group of a carboxamide unit in an adjacent foldamer molecule.

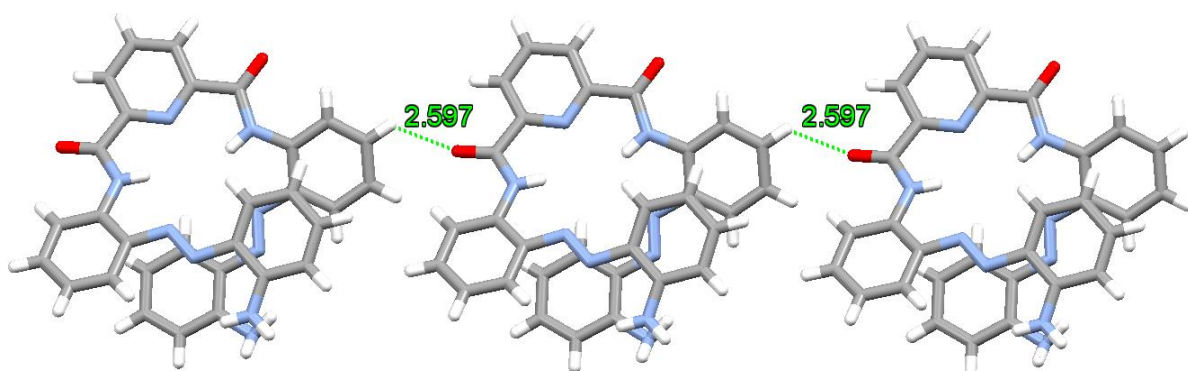


Figure S55. Solid state analysis of **1·THF** highlighting the presence of an intermolecular C-H \cdots O hydrogen-bonding interaction¹⁷ between an aromatic proton on a foldamer molecule and O atom of a carbonyl group of a carboxamide unit in an adjacent foldamer molecule.

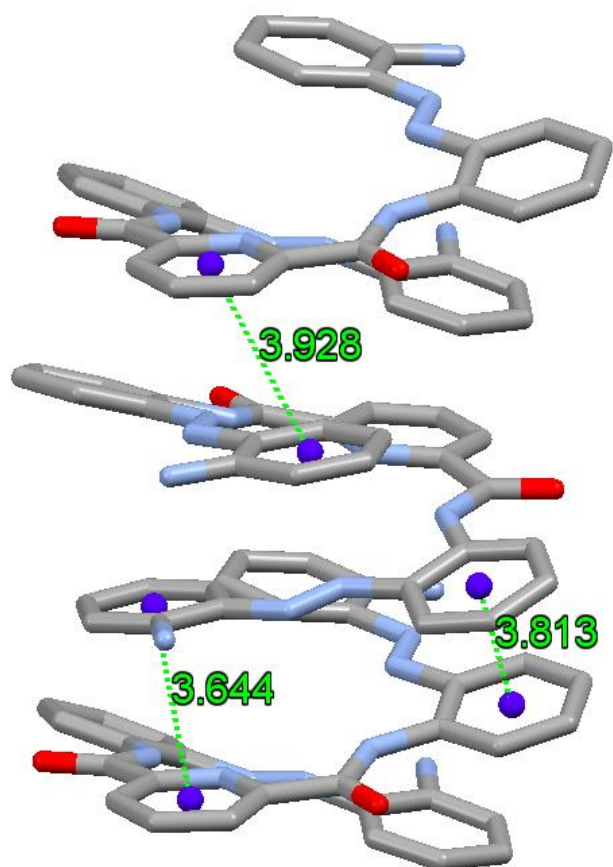


Figure S56. Solid state analysis of the offset face-to-face π - π stacking interactions¹⁸ observed between molecules of **1•THF**.

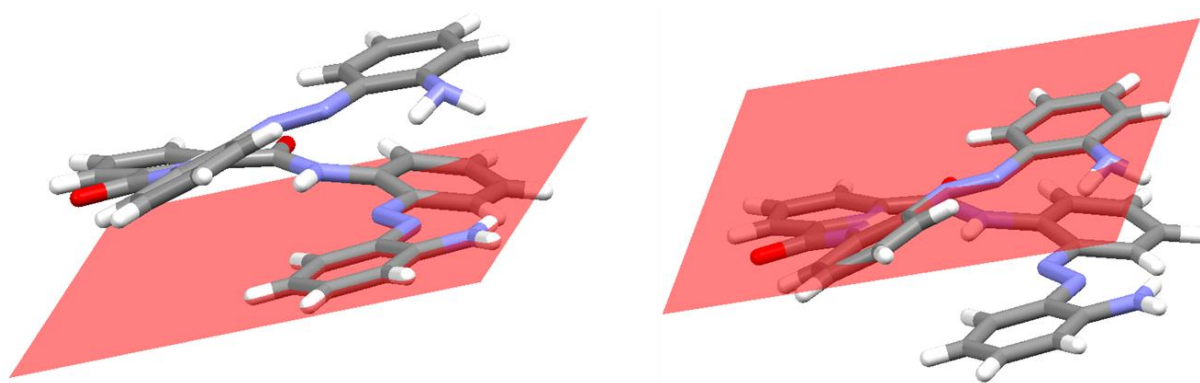


Figure S57. Solid state analysis of a foldamer molecule in the unit cell of **1•THF** highlighting the plane of the terminal aniline groups.

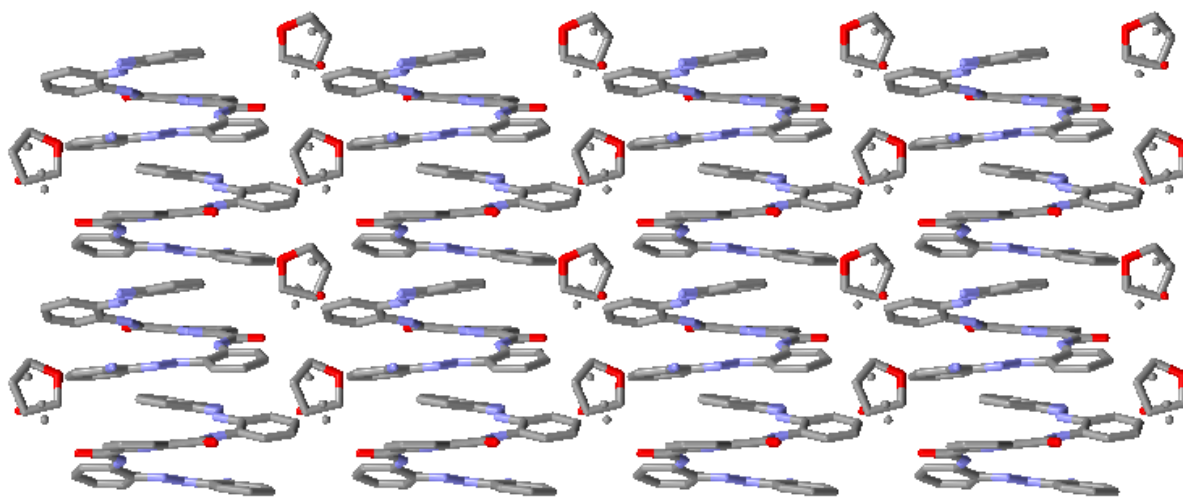


Figure S58. Solid state analysis showing the crystal packing of **1·THF** as viewed along the *a* axis. H atoms have been removed for clarity.

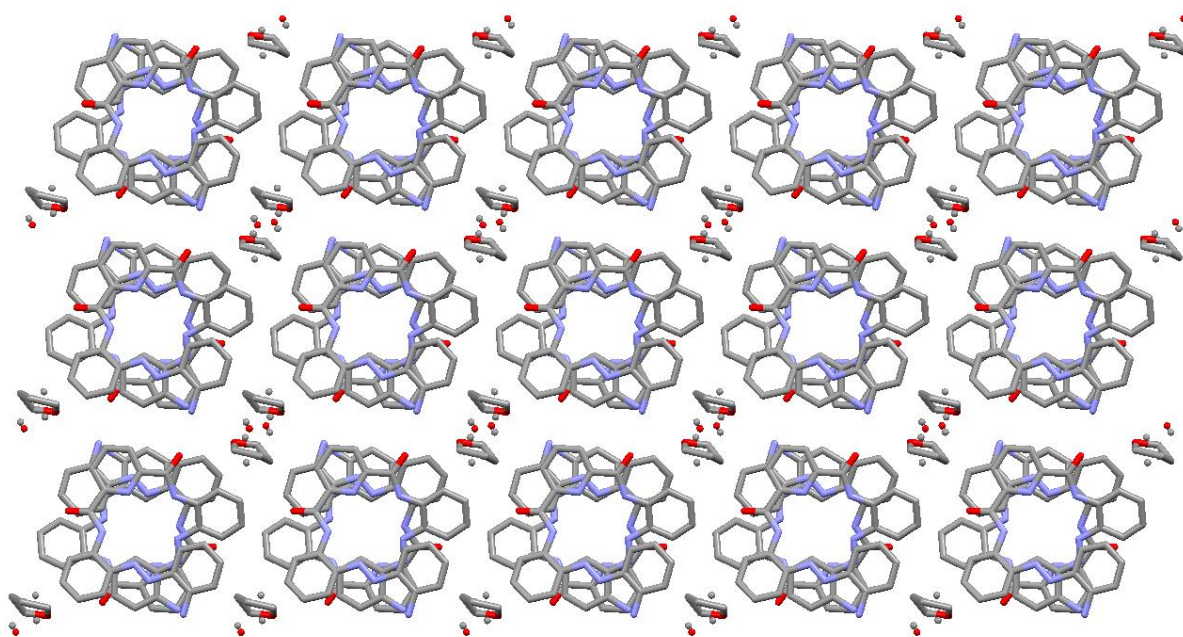


Figure S59. Solid state analysis showing the crystal packing of **1·THF** as viewed along the *b* axis. H atoms have been removed for clarity.

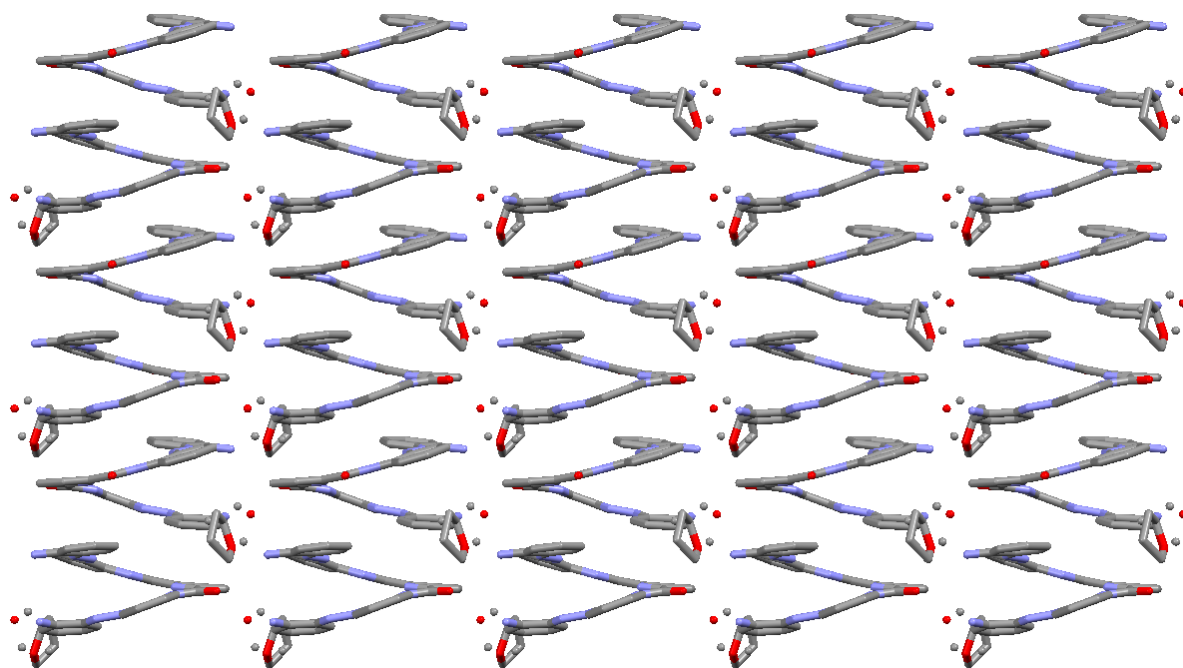


Figure S60. Solid state analysis showing the crystal packing of **1·THF** as viewed along the *c* axis. H atoms have been removed for clarity.

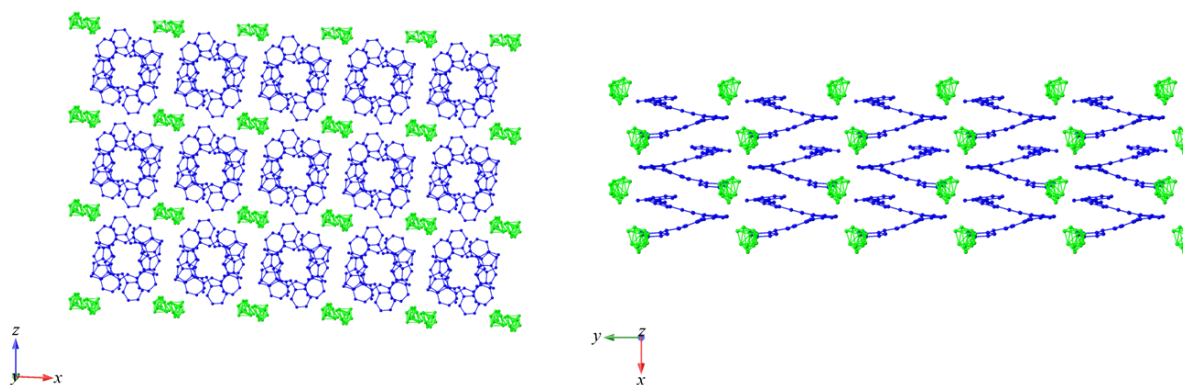


Figure S61. Solid state analysis showing the crystal packing of **1·THF** showing columns and rows of right-handed stacks. Hydrogen atoms have been removed for clarity, solvent molecules are shown in green, and molecules have been coloured in accordance with handedness, where blue represents right (P).

e) Solid State Analysis of 1-butanone

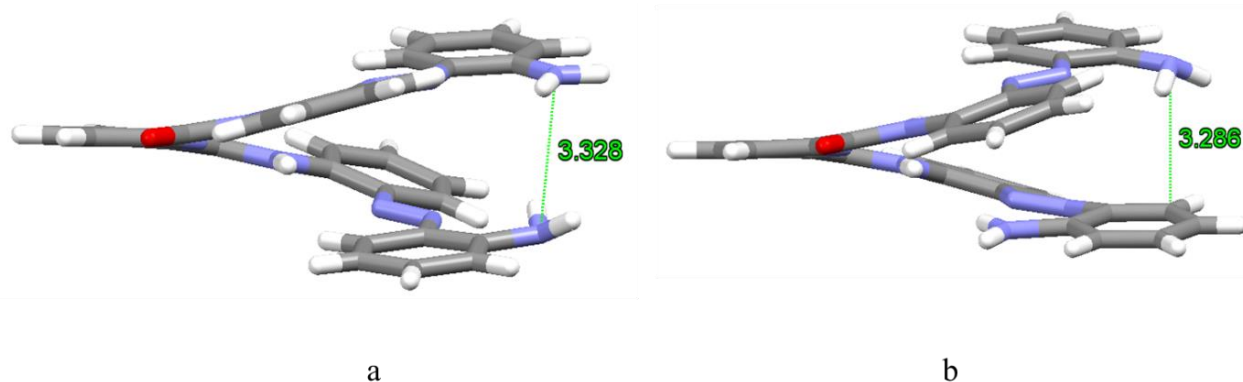


Figure S62. Solid state analysis of **1-butanone**, showing helical pitch with the majority component shown as ‘a’ at 69.5(7)% occupancy and the minority component shown as ‘b’ with a 30.5(7)% occupancy, showing helical pitch. The structure shows positional disorder of the aniline moiety at one end of the molecule.

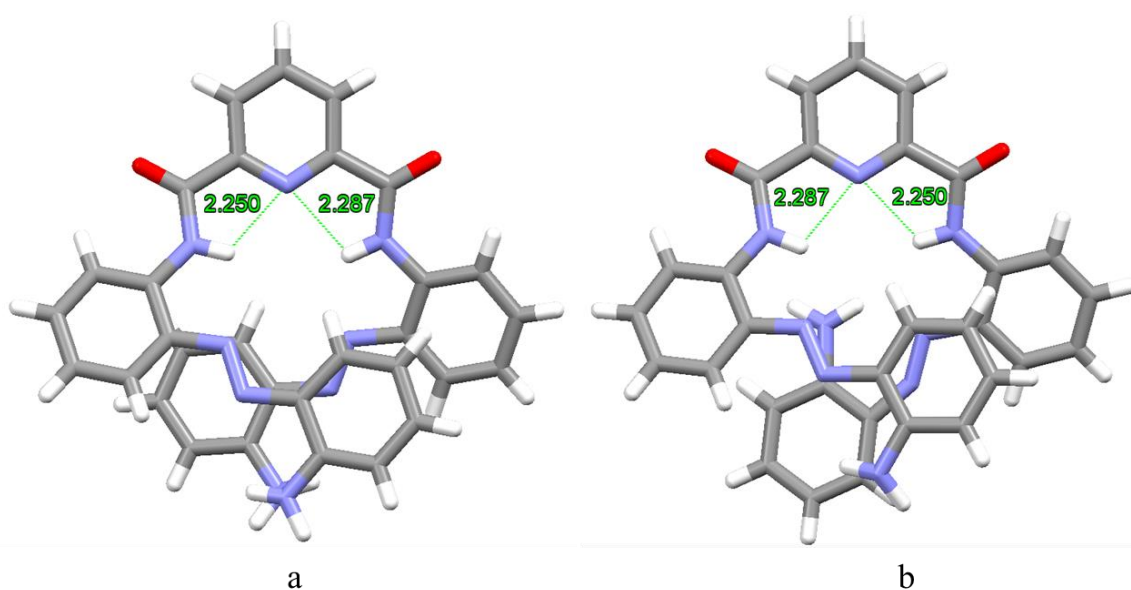


Figure S63. Solid state analysis of **1-butanone** in the unit cell highlighting the presence of bifurcated¹⁴ intramolecular N-H...N hydrogen bonding interactions¹⁴ involving the N atom of the pyridine and the two NH's of the adjacent amide bonds leading to the *syn-syn* conformation about the central pyridinecarboxamide unit.¹⁵ Where the disorder component is denoted using ‘a’ for the majority occupancy component and ‘b’ for the minority occupancy component.

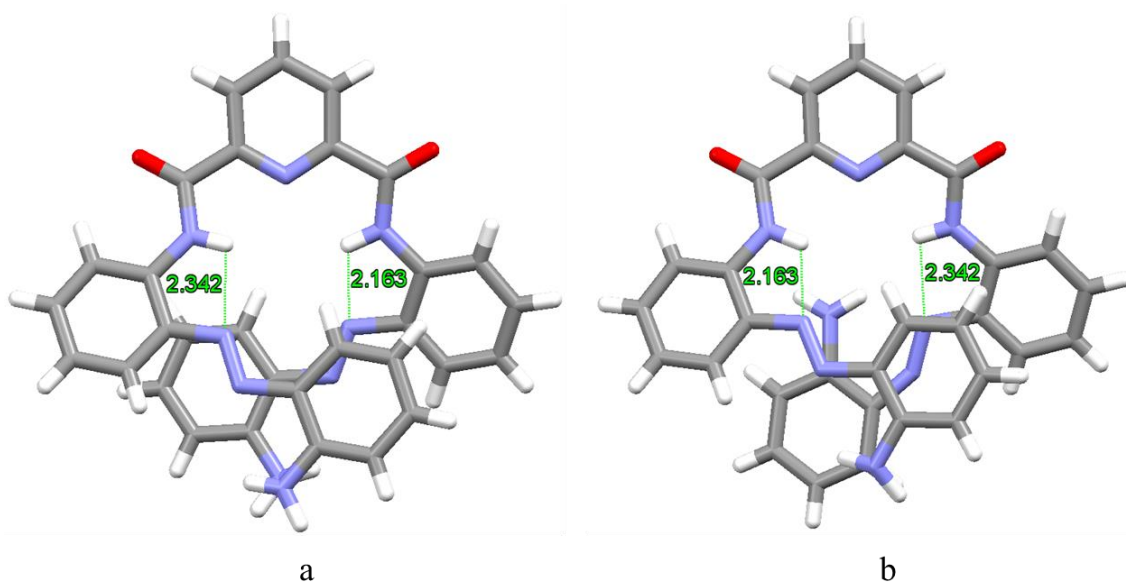


Figure S64. Solid state analysis of **1•butanone** in the unit cell highlighting the close contacts between the pyridyl amide NHs and the adjacent azo N atoms.¹⁶ Where the disorder component is denoted using 'a' for the majority occupancy component and 'b' for the minority occupancy component.

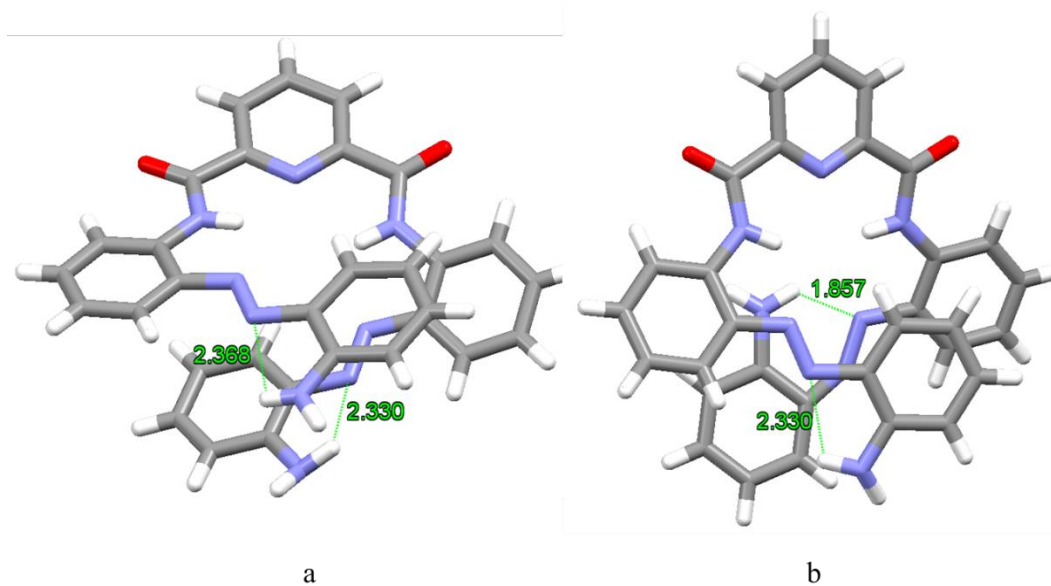


Figure S65. Solid state analysis of **1•butanone** in the unit cell highlighting the close contacts between the terminal acetyl amide and the adjacent azo N atoms.¹⁶ Where the disorder component is denoted using 'a' for the majority occupancy component and 'b' for the minority occupancy component.

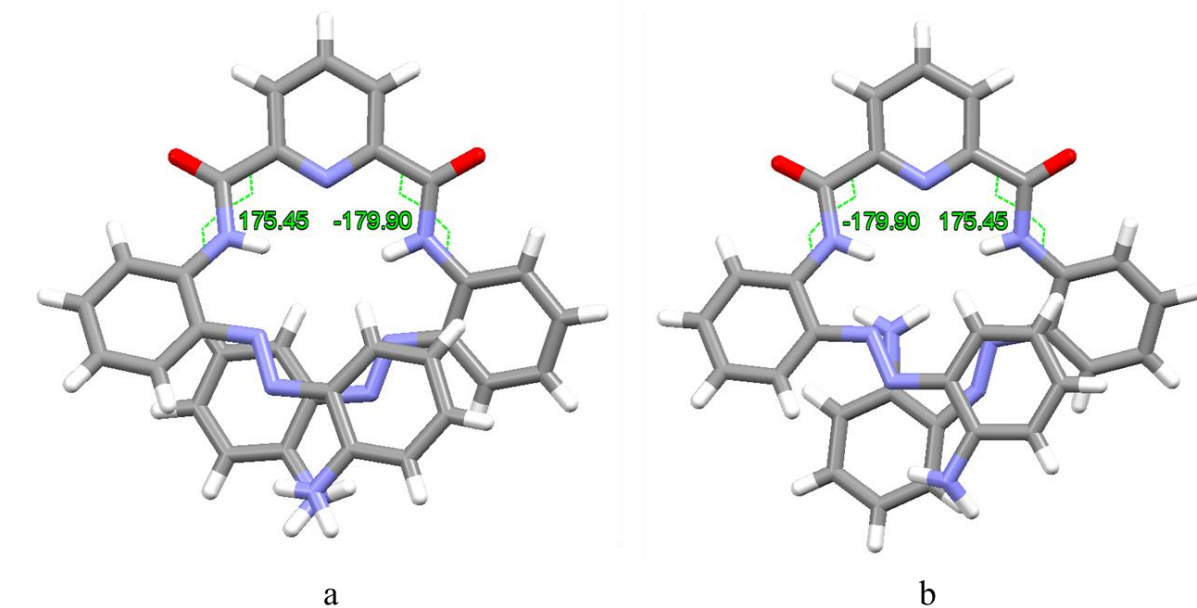


Figure S66. Solid state analysis of **1•butanone** in the unit cell highlighting the torsion angles of the internal peptide bonds. Where the disorder component is denoted using ‘a’ for the majority occupancy component and ‘b’ for the minority occupancy component.

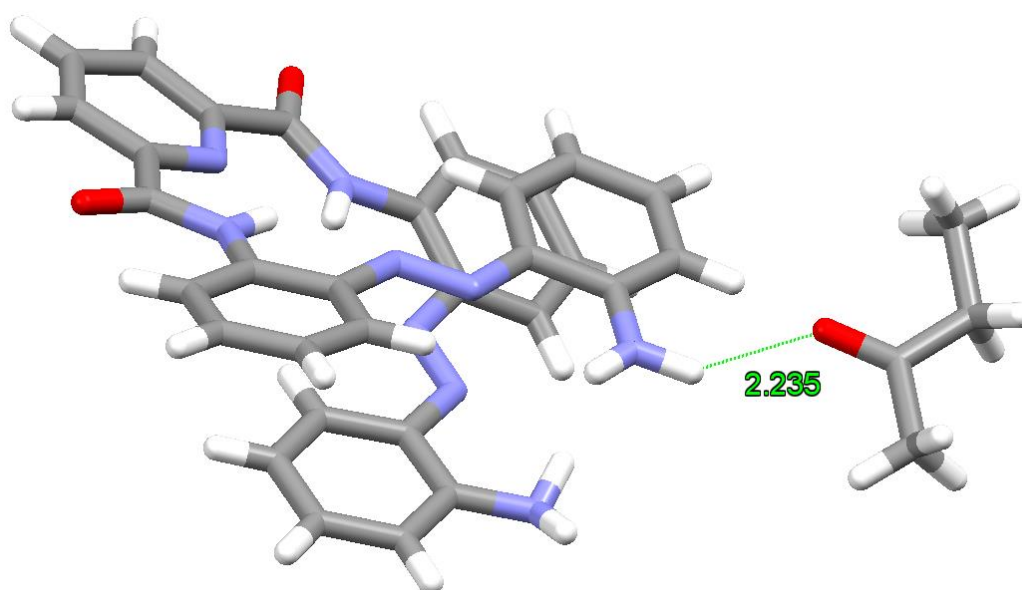


Figure S67. Solid state analysis of the majority component of **1•butanone** highlighting the presence of intermolecular N-H...O hydrogen-bonding interactions¹⁷ between an NH of a terminal amine functionality on the foldamer molecule and the O atom of a butanone solvent molecule.

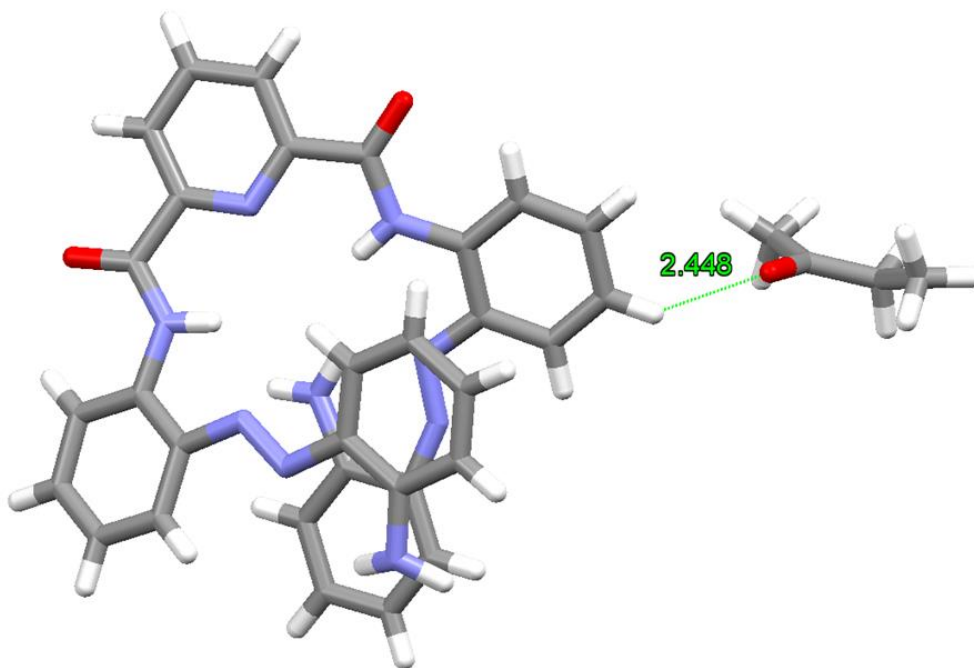


Figure S68. Solid state analysis of the minority component of **1•butanone** highlighting the presence of intermolecular N-H...O hydrogen-bonding interactions^{17,19} between an NH of a terminal amine functionality on the foldamer molecule and the O atom of a butanone solvent molecule.

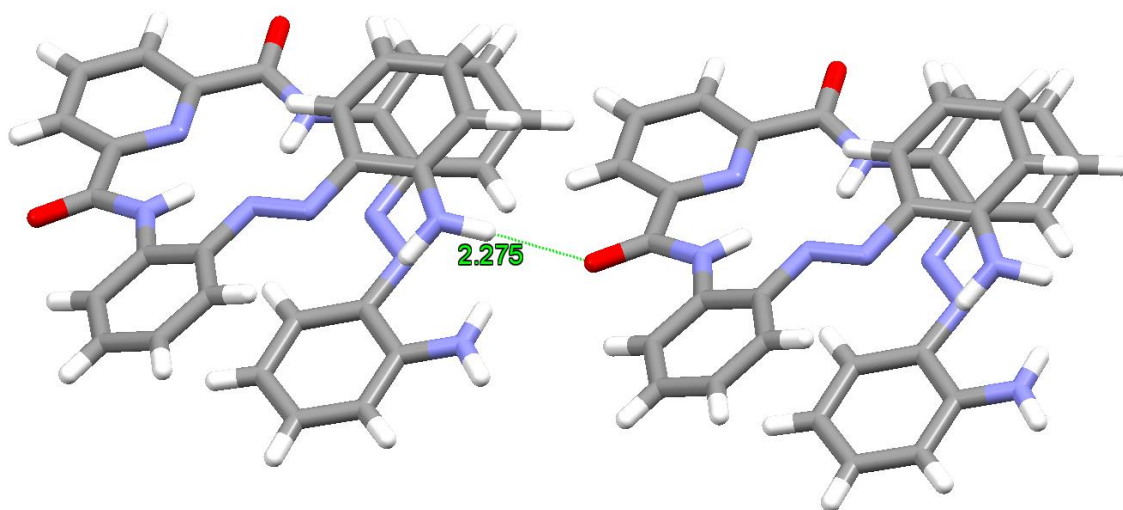


Figure S69. Solid state analysis of **1•butanone** highlighting the presence of an intermolecular N-H...O hydrogen-bonding interaction¹⁷ between the NH atoms of the terminal amine functionalities on one molecule and O atom of a carbonyl group of a carboxamide unit in an adjacent foldamer molecule. This interaction is consistent as the disordered aniline is not participating.

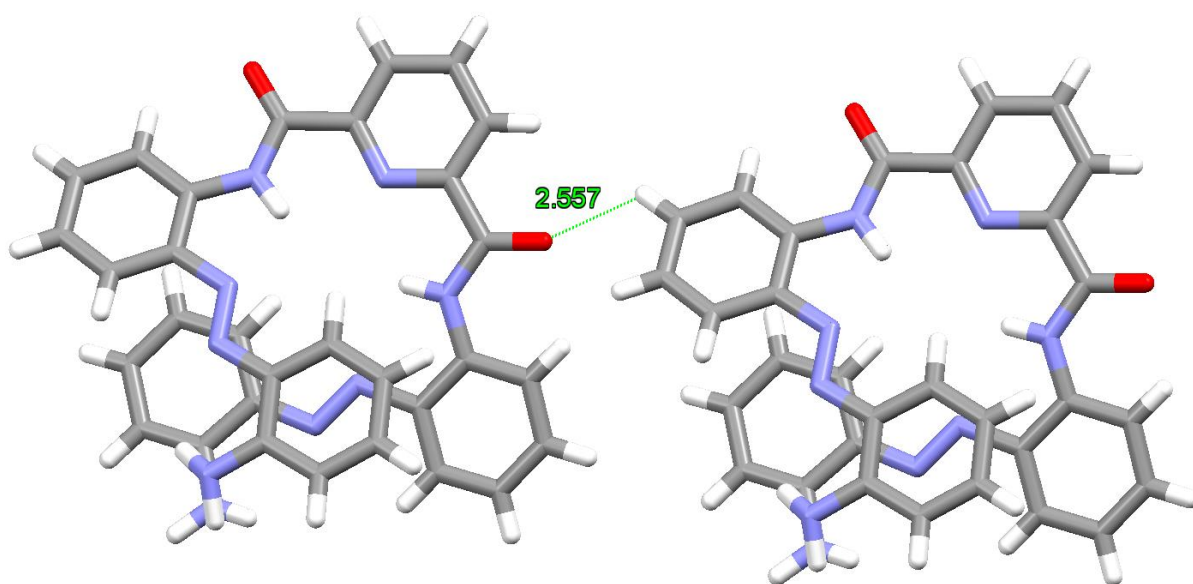


Figure S70. Solid state analysis of **1•butanone** highlighting the presence of an intermolecular C-H...O hydrogen-bonding interaction between an aromatic proton on a foldamer molecule and O atom of a carbonyl group of a carboxamide unit in an adjacent foldamer molecule. This interaction is consistent as the disordered aniline is not participating.

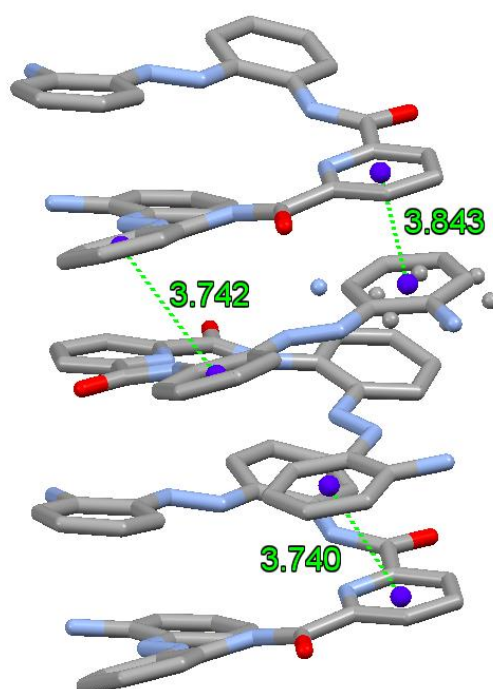


Figure S71. Solid state analysis of the offset face-to-face π - π stacking interactions¹⁸ observed between molecules of **1•butanone** when considering the majority component of the disordered aniline.

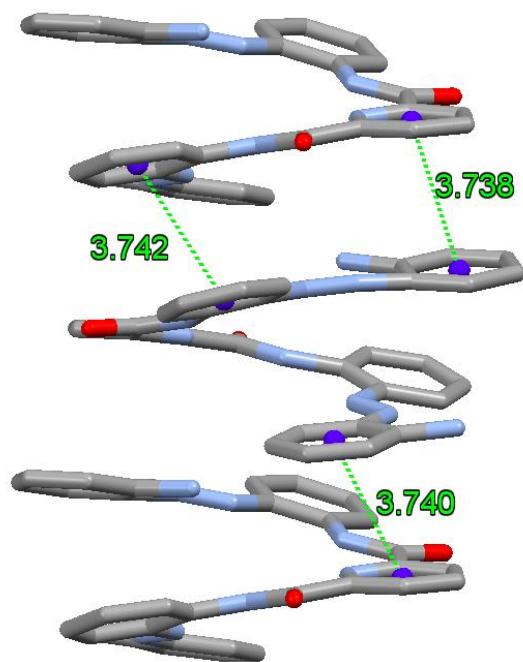


Figure S72. Solid state analysis of the offset face-to-face π - π stacking interactions¹⁸ observed between molecules of **1-butanol** when considering the minority component of the disordered aniline.

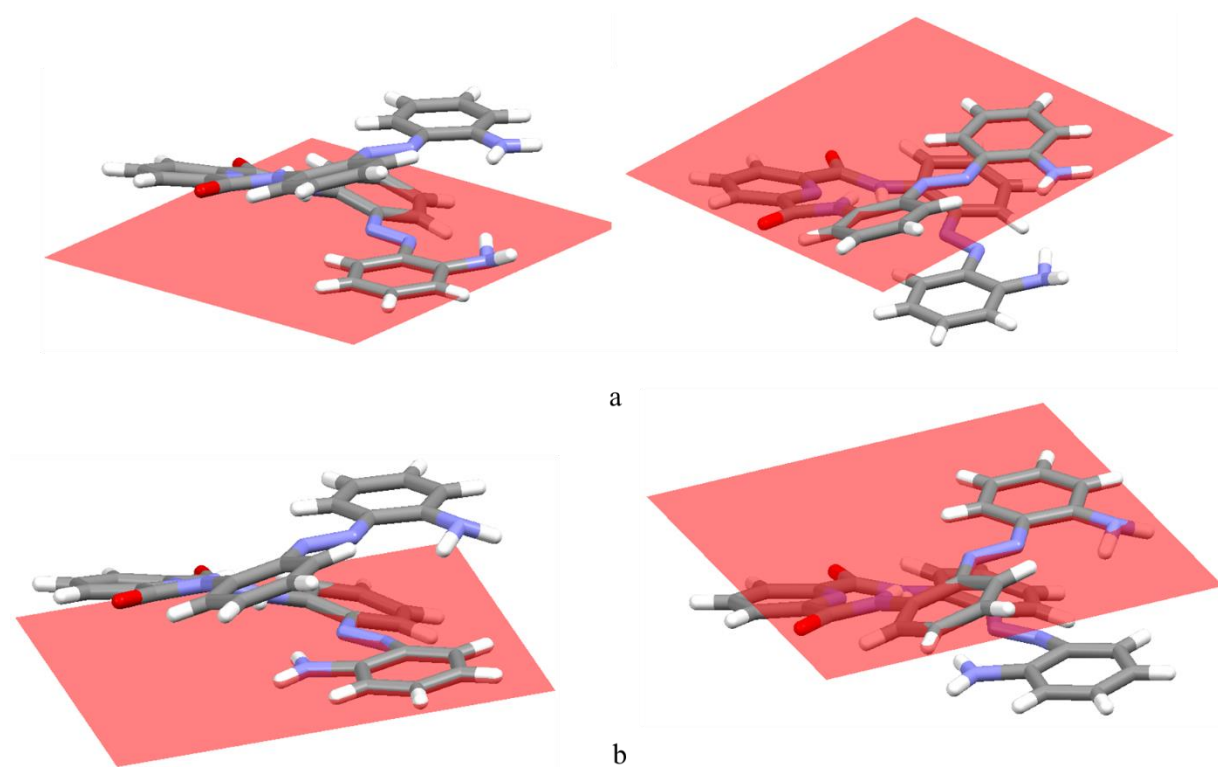


Figure S73. Solid state analysis of a foldamer molecule in the unit cell of **1-butanol**, where the disordered occupancy is denoted using 'a' for the majority component and 'b' for the minority component, highlighting the plane of the terminal aniline groups.

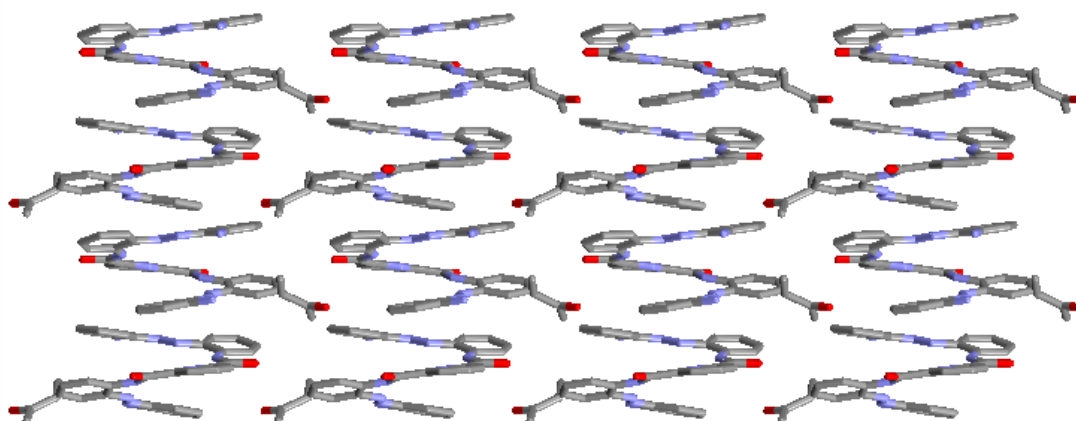


Figure S74. Solid state analysis showing the crystal packing of **1-butanone** as viewed along the *a* axis when considering the majority component of the disordered aniline. H atoms have been removed for clarity.

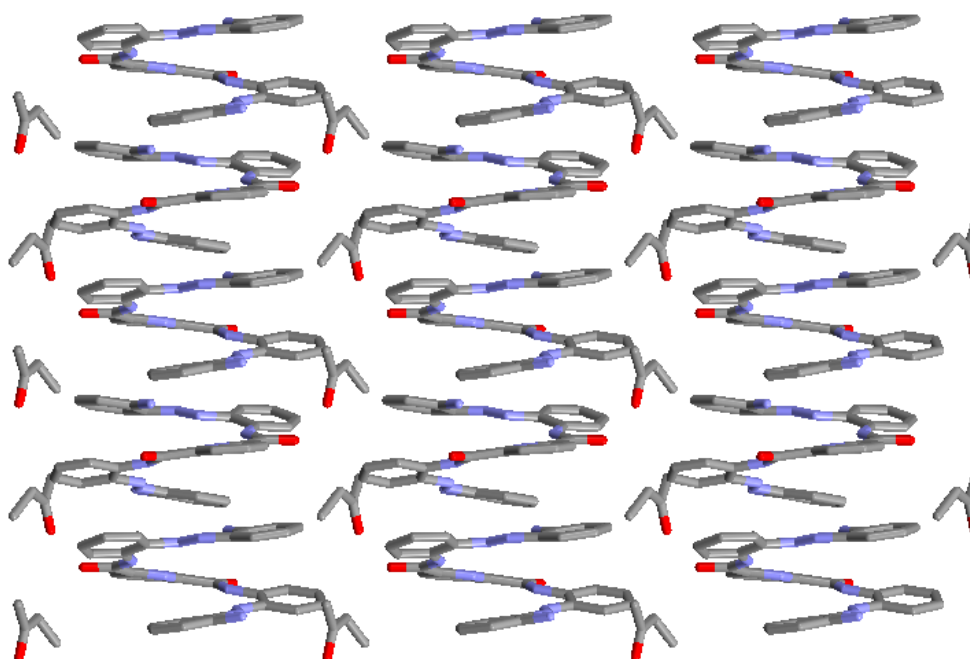


Figure S75. Solid state analysis showing the crystal packing of **1-butanone** as viewed along the *a* axis when considering the minority component of the disordered aniline. H atoms have been removed for clarity.

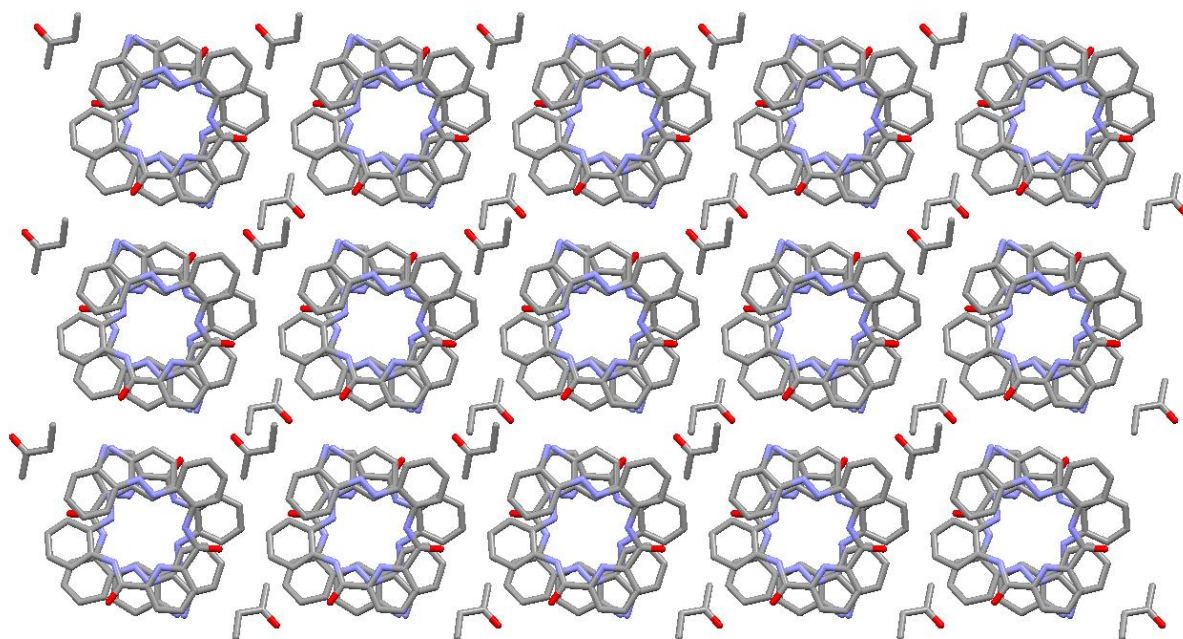


Figure S76. Solid state analysis showing the crystal packing of **1•butanone** as viewed along the *b* axis when considering the majority component of the disordered aniline. H atoms have been removed for clarity.

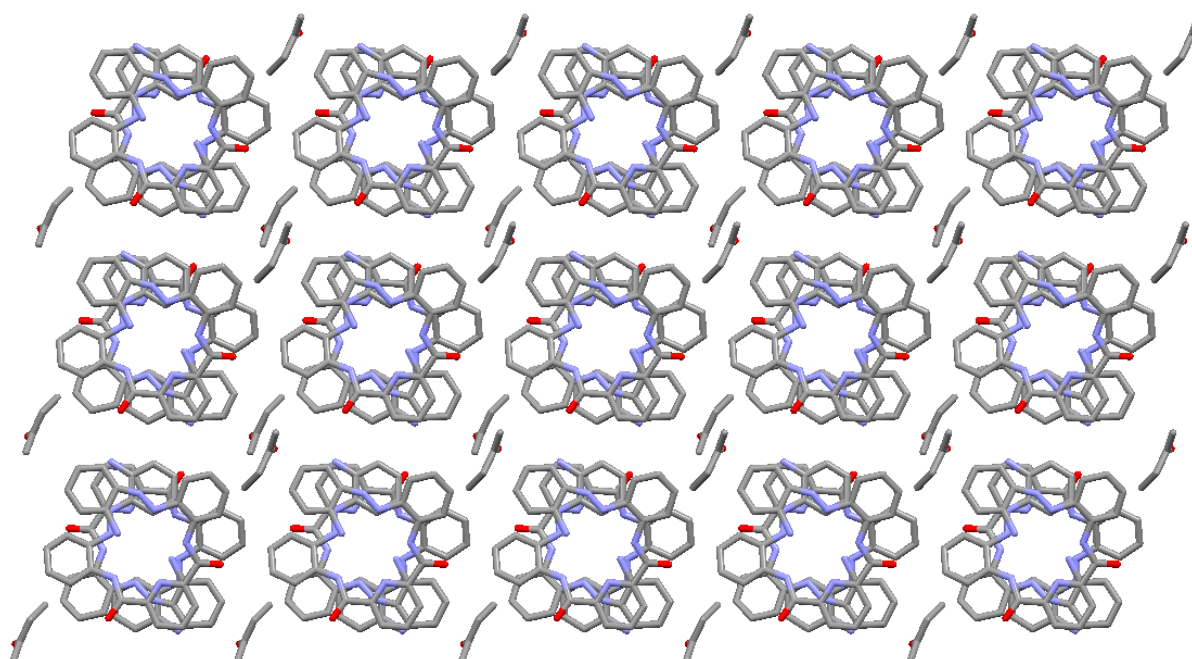


Figure S77. Solid state analysis showing the crystal packing of **1•butanone** as viewed along the *b* axis when considering the minority component of the disordered aniline. H atoms have been removed for clarity.

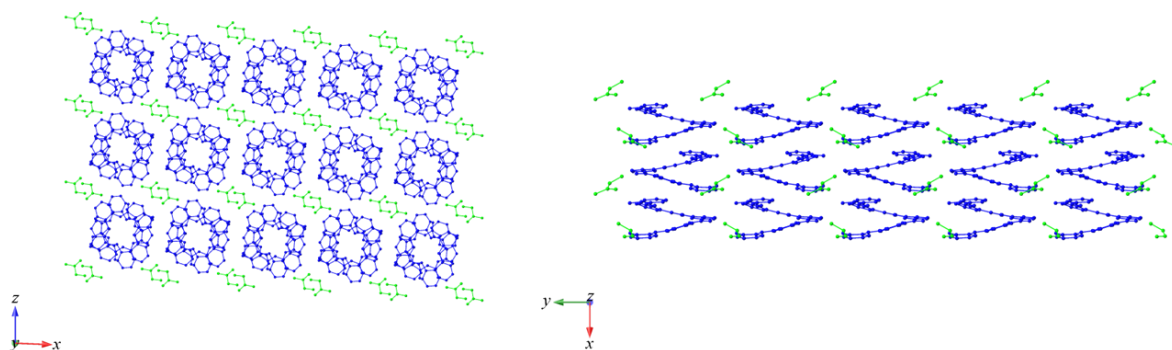


Figure S78. Solid state analysis showing the crystal packing of the majority disorder component of **1-butanone** with a chemical occupancy of 69.5(7)% showing columns and rows of right-handed stacks. Hydrogen atoms have been removed for clarity, solvent molecules are shown in green, and molecules have been coloured in accordance with handedness, where blue represents right (P).

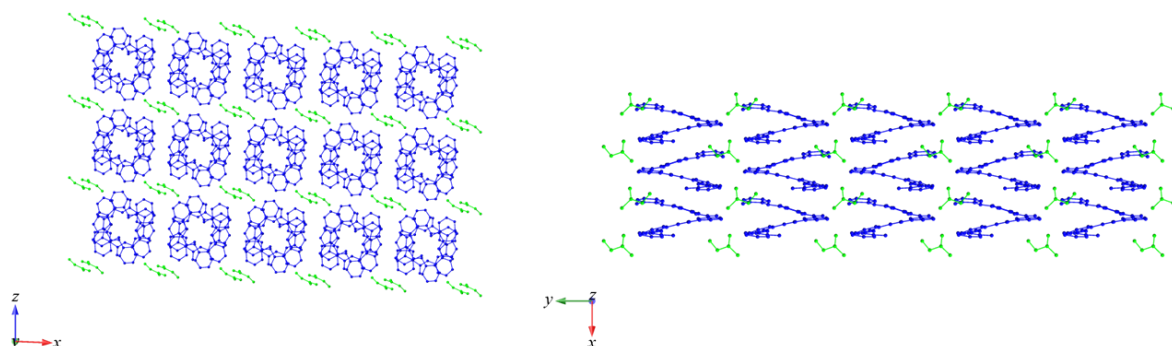


Figure S79. Solid state analysis showing the crystal packing of the minority disorder component of **1-butanone** with a chemical occupancy of 30.5(7)% showing columns and rows of right-handed stacks. Hydrogen atoms have been removed for clarity, solvent molecules are shown in green, and molecules have been coloured in accordance with handedness, where blue represents right (P).

f) Solid state analysis of 1·DCM

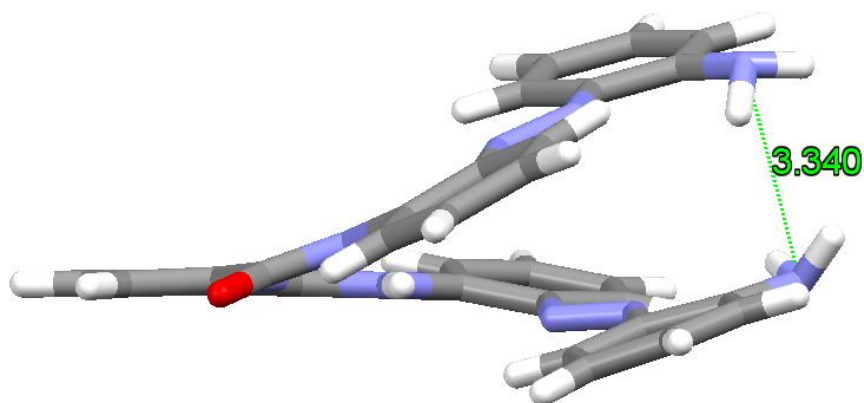


Figure S80. Solid state analysis of **1·DCM**, showing helical pitch (distance between N atoms at each terminus).

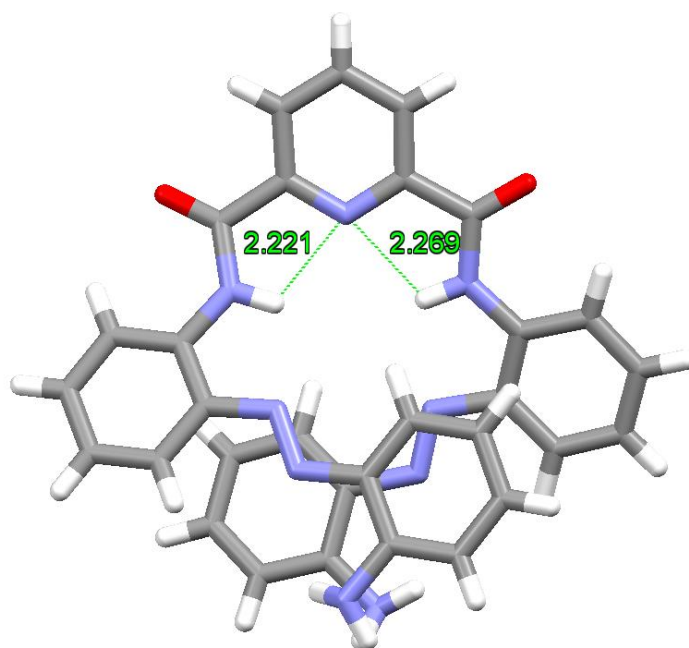


Figure S81. Solid state analysis of **1·DCM** in the unit cell highlighting the presence of bifurcated¹⁴ intramolecular N-H...N hydrogen bonding interactions involving the N atom of the pyridine and the two NH's of the adjacent amide bonds leading to the *syn-syn* conformation about the central pyridinecarboxamide unit.¹⁵

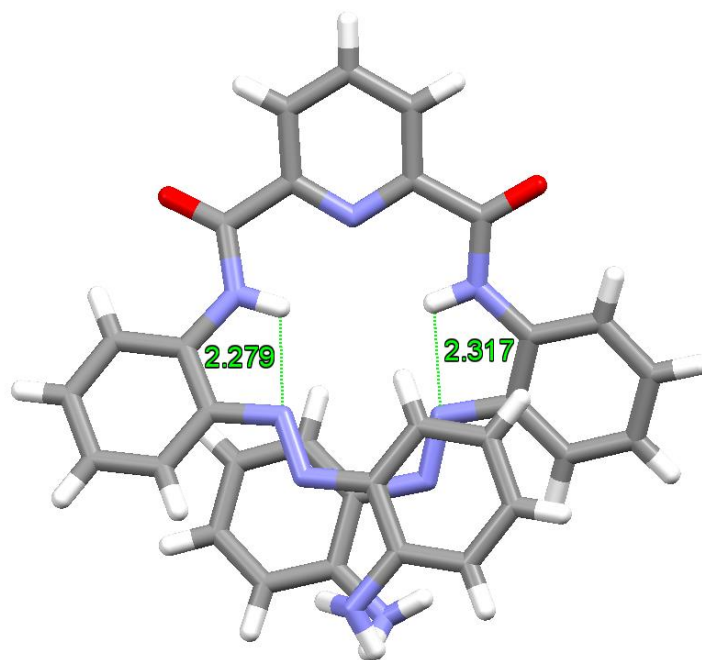


Figure S82. Solid state analysis of **1-DCM** in the unit cell highlighting the close contacts between the pyridyl amide NHs and the adjacent azo N atoms.¹⁶

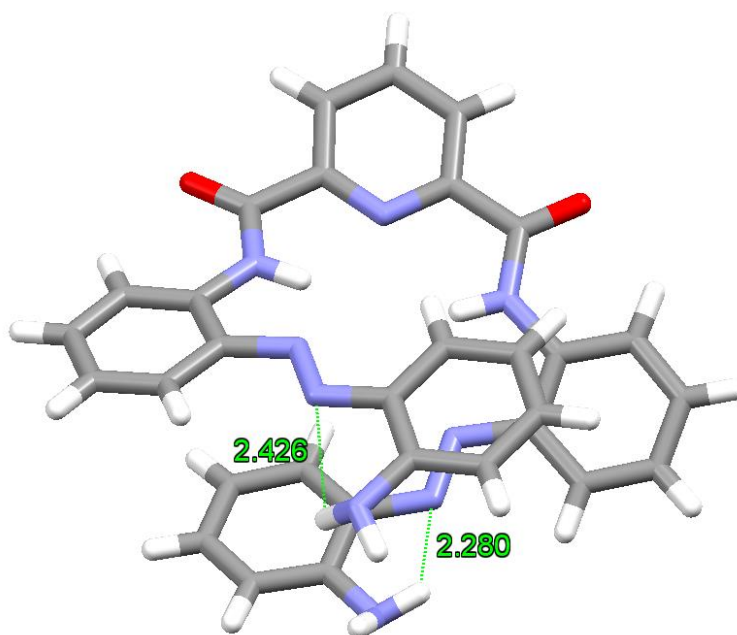


Figure S83. Solid state analysis of **1-DCM** in the unit cell highlighting the close contacts between the terminal acetyl amide and the adjacent azo N atoms.¹⁶

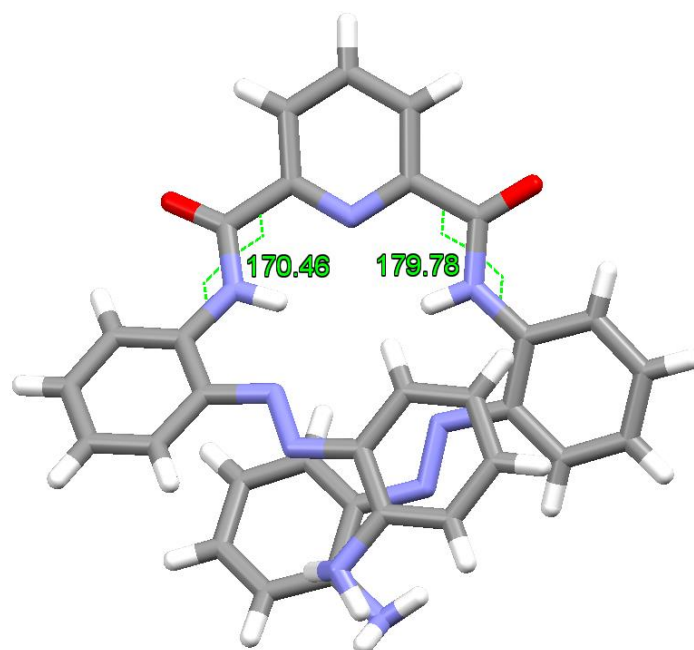


Figure S84. Solid state analysis of **1·1·DCM** in the unit cell highlighting the torsion angles of the internal peptide bonds.

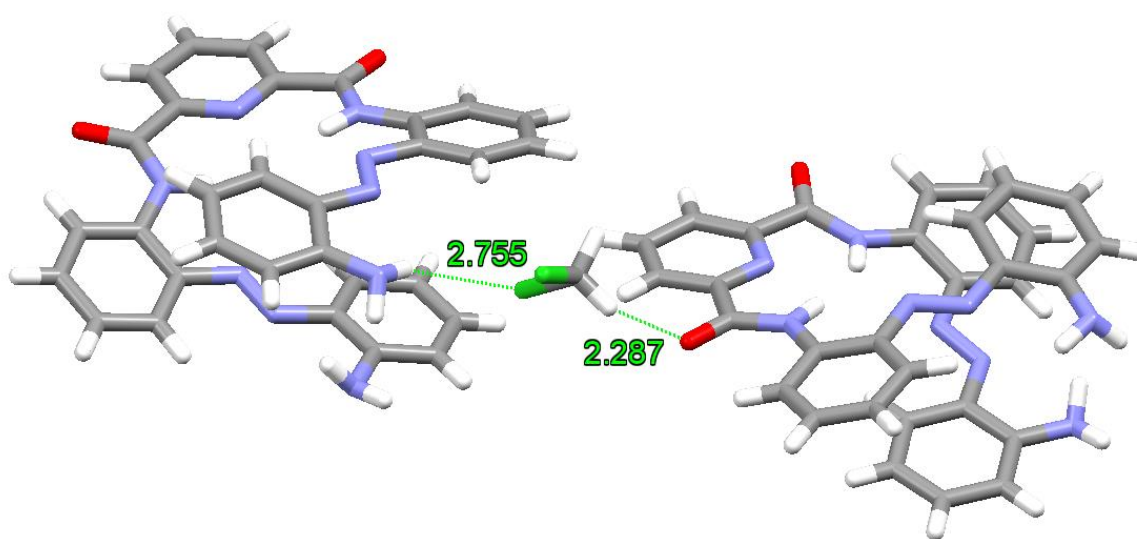


Figure S85. Solid state analysis of **1·DCM** highlighting the presence of intermolecular N-H...Cl and C-H...O hydrogen-bonding interactions.^{17,19} The interactions are formed between the NH of one of terminal amine functionalities of a foldamer molecule and a chloride atom on a dichloromethane solvent molecule and between O atom of a carbonyl group in the carboxamide unit of a foldamer and an aliphatic proton on a dichloromethane solvent molecule.

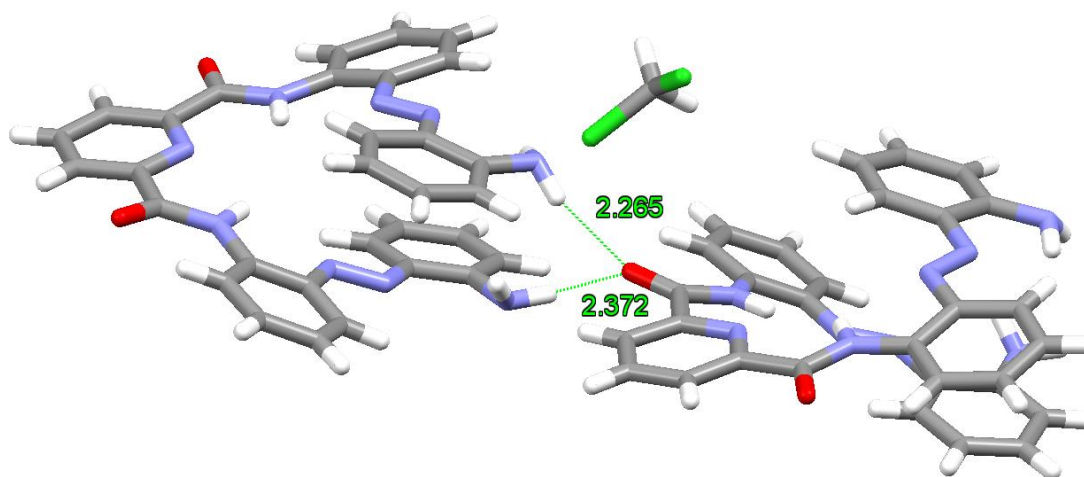


Figure S86. Solid state analysis of **1·1·DCM** highlighting the presence of an intermolecular bifurcated N-H...O hydrogen-bonding interaction between the NH atoms of the terminal amine functionalities on one molecule and O atom of a carbonyl group of a carboxamide unit in an adjacent foldamer molecule.

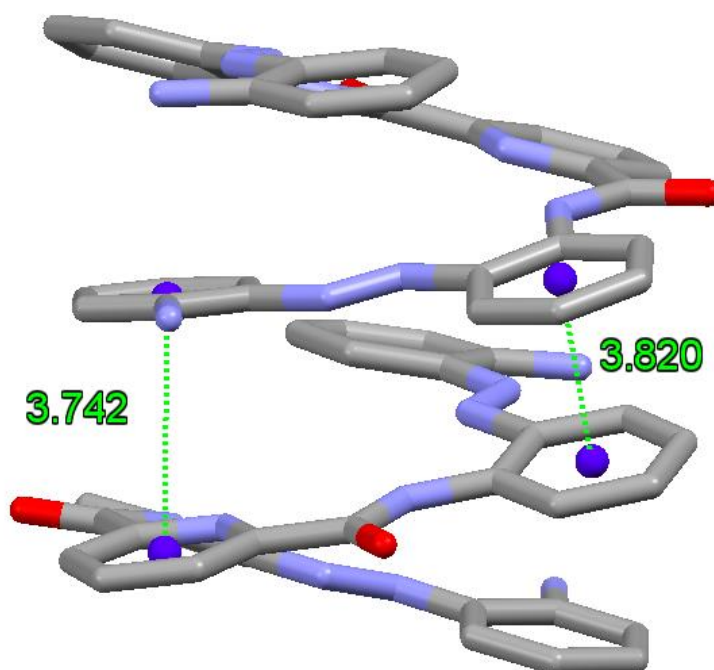


Figure S87. Solid state analysis of the offset face-to-face π - π stacking interactions¹⁸ observed between molecules of **1·DCM**. Hydrogen atoms have been removed for clarity.

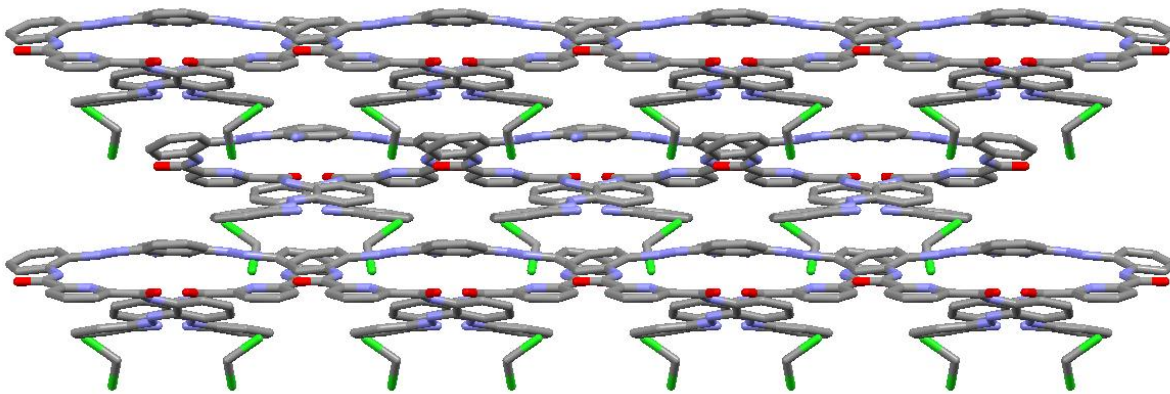


Figure S88. Solid state analysis showing the crystal packing of **1•DCM** as viewed along the *a* axis. H atoms have been removed for clarity.

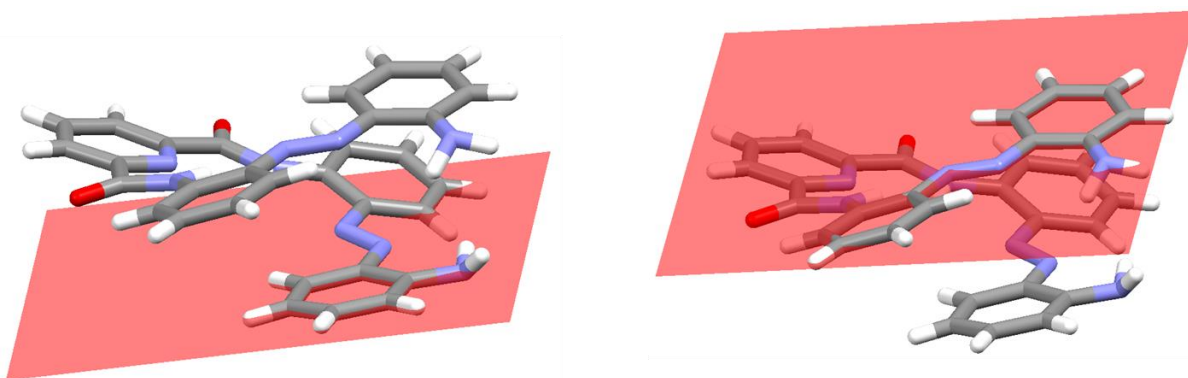


Figure S89. Solid state analysis of a foldamer molecule in the unit cell of **1•DCM**, highlighting the plane of the terminal aniline groups.

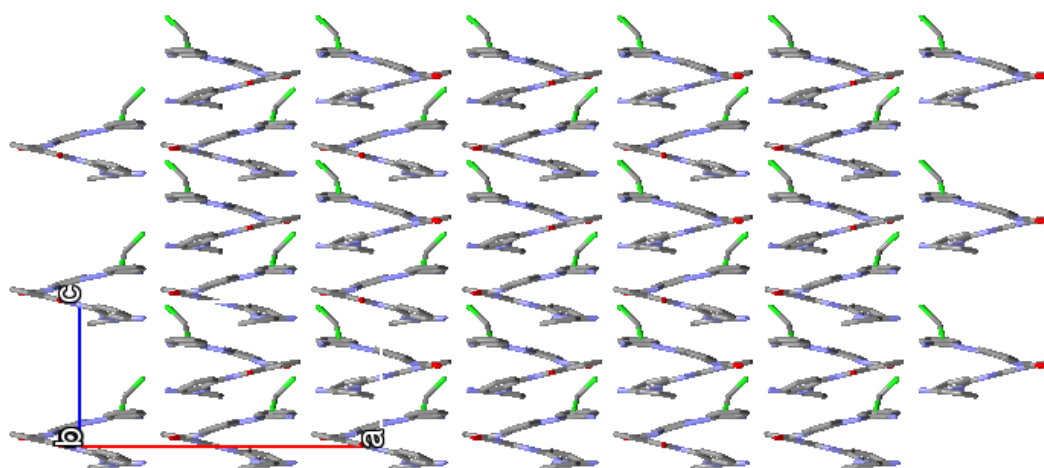


Figure S90. Solid state analysis showing the crystal packing of **1•DCM** as viewed along the *b* axis. H atoms have been removed for clarity.

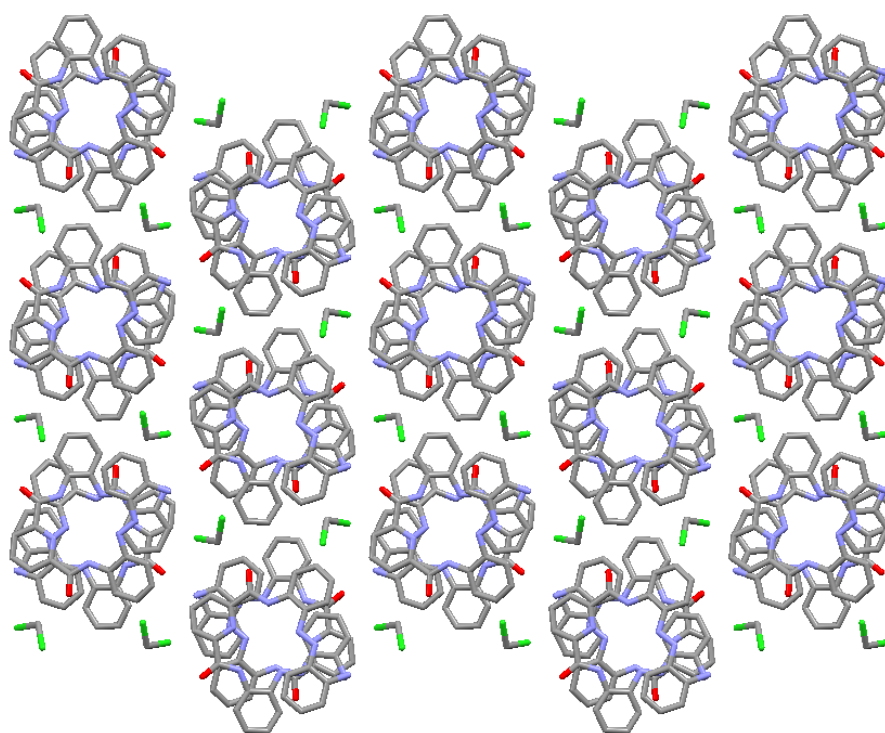


Figure S91. Solid state analysis showing the crystal packing of **1•DCM** as viewed along the *c* axis. H atoms have been removed for clarity.

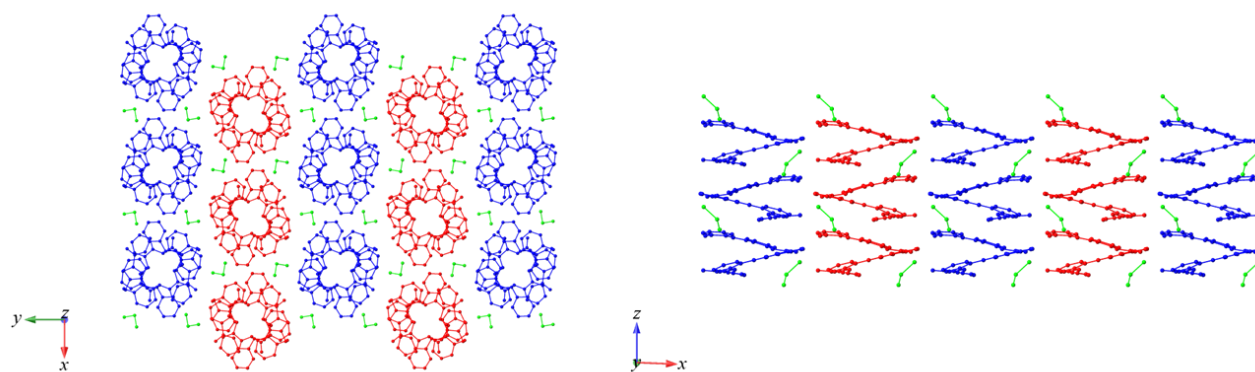


Figure S92. Solid state analysis showing the crystal packing of **1·DCM** showing columns of like-handed stacks, which alternate handedness between columns. Hydrogen atoms have been removed for clarity, solvent molecules are shown in green, molecules have been coloured in accordance with handedness, where red represents left (M), and blue represents right (P).

g) Solid state analysis of **1·MeOH**

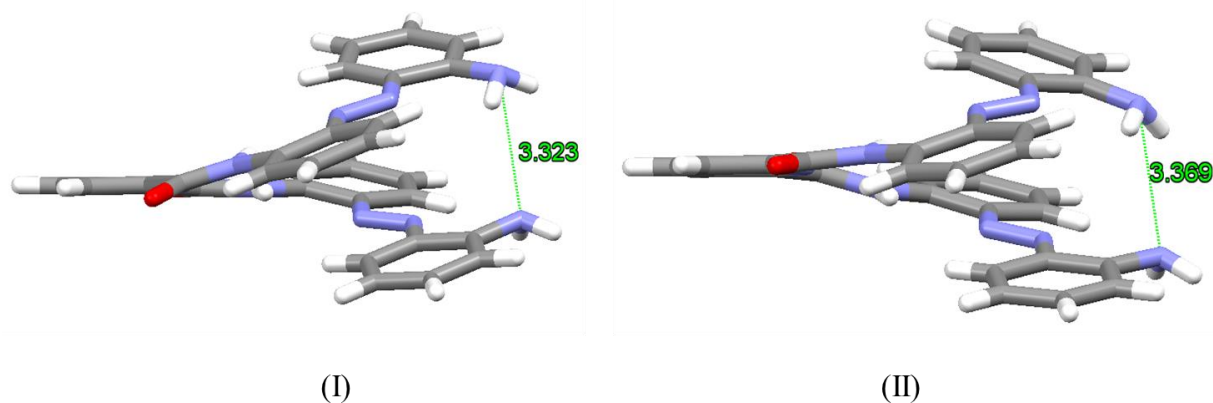


Figure S93. Solid state analysis of the two crystallographically unique molecules in the unit cell of **1·MeOH**, showing helical pitch (distance between N atoms at each terminus).

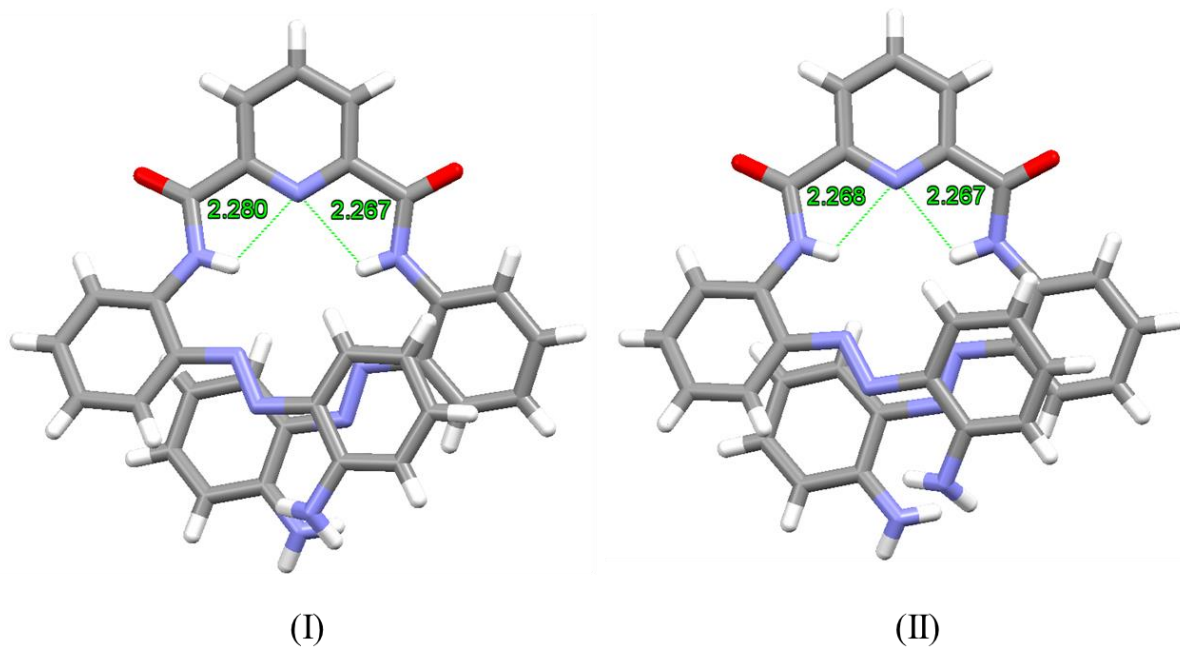


Figure S94. Solid state analysis of the two crystallographically unique molecules of **1·MeOH** in the unit cell, highlighting the presence of bifurcated¹⁴ intramolecular N-H···N hydrogen bonding interactions¹⁴ involving the N atom of the pyridine and the two NH's of the adjacent amide bonds leading to the *syn-syn* conformation about the central pyridinecarboxamide unit.¹⁵

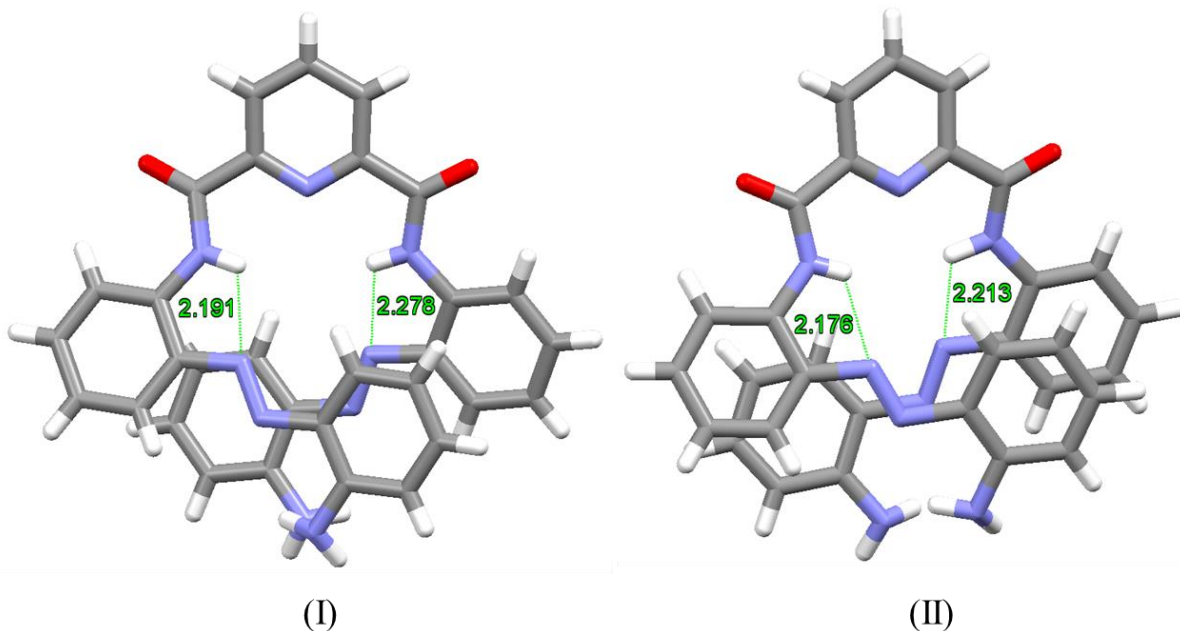


Figure S95. Solid state analysis of the two crystallographically unique molecules in the unit cell of **1·MeOH**, highlighting the close contacts between the pyridyl amide NHs and the adjacent azo N atoms.¹⁶

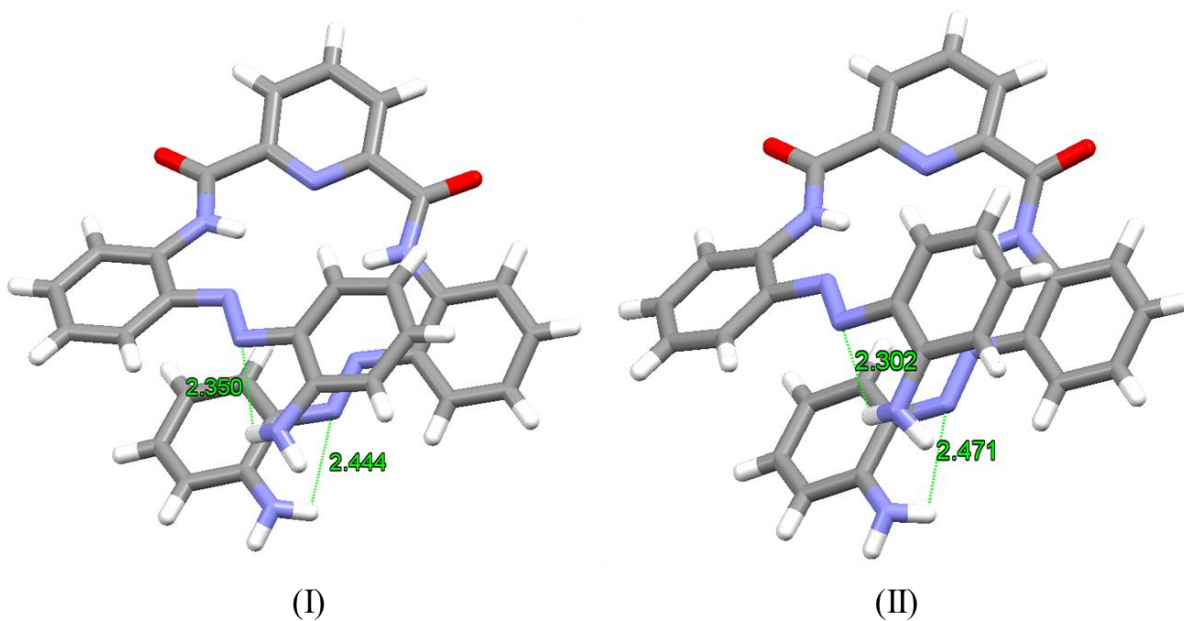


Figure S96. Solid state analysis of the two crystallographically unique molecules in the unit cell of **1·MeOH**, highlighting the close contacts between the terminal acetyl amide and the adjacent azo N atoms.¹⁶

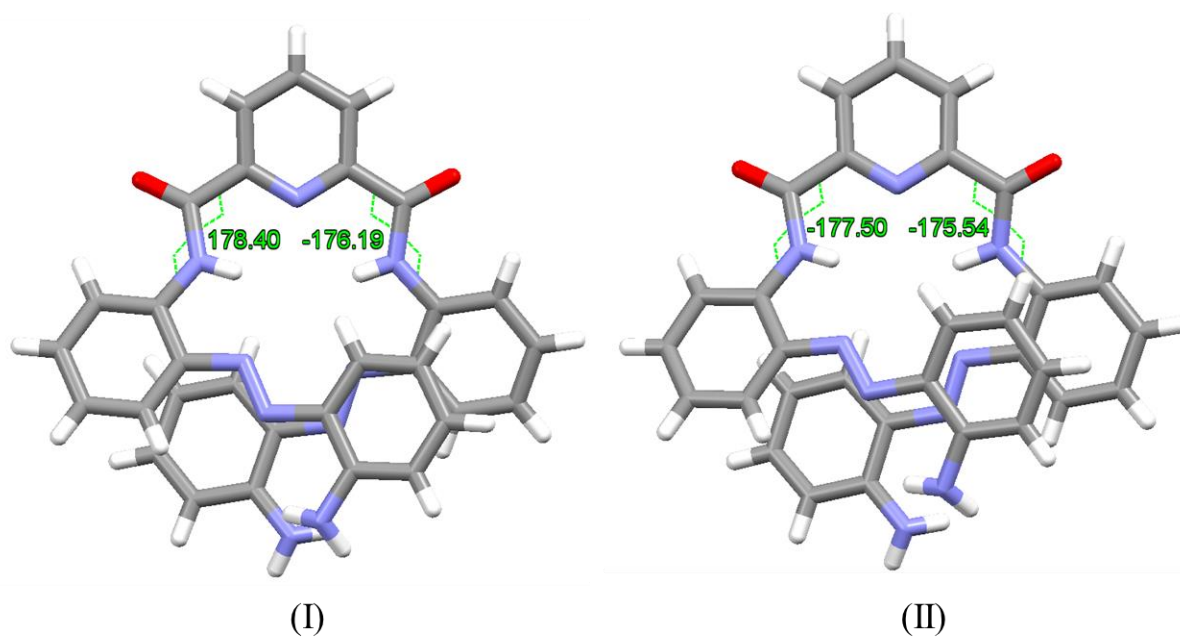


Figure S97. Solid state analysis of the two crystallographically unique molecules in the unit cell of **1·MeOH**, highlighting the torsion angles of the internal peptide bonds.

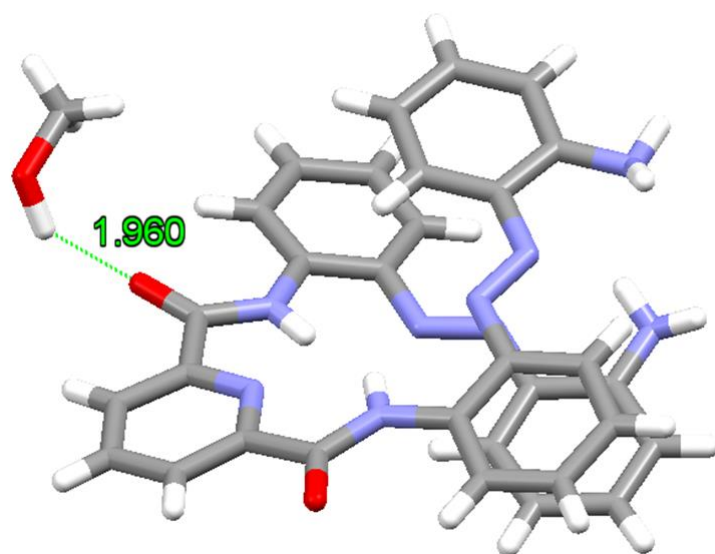


Figure S98. Solid state analysis of **1**·MeOH highlighting the presence of intermolecular O-H···O hydrogen-bonding interactions⁹ between a solvent molecule of methanol and the O atom of a carbonyl group of a molecule of I in the unit cell.

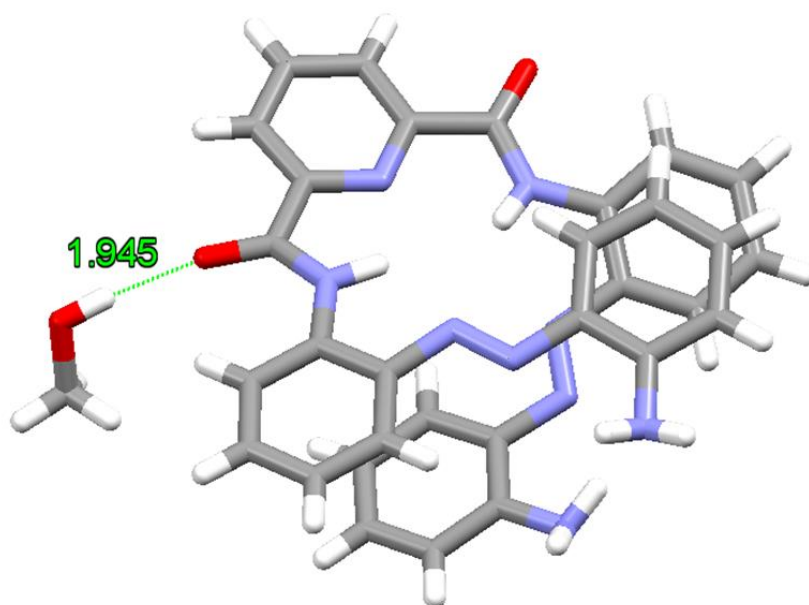


Figure S99. Solid state analysis of **1**·MeOH highlighting the presence of intermolecular O-H···O hydrogen-bonding interactions¹⁷ between a solvent molecule of methanol and the O atom of a carbonyl group of a molecule of II in the unit cell.

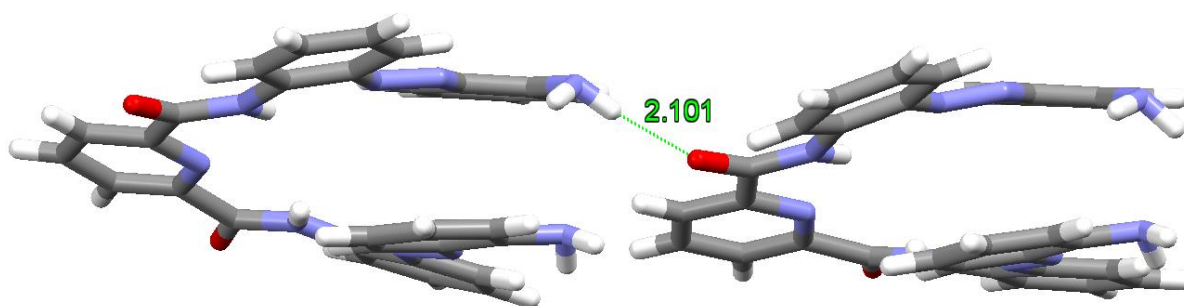


Figure S100. Solid state analysis of **1•MeOH** highlighting the presence of intermolecular N-H...O hydrogen-bonding interactions¹⁷ between the proton on the aniline ring of molecule of foldamer I and the O atom of a carbonyl group of foldamer molecule II.

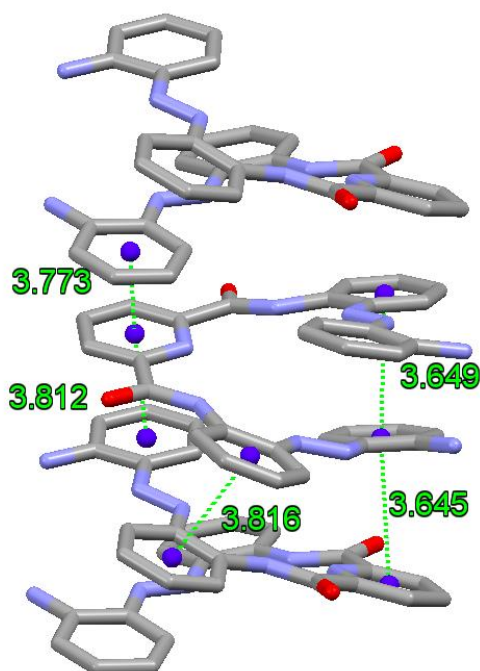


Figure S101. Solid state analysis of the offset face-to-face π - π stacking interactions¹⁸ observed between molecules of **1•MeOH**. Stacking in a I to II to I motif. Hydrogen atoms have been removed for clarity.

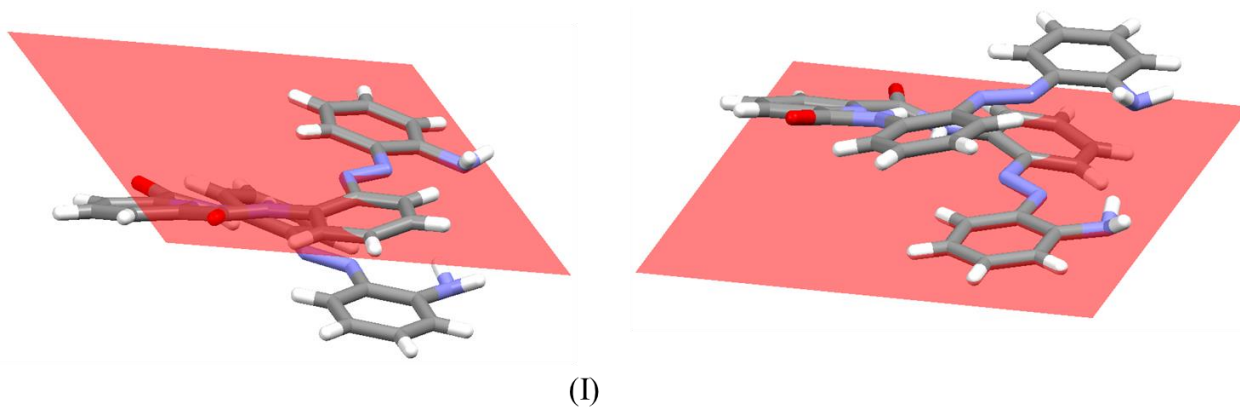


Figure S102. Solid state analysis of molecule I in the unit cell of **1•MeOH**, highlighting the plane of the terminal aniline groups.

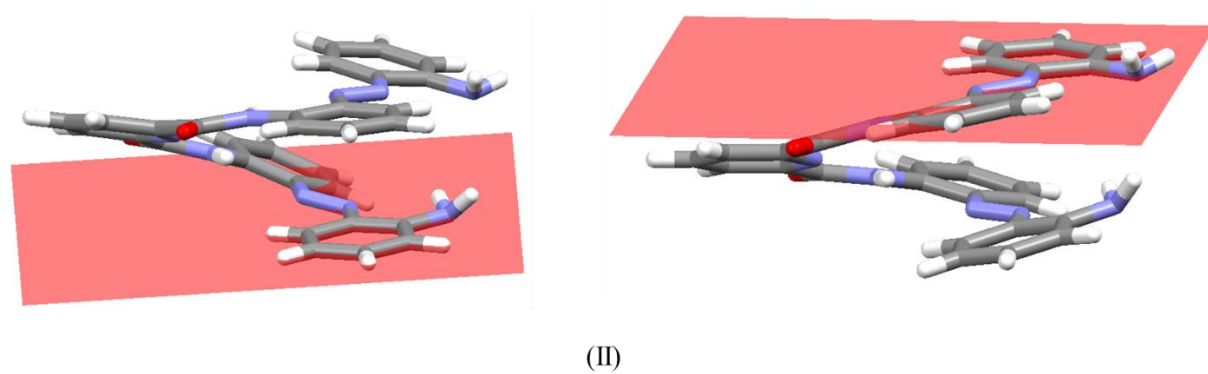


Figure S103. Solid state analysis of molecule II in the unit cell of **1•MeOH**, highlighting the plane of the terminal aniline groups.

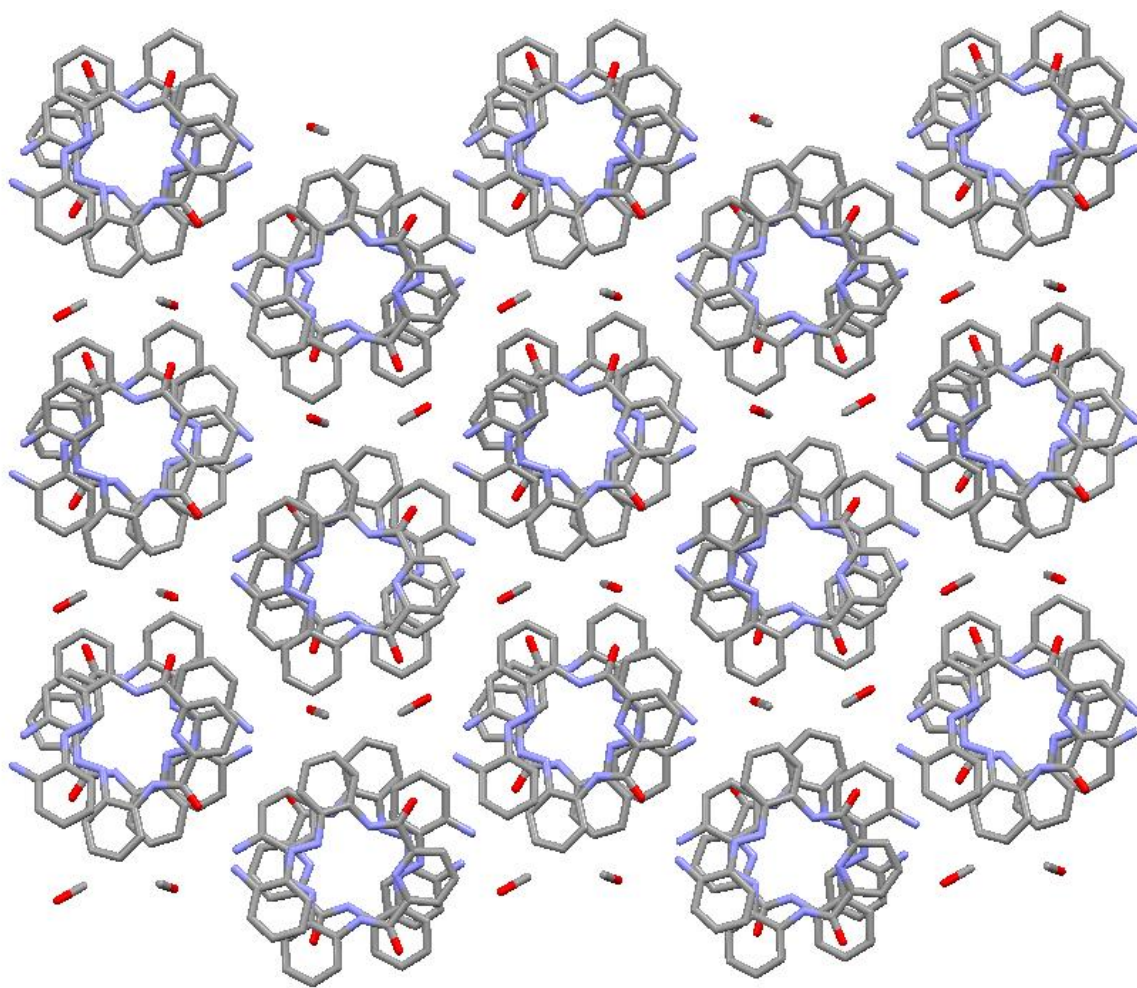


Figure S104. Solid state analysis showing the crystal packing of **1·MeOH** as viewed along the *b* axis. H atoms have been removed for clarity.

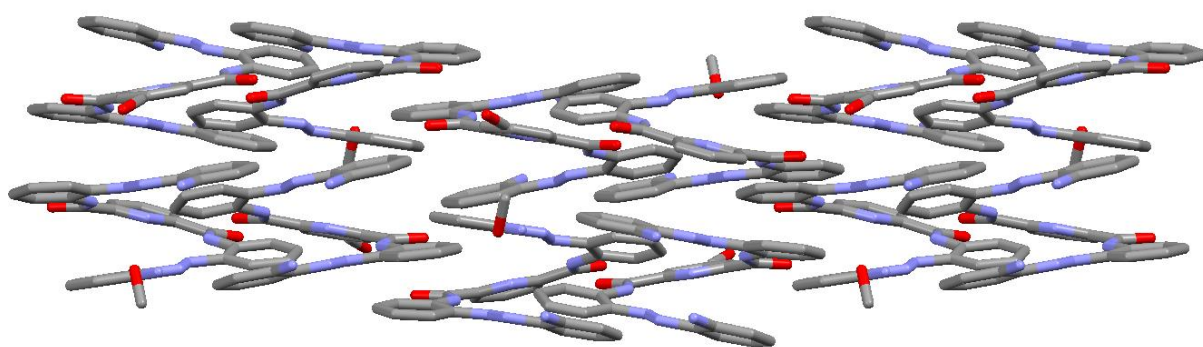


Figure S105. Solid state analysis showing the crystal packing of **1·MeOH** as viewed along the *a* axis. H atoms have been removed for clarity.

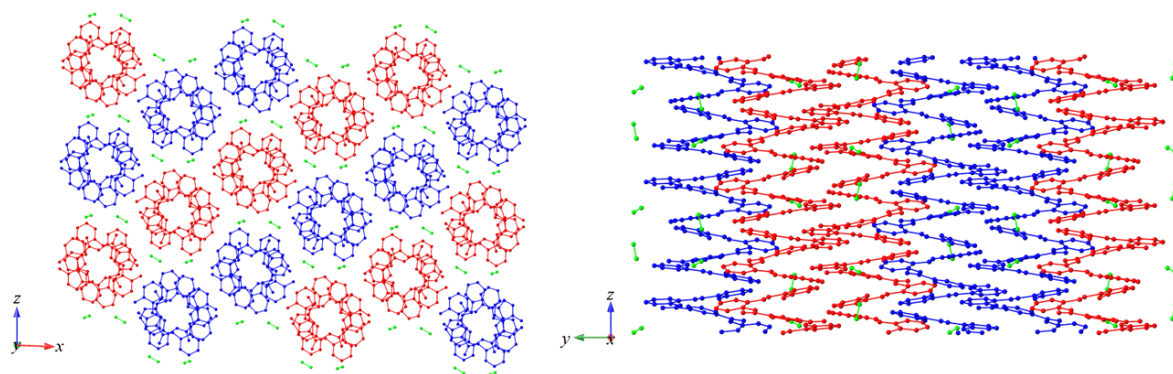


Figure S106. Solid state analysis showing the crystal packing of **1·MeOH** showing columns of like-handed stacks, which alternate handedness between a diagonal array of columns. Hydrogen atoms have been removed for clarity, solvent molecules are shown in green, molecules have been coloured in accordance with handedness, where red represents left (M), and blue represents right (P).

h) Solid state analysis of 1·DMSO



Figure S107. Solid state analysis of **1·DMSO**, showing helical pitch (distance between N atoms at each terminus) with the majority component shown as 'a' at 64.6(10)% occupancy and the minority component shown as 'b' with a 35.6(10)% occupancy, showing helical pitch. The structure shows positional disorder of the aniline moiety at one end of the molecule.

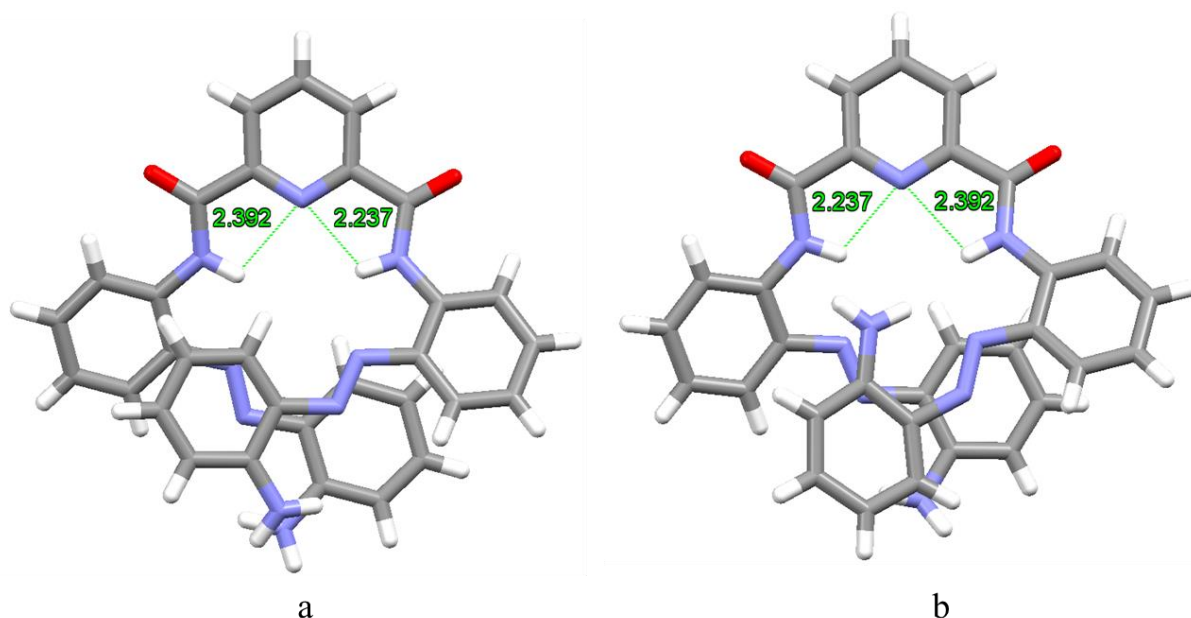


Figure S108. Solid state analysis of **1·DMSO** in the unit cell highlighting the presence of bifurcated¹⁴ intramolecular N-H...N hydrogen bonding interactions involving the N atom of the pyridine and the two NH's of the adjacent amide bonds leading to the *syn-syn* conformation

about the central pyridinecarboxamide unit.¹⁵ Where the disorder component is denoted using ‘a’ for the majority occupancy component and ‘b’ for the minority occupancy component.

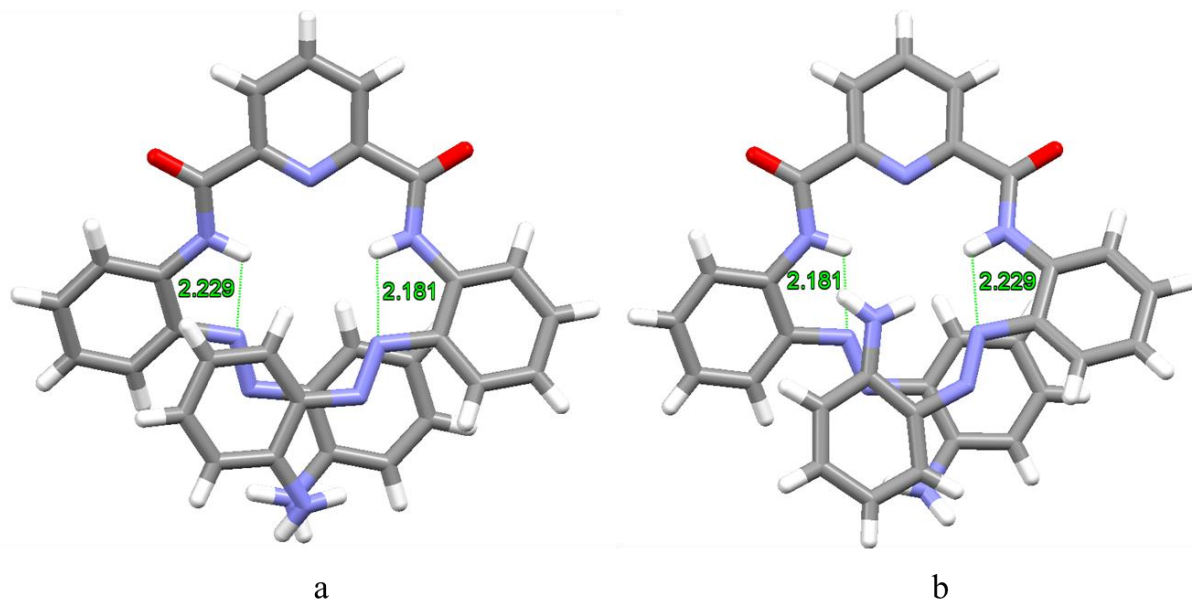


Figure S109. Solid state analysis of **1·DMSO** in the unit cell highlighting the close contacts between the pyridyl amide NHs and the adjacent azo N atoms.¹⁶ Where the disorder component is denoted using ‘a’ for the majority occupancy component and ‘b’ for the minority occupancy component.

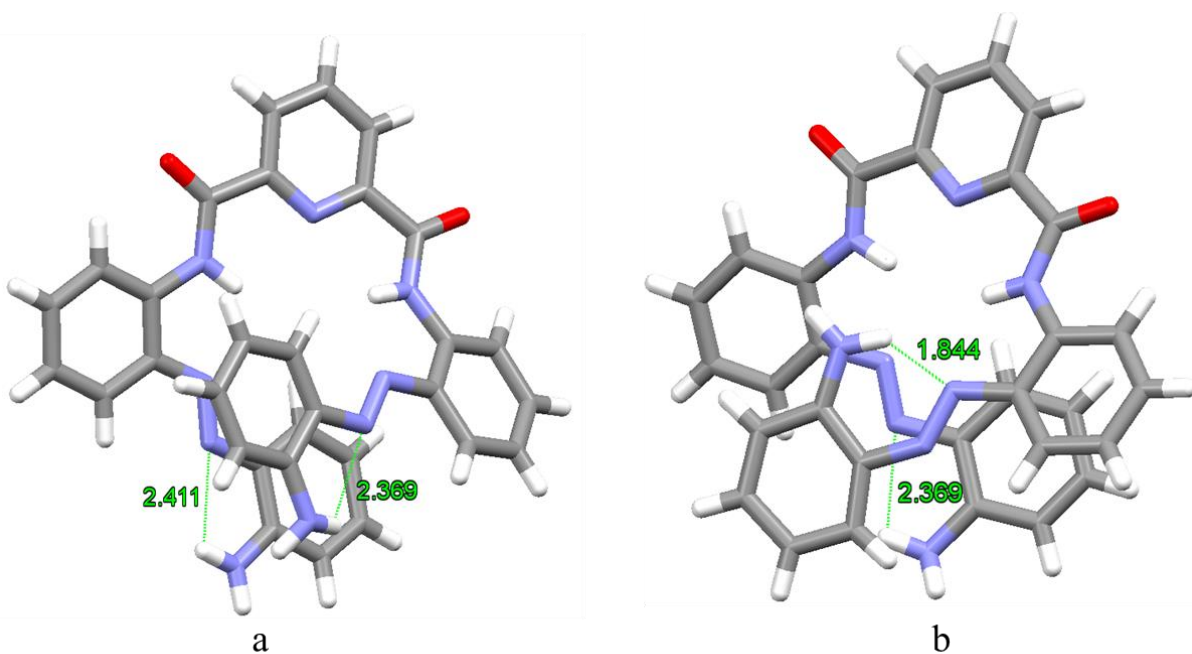


Figure S110. Solid state analysis of **1·DMSO** in the unit cell highlighting the close contact between the terminal amine functionality and the adjacent azo N atom.¹⁶ Where the disorder component is denoted using ‘a’ for the majority occupancy component and ‘b’ for the minority occupancy component.

component is denoted using 'a' for the majority occupancy component and 'b' for the minority occupancy component.

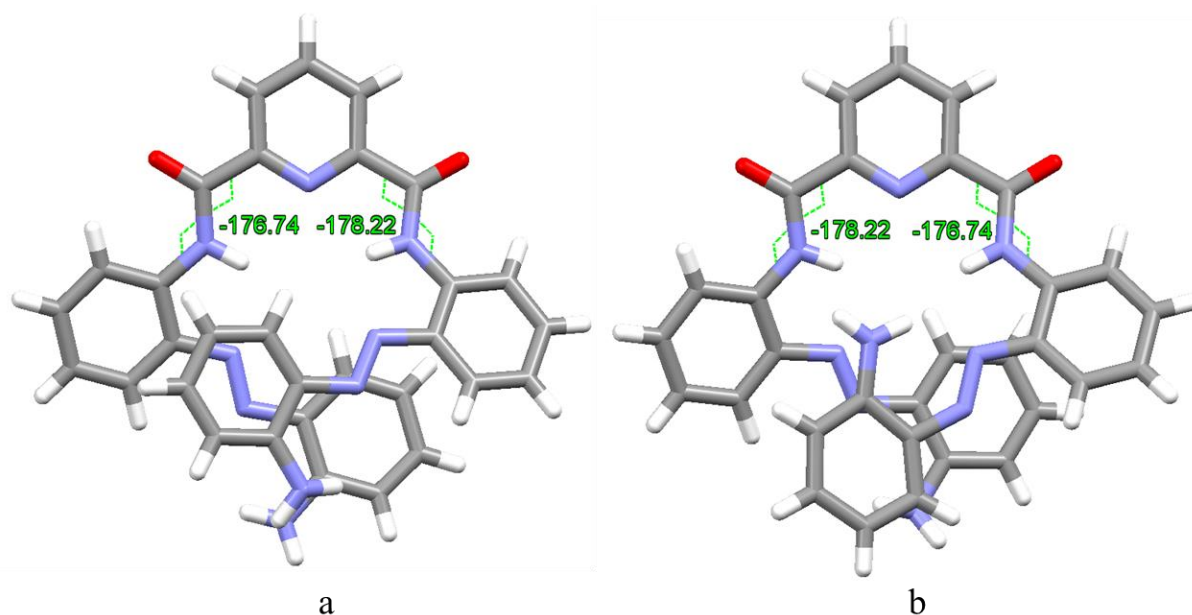


Figure S111. Solid state analysis of **1·DMSO** in the unit cell highlighting the torsion angles of the internal peptide bonds. Where the disorder component is denoted using 'a' for the majority occupancy component and 'b' for the minority occupancy component.

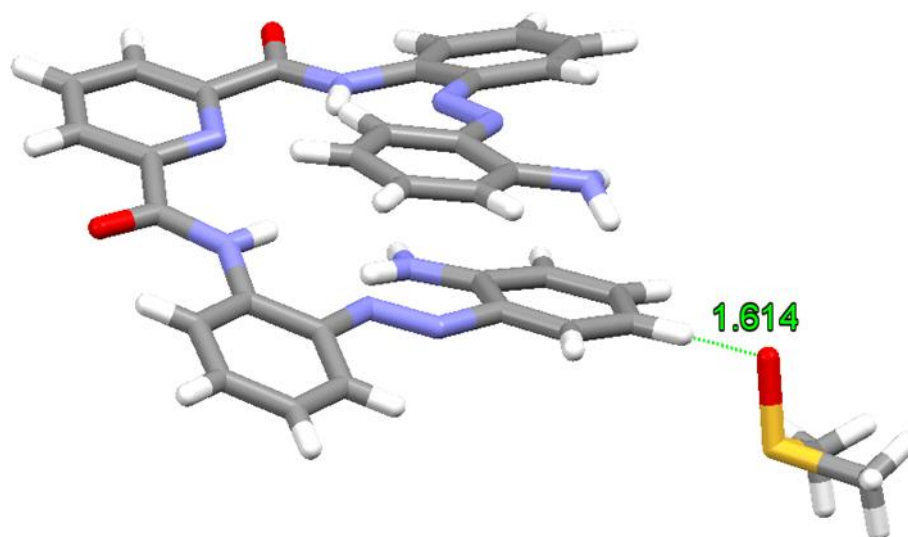


Figure S112. Solid state analysis of **1·DMSO** highlighting the presence of an intermolecular C-H...O hydrogen-bonding interaction¹⁹ between an aromatic proton on one foldamer and the O atom DMSO molecule.

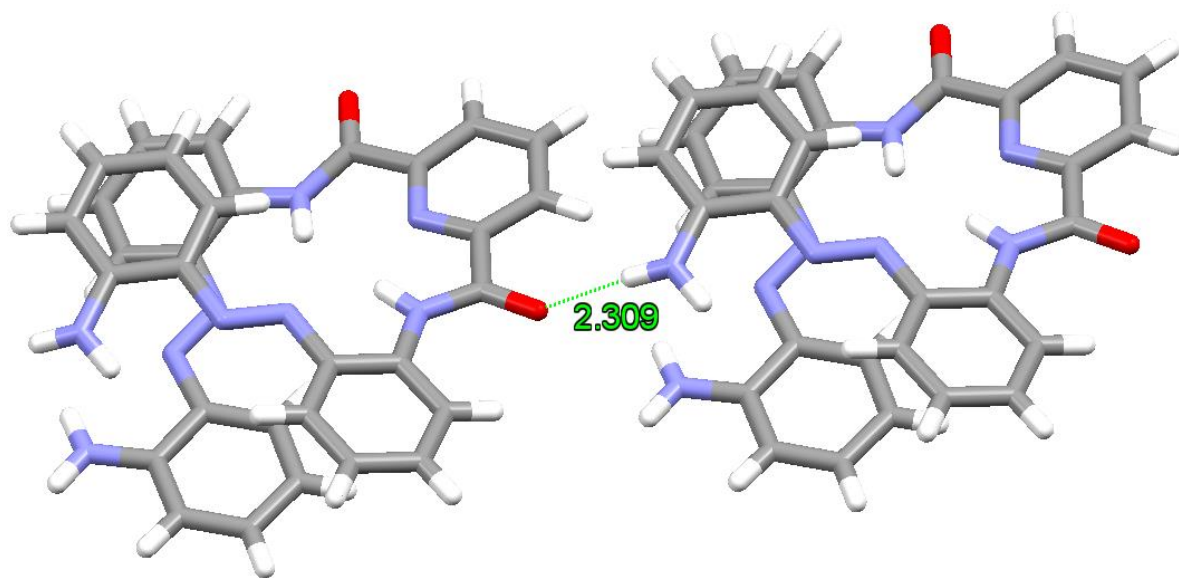


Figure S113. Solid state analysis of **1·DMSO** highlighting the presence of an intermolecular C-H...O hydrogen-bonding interaction¹⁷ within the majority occupancy component between an aromatic proton on one foldamer and the O atom of a carbonyl group of a carboxamide unit in an adjacent foldamer molecule. This interaction is observed in both parts as the positional disorder is localised on only one aniline moiety.

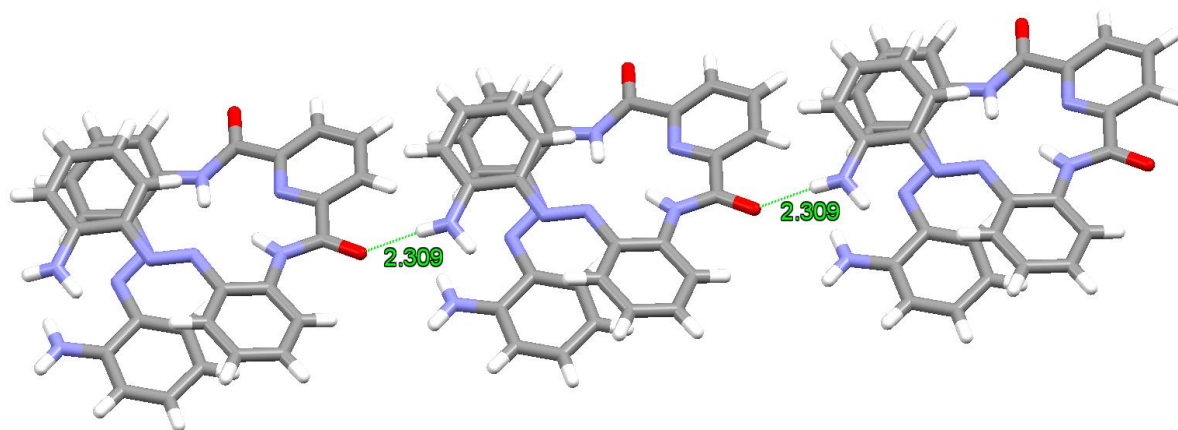


Figure S114. Solid state analysis of **1·DMSO** highlighting the presence of an intermolecular C-H...O hydrogen-bonding chain within the majority occupancy component between an aromatic proton on one foldamer and the O atom of a carbonyl group of a carboxamide unit in an adjacent foldamer molecule. This interaction is observed in both parts as the positional disorder is localised on only one aniline moiety.

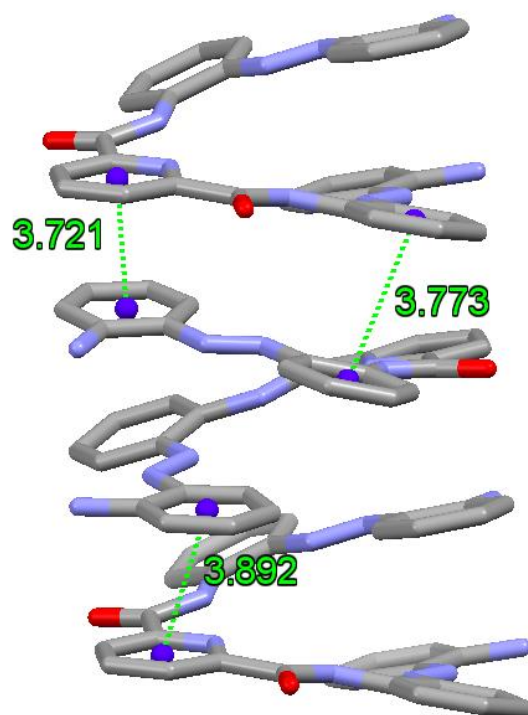


Figure S115. Solid state analysis of the offset face-to-face π - π stacking interactions¹⁸ observed between molecules of **1•DMSO** when observing the majority component.

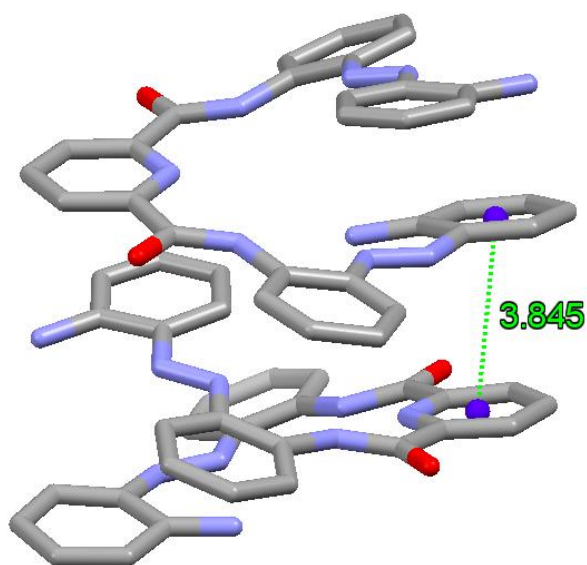


Figure S116. Solid state analysis of the additional offset face-to-face π - π stacking interaction¹⁸ observed between molecules of **1•DMSO** when the positional disorder of aniline is considered.

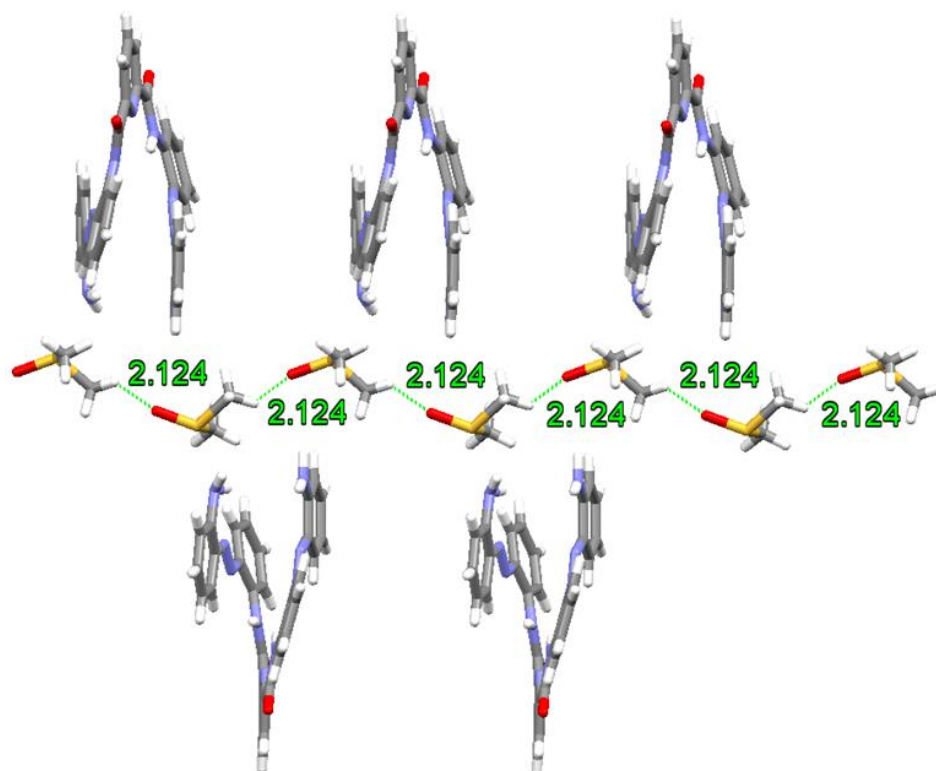


Figure S117. Solid state analysis of **1·DMSO** highlighting the presence of an intermolecular C-H \cdots O hydrogen-bonding interactions between the aliphatic protons of the DMSO solvent molecule and the O atom of on an adjacent DMSO solvent molecule.

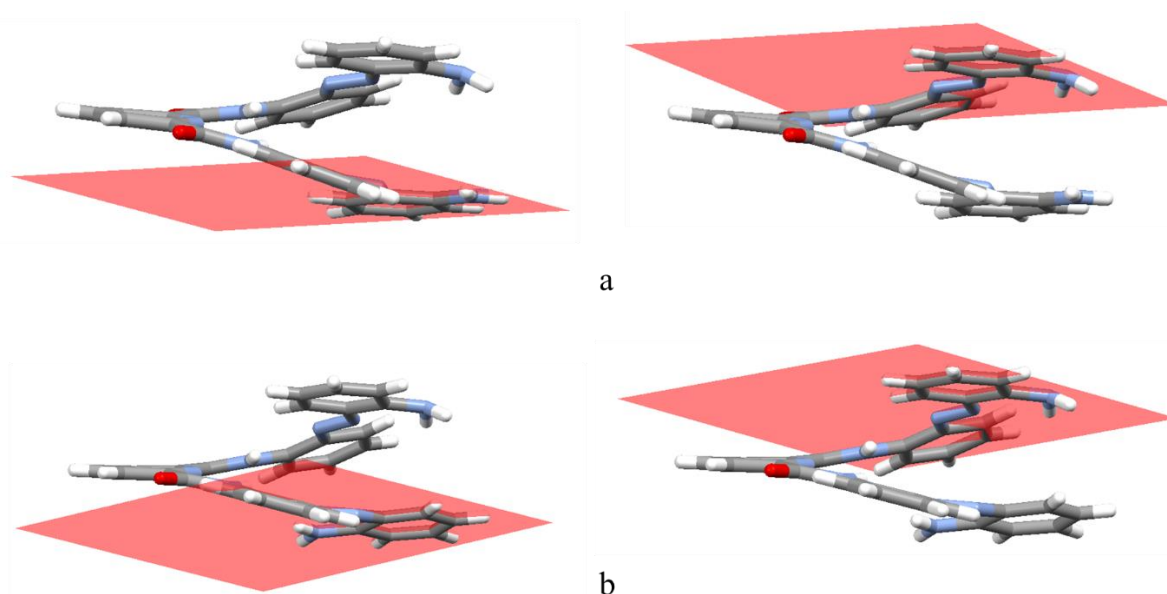


Figure S118. Solid state analysis of a foldamer molecule in the unit cell of **1·DMSO**, where the disordered occupancy is denoted using ‘a’ for the majority component and ‘b’ for the minority component, highlighting the plane of the terminal aniline groups.

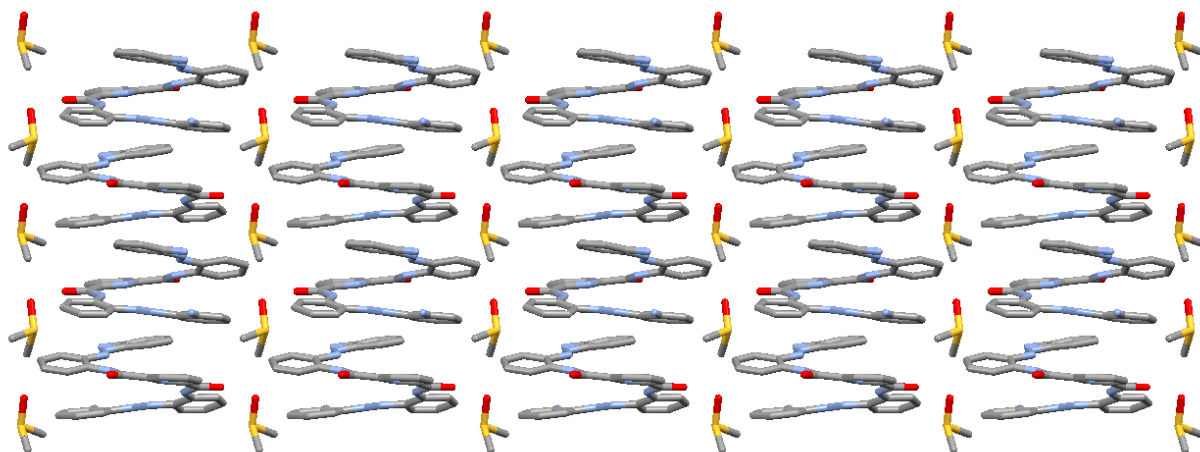


Figure S119. Solid state analysis showing the crystal packing of **1·DMSO** as viewed along the *a* axis for the majority component. H atoms have been removed for clarity.

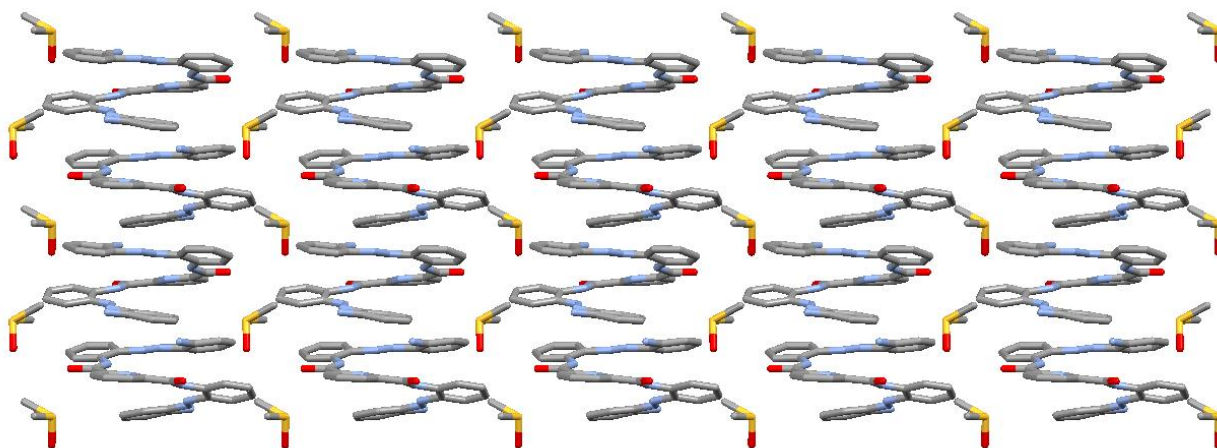


Figure S120. Solid state analysis showing the crystal packing of **1·DMSO** as viewed along the *a* axis for the minority component. H atoms have been removed for clarity.

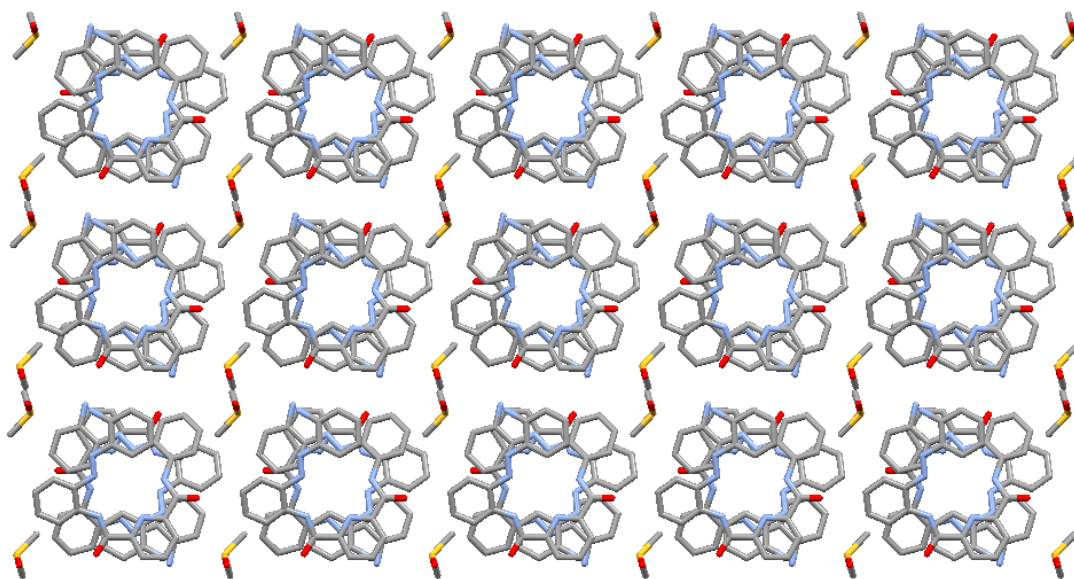


Figure S121. Solid state analysis showing the crystal packing of **1•DMSO** as viewed along the *b* axis for the majority component. H atoms have been removed for clarity.

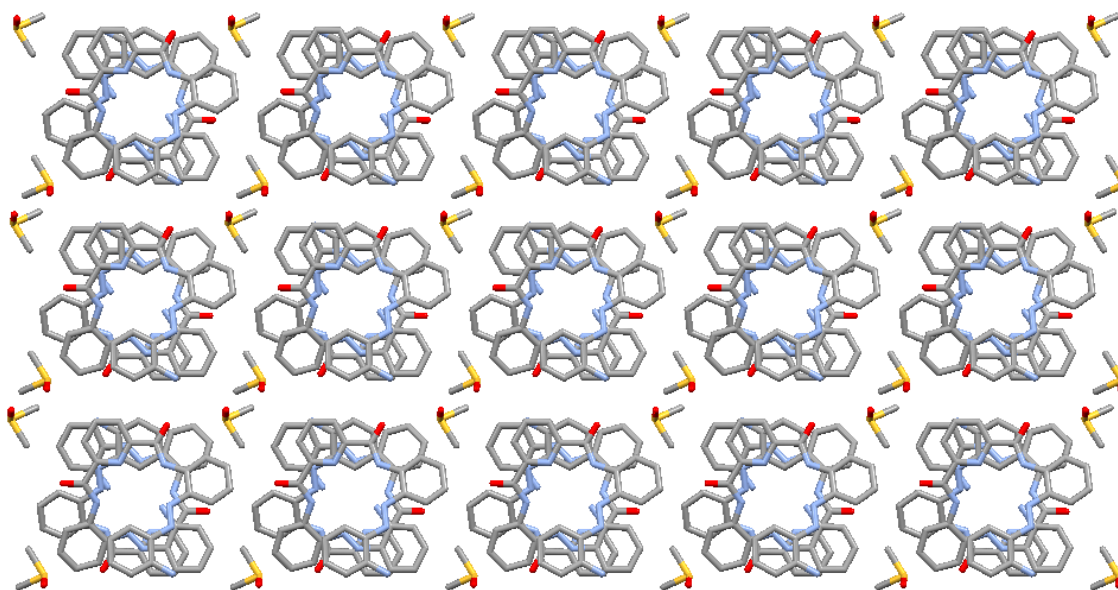


Figure S122. Solid state analysis showing the crystal packing of **1•DMSO** as viewed along the *b* axis for the minority component. H atoms have been removed for clarity.

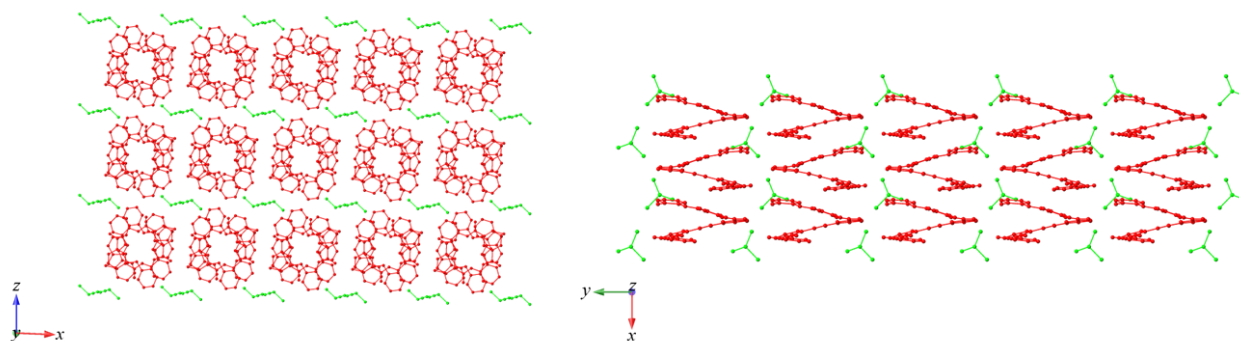


Figure S123. Solid state analysis showing the crystal packing of the majority disorder component of **1•DMSO** with a chemical occupancy of 64.6(1)% showing columns and rows of left-handed stacks. Hydrogen atoms have been removed for clarity, solvent molecules are shown in green, and molecules have been coloured in accordance with handedness, where red represents right (P).

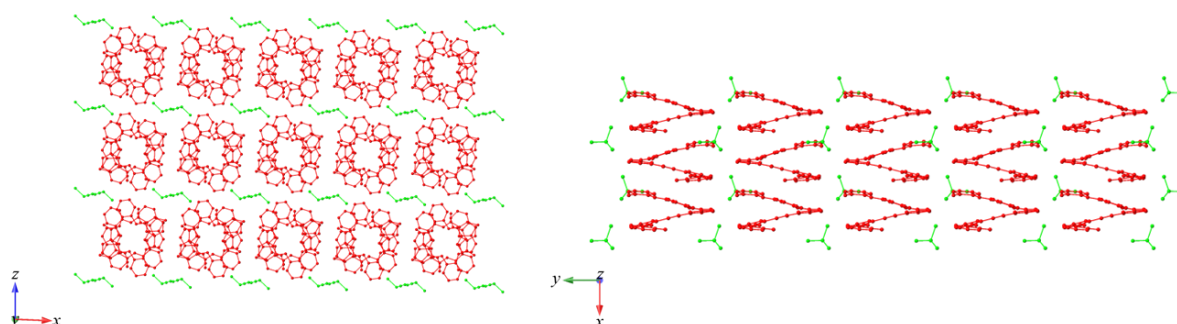


Figure S124. Solid state analysis showing the crystal packing of the minority disorder component of **1•DMSO** with a chemical occupancy of 35.4(1)% showing columns and rows of left-handed stacks. Hydrogen atoms have been removed for clarity, solvent molecules are shown in green, and molecules have been coloured in accordance with handedness, where red represents right (P).

Cavity space and channel calculation

Cavity spaces and channels of crystal structures were calculated using the MoloVol²⁰ program with a grid resolution of 0.1 Å and optimisation depth of 4. Single probe mode was used, and probe radii were varied and are specified in the tables below. The surfaces were visualised using Pymol²¹ and set as level 2.0 surfaces (molecular and cavity surface). The surfaces of the cavities have been colourised in order of decreasing volume; red, orange, yellow, green, blue, magenta, purple, and cyan. Fragmented cavities produced as a result of the unit cell boundaries have been merged to calculate total volume of a given cavity and visualised as such. Tunnel radii have been calculated by rearranging $V=\pi r^2 h$, where h is the length of unit cell axis and V is calculated cavity space from MoloVol.

a) Void Analysis of 1A and 1A'

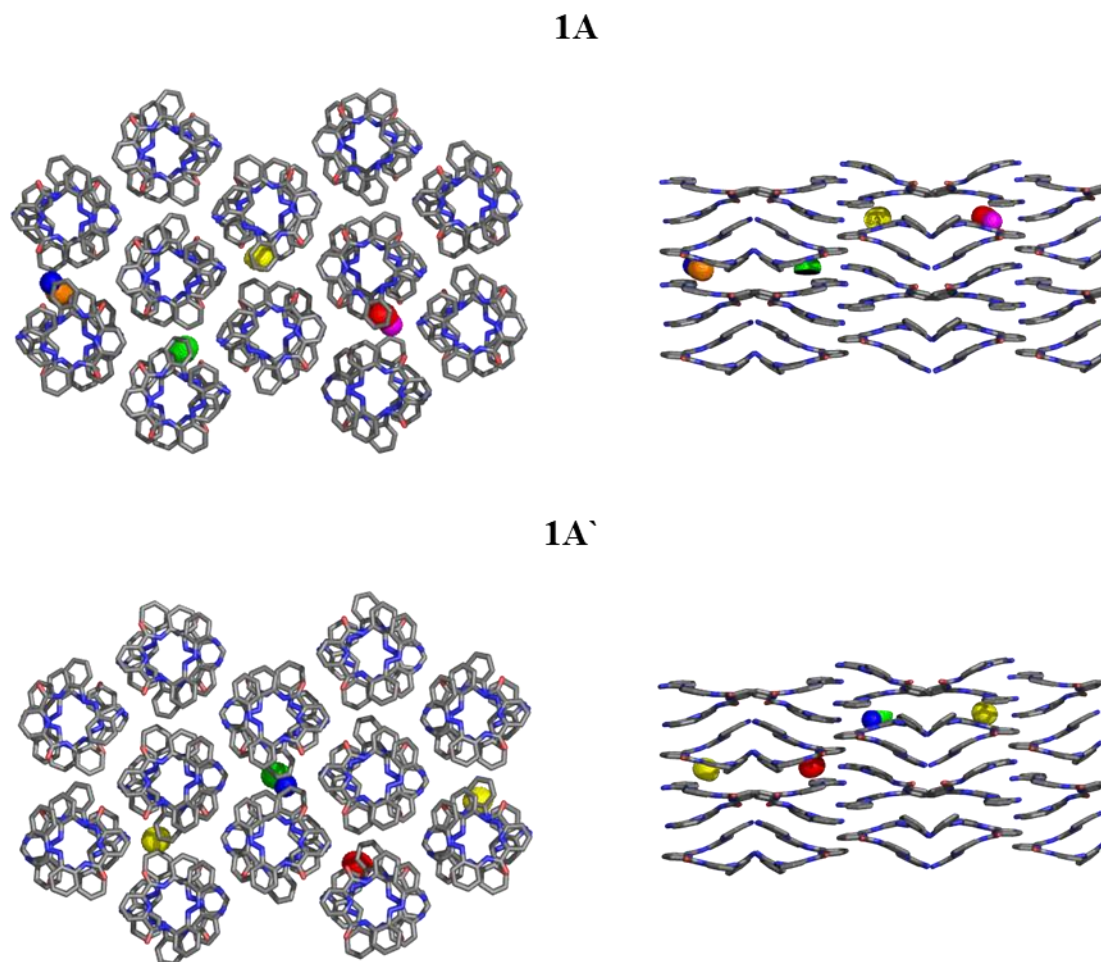


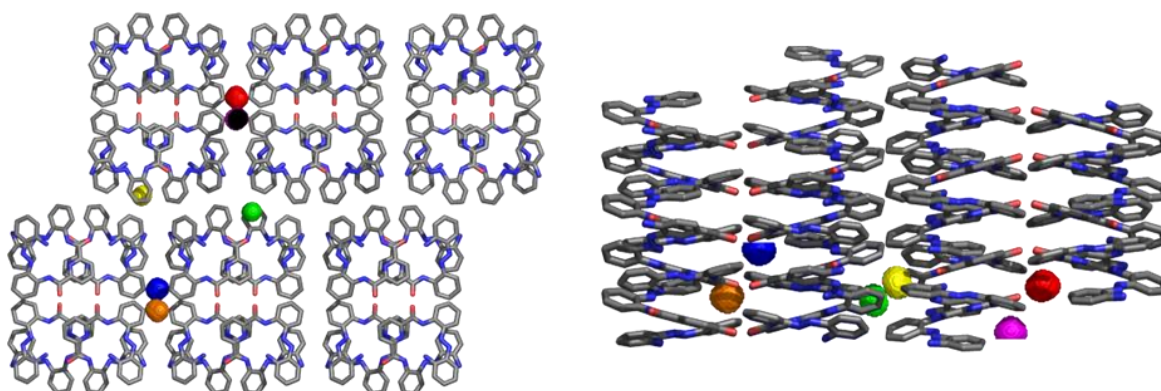
Figure S125. Visualisation of cavities in **1A** and **1A'** calculated using MoloVol.²⁰

Structure	Probe radius/Å	Cav1/Å ³	Cav2/Å ³	Cav3/Å ³	Cav4/Å ³	Cav5/Å ³	Cav6/Å ³	Cav7/Å ³
1A	1.1	9.511	4.91	9.013	7.66	4.47	4.41	2.39
1A'	1.1	10.58	10.57	10.37	6.24	4.64	-	-

Table S12. Cavity analysis of crystal structures **1A** and **1A'**, cavities have been coloured as mentioned above in 'Cavity space and channel calculation'.

b) Void Analysis of **1B**

1B part 1



1B part 2

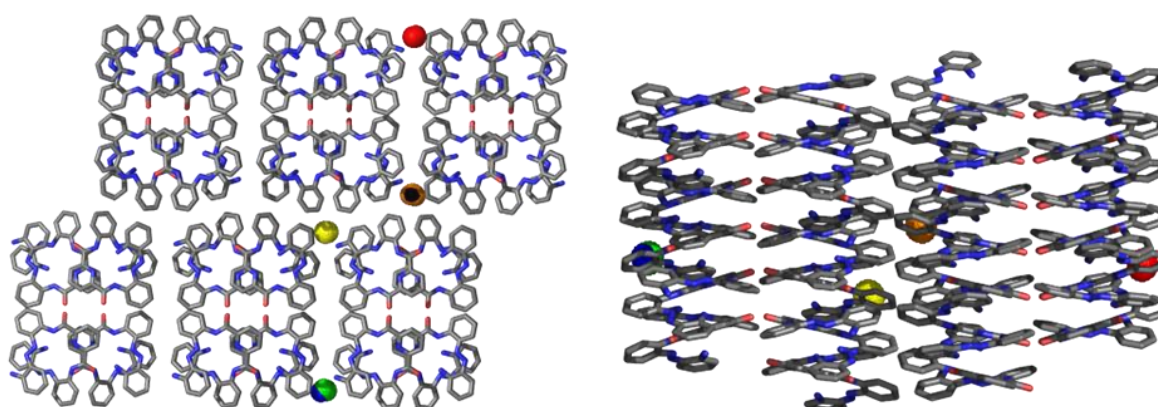


Figure S126. Visualisation of cavities for both disorder components in **1B** calculated using MoloVol.²⁰

Part	Probe radius/ Å	Cav1/Å ³	Cav2/Å ³	Cav3/Å ³	Cav4/Å ³	Cav5/Å ³	Cav6/Å ³
1	1.0	8.152	8.03	6.599	6.268	6.058	5.979
2	1.1	8.573	8.488	8.329	7.026	2.751	-

Table S13. Cavity analysis of both disorder components of the crystal structure of **1B**, cavities have been coloured as mentioned above in ‘Cavity space and channel calculation’.

c) Void Analysis of **1·THF**

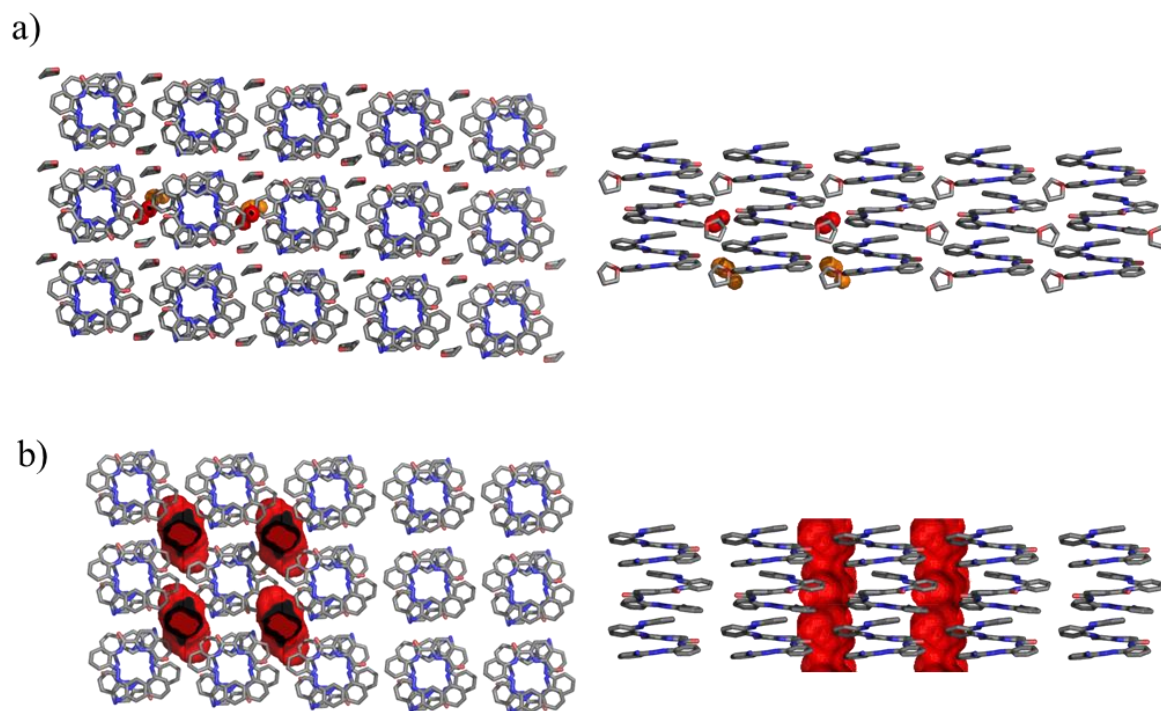


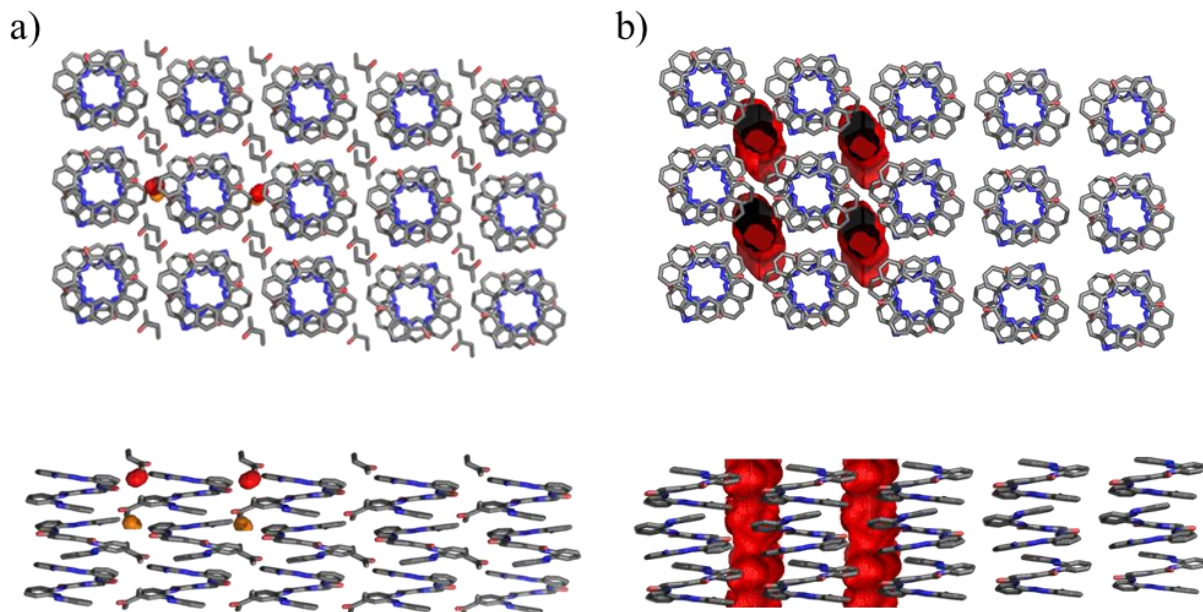
Figure S127. Visualisation of cavities in of **1·THF** calculated using MoloVol.²⁰ Tunnels are observed upon removal of solvent from .CIF files and are depicted as three dimensional slices down the *b* axis.

Probe radius/Å	Solvent	Cav1/Å ³	Cav2/Å ³	Channel volume per unit cell/Å ³	Channel radius/Å
0.9	Y	8.9043	8.90431	-	-
1.2	N	-	-	256.875	7.847

Table S14. Cavity analysis of crystal structures a) **1·THF** and b) **1·THF** with solvent excluded from .CIF data, cavities have been coloured as mentioned above in 'Cavity space and channel calculation'.

d) Void Analysis of 1-butanone

1-butanone part 1



1-butanone part 2

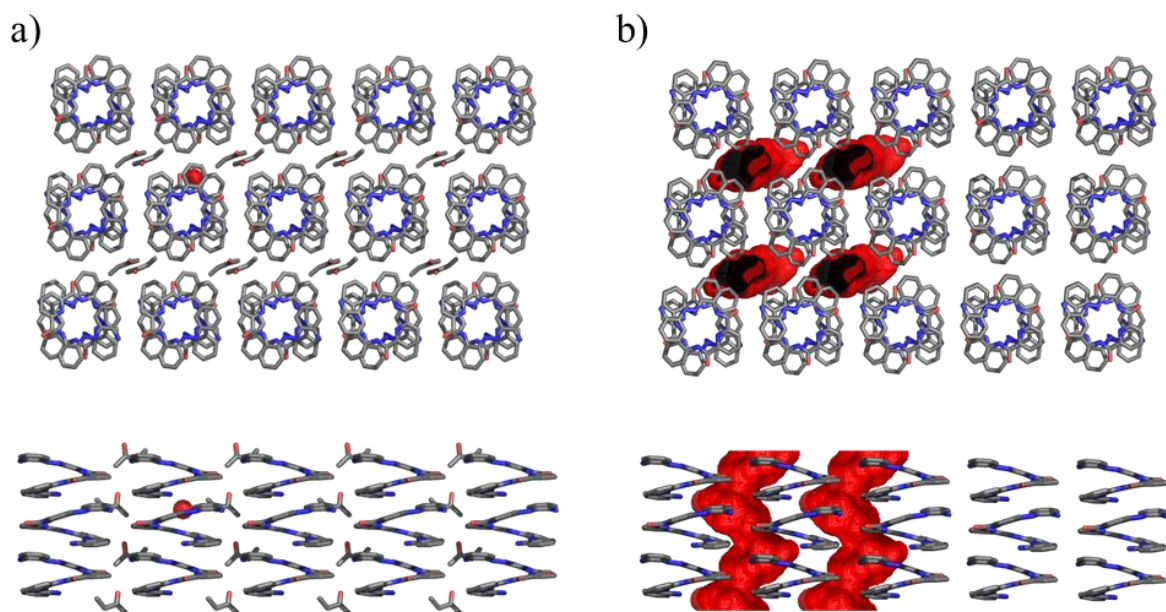


Figure S128. Visualisation of cavities in of a) **1•butanone** and b) **1•butanone** with solvent excluded from .CIF data, calculated using MoloVol.²⁰ Showing both components of the crystal structure, part 1 and part 2.

Part	Probe radius/Å	Solvent	Cav1/Å ³	Cav2/Å ³	Tunnel volume per unit cell/ Å ³	Tunnel radius/Å
1a	0.9	No	5.83	4.75	-	-
1b	1.2	Yes	-	-	296.15	4.53
2a	1.0	No	4.53	-	-	-
2b	1.2	Yes	-	-	287.74	4.41

Table S15. Cavity analysis of both part 1 (majority disorder component) and part 2 (minority disorder component) of crystal structures a) **1•butanone** and b) **1•butanone** with solvent excluded from .CIF data, cavities have been coloured as mentioned above in ‘Cavity space and channel calculation’.

e) Void Analysis of 1•DCM

1-DCM

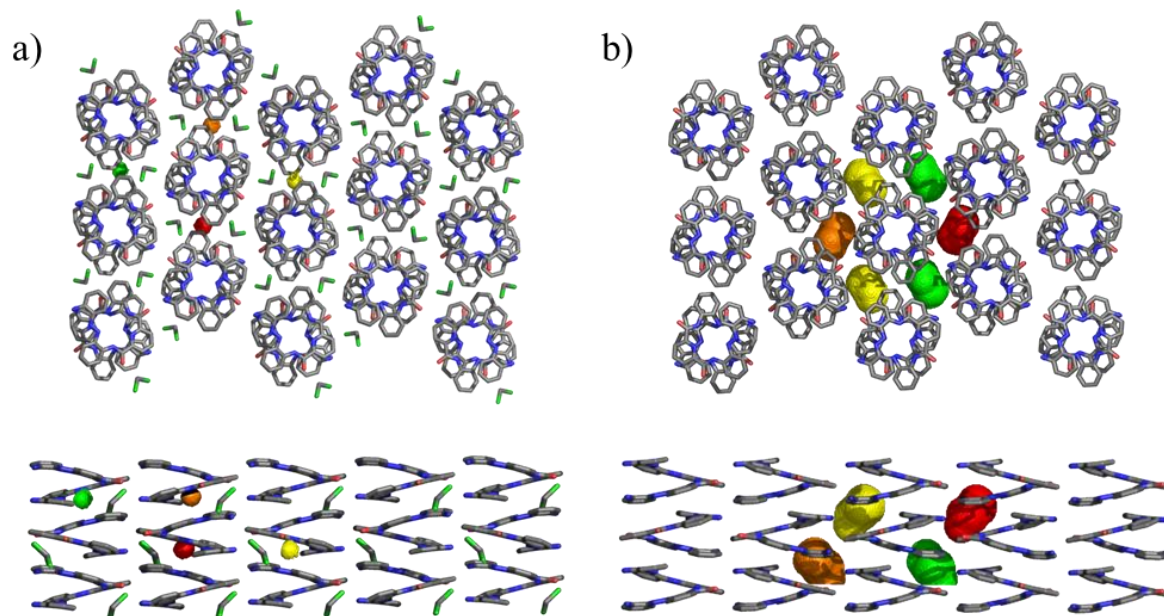


Figure S129. Visualisation of cavities in of a) **1•DCM** and b) **1•DCM** with solvent excluded from .CIF data, calculated using MoloVol.²⁰

Probe radius/Å	Solvent	Cav1/Å ³	Cav2/Å ³	Cav3/Å ³	Cav4/Å ³
0.9	Yes	6.04232	6.024	5.55368	3.744
1.6	No	73.272	66.6544	73.2111	66.9523

Table S16. Cavity analysis of crystal structures a) **1•DCM** and b) **1•DCM** with solvent excluded from .CIF data, cavities have been coloured as mentioned above in 'Cavity space and channel calculation'.

f) Void Analysis of **1·MeOH**

1·MeOH

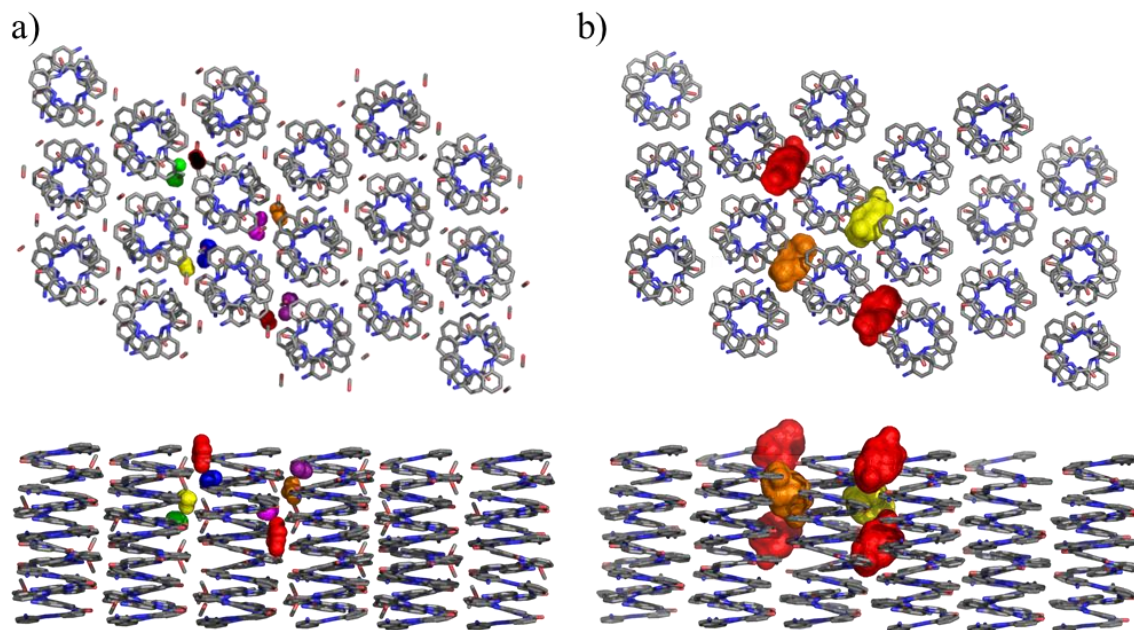


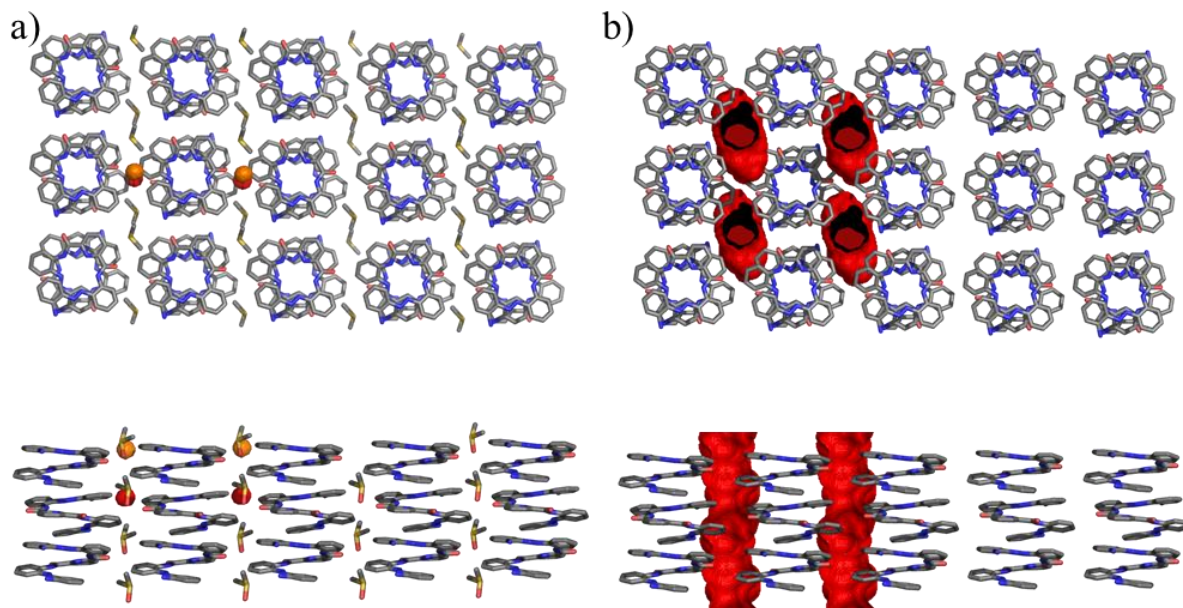
Figure S130. Visualisation of cavities in a) **1·MeOH** and b) **1·MeOH** with solvent excluded from .CIF data, calculated using MoloVol.²⁰

Probe radius/Å	Solvent	Cav1/Å ³	Cav2/Å ³	Cav3/Å ³	Cav4/Å ³
0.9	Yes	6.04232	6.024	5.55368	3.744
1.6	No	73.272	66.6544	73.2111	66.9523

Table S17. Cavity analysis of crystal structures a) **1·MeOH** and b) **1·MeOH** with solvent excluded from .CIF data, cavities have been coloured as mentioned above in ‘Cavity space and channel calculation’.

g) Void Analysis of **1**·DMSO

1·DMSO part 1



1·DMSO part 2

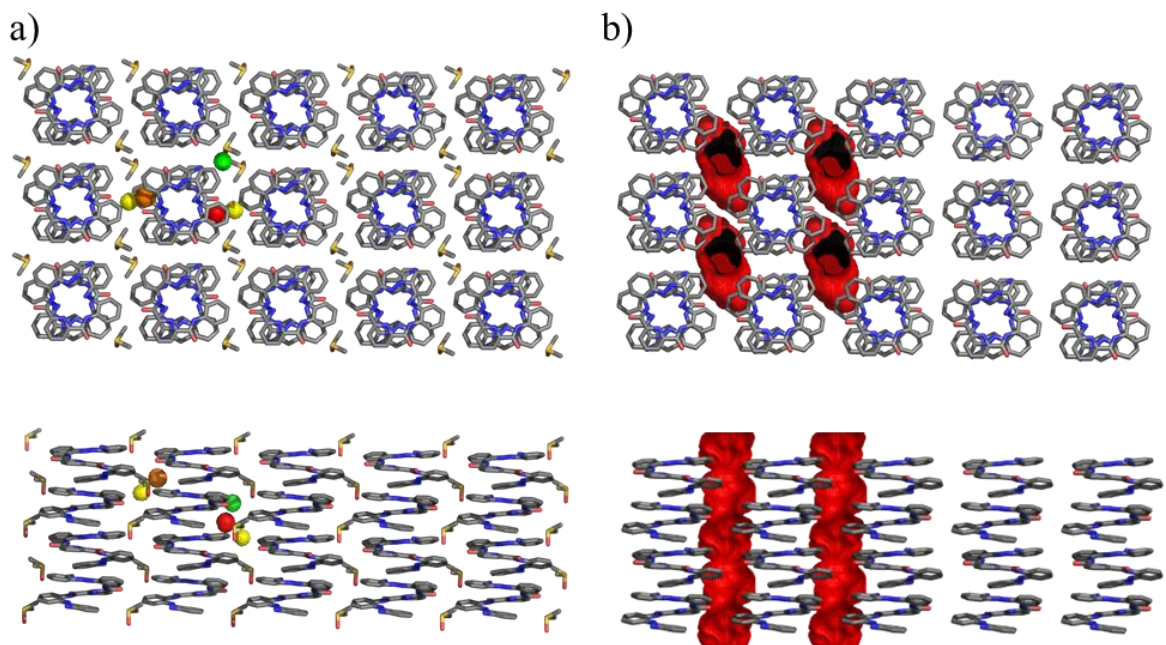


Figure S131. Visualisation of cavities in of **1**·DMSO calculated using MoloVol.²⁰ Showing both components of the crystal structure, part 1 and part 2.

Part	Probe radius/Å	Solvent	Cav1/Å ³	Cav2/Å ³	Tunnel volume per unit cell/ Å ³	Tunnel radius/Å
1a	0.9	Yes	4.88652	4.54729	-	-
1b	1.2	No	-	-	285.829	4.359
2a	1.0	Yes	6.897	6.751	-	-
2b	1.2	No	-	-	282.826	4.313

Table S18.19 Cavity analysis of both part 1 (majority disorder component) and part 2 (minority disorder component) of crystal structures a) **1·DMSO** and b) **1·DMSO** with solvent excluded from .CIF data, cavities have been coloured as mentioned above in ‘Cavity space and channel calculation’.

References

- 1 A. R. Davis, S. Ozturk, C. C. Seaton, L. Male and S. J. Pike, *Chem. A Eur. J.*, 2024, **30**, e202402892.
- 2 S. J. Pike, A. Heliot and C. C. Seaton, *CrystEngComm.*, 2020, **22**, 5040–5048.
- 3 CrysAlisPro, Rigaku Oxford Diffraction, 2020 & 2021.
- 4 D. Allan, H. Nowell, S. Barnett, M. Warren, A. Wilcox, J. Christensen, L. Saunders, A. Peach, M. Hooper, L. Zaja, S. Patel, L. Cahill, R. Marshall, S. Trimmell, A. Foster, T. Bates, S. Lay, M. Williams, P. Hathaway, G. Winter, M. Gerstel and R. Wooley, *Crystals*, **2017**, 7, 336.
- 5 J. Beilsten-Edmands et al., *Acta Cryst.*, **2020**, D76, 385-399.
- 6 P. R. Evans and G. N. Murshudov, *Acta Cryst.*, **2013**, D69, 1204-1214.
- 7 M. D. Winn, C. C. Ballard, K. D. Cowtan, E. J. Dodson, P. Emsley, P. R. Evans, R. M. Keegan, E. B. Krissinel, A. G. W. Leslie, A. McCoy, S. J. McNicholas, G. N. Murshudov, N. S. Pannu, E. A. Potterton, H. R. Powell, R. J. Read, A. Vagin and K. S. Wilson, *Acta Cryst.*, **2011**, D67, 235–242.
- 8 G. Winter, *J. Appl. Cryst.*, **2010**, 43, 186–190.
- 9 G. Winter, D. G. Waterman, J. M. Parkhurst, A. S. Brewster, R. J. Gildea, M. Gerstel, L. Fuentes-Montero, M. Vollmar, T. Michels-Clark, I. D. Young, N. K. Sauter and G. Evans, *Acta Cryst.*, **2018**, D74, 85–97.
- 10 O. V. Dolomanov, L. J. Bourhis, R. J. Gildea, J. A. K. Howard and H. Puschmann, *J. Appl. Cryst.*, **2009**, 42, 339–341.
- 11 I. G. M. Sheldrick, *Acta Cryst.*, Sect. A Struct. Chem., **2015**, A71, 3–8.
- 12 G. M. Sheldrick, *Acta Cryst.*, Sect. C Struct. Chem., **2015**, C71, 3–8.

- 13 C. F. Macrae, I. Sovago, S. J. Cottrell, P. T. A. Galek, P. McCabe, E. Pidcock, M. Platings, G. P. Shields, J. S. Stevens, M. Towler and P. A. Wood, *J. Appl. Cryst.*, 2020, 53, 226–235.
- 14 I. Rozas, I. Alkorta and J. Elguero, *J. Phys. Chem. A*, 1998, **102**, 9925–9932.
- 15 Y. Hamuro, S. J. Geib and A. D. Hamilton, *Angew. Chemie Int. Ed. English*, 1994, **33**, 446–448.
- 16 C. Tie, J. C. Gallucci and J. R. Parquette, *J. Am. Chem. Soc.*, 2006, **128**, 1162–1171.
- 17 S. Horowitz and R. C. Trievel, *J. Biol. Chem.*, 2012, **287**, 41576–41582.
- 18 M. Egli, V. Tereshko, G. N. Mushudov, R. Sanishvili, X. Liu and F. D. Lewis, *J. Am. Chem. Soc.*, 2003, **125**, 10842–10849.
- 19 S. Sarkhel and G. R. Desiraju, *Proteins Struct. Funct. Bioinforma.*, 2003, 54, 247–259.
- 20 J. B. Maglic and R. Lavendomme, *J. Appl. Crystallogr.*, 2022, 55, 1033–1044.
- 21 The PyMOL Molecular Graphics System, Version 3.0 Schrödinger, LLC, .